AEDC-TR-73-112

$\varphi . 1$

NUMERICAL CALCULATION OF THE SUBSONIC AND TRANSONIC TURBULENT BOUNDARY LAYER ON AN INFINITE YAWED AIRFOIL

John C. Adams, Jr.

ARO, Inc.

July 1973

VON KÁRMÁN GAS DYNAMICS FACILITY
ARNOLD ENGINEERING DEVELOPMENT CENTER
AIR FORCE SYSTEMS COMMAND
ARNOLD AIR FORCE STATION, TENNESSEE

NOTICES

NUMERICAL CALCULATION OF THE SUBSONIC AND TRANSONIC TURBULENT BOUNDARY LAYER ON AN INFINITE YAWED AIRFOIL

John C. Adams, Jr.

ARO, Inc.

Approved for public release; distribution unlimited.

FOREWORD

The work reported herein was conducted at the Arnold Engineering Development Center (AEDC), Air Force Systems Command (AFSC), under Program Element 65802F.

The results of research presented were obtained by ARO, Inc. (a subsidiary of Sverdrup & Parcel and Associates, Inc.), contract operator of AEDC, AFSC, Arnold Air Force Station, Tennessee. The research was conducted from April 1972 through April 1973 under ARO Project Nos. VF203 and VD205, and the manuscript was submitted for publication on April 30, 1973.

This technical report has been reviewed and is approved.

ELTON R. THOMPSON
Research and Development Division
Directorate of Technology

ROBERT O. DIETZ
Director of Technology

ABSTRACT

Formulation and application of a three-dimensional compressible turbulent boundary-layer analysis is presented for subsonic and transonic flow over a yawed airfoil of infinite extent. The governing turbulent boundary-layer equations are integrated using an implicit finite-difference procedure in conjunction with a scalar eddy viscosity model of three-dimensional turbulence. Comparisons with other analysis techniques as well as experimental measurements under subsonic wind tunnel conditions are presented to establish and ascertain the basic validity and applicability of the current technique. Also considered are the effects of a hot wall on the transonic, three-dimensional, turbulent boundary layer which have practical application to transonic Space Shuttle reentry, where the wing surface temperature may reach soak values on the order of twice the free-stream stagnation temperature because of the hypersonic high-heating phase of the reentry trajectory. Ground testing of Space Shuttle configurations under continuous transonic flow conditions with an adiabatic wall may not be totally applicable to actual Shuttle entry; airfoil static stall angle, maximum lift coefficient, local skin-friction, and other turbulent boundary-layer parameters are strongly affected by hot-wall relative to adiabatic-wall conditions.

CONTENTS

APPENDIXES

I. ILLUSTRATIONS

Figure

NOMENCLATURE

A_*	van Driest damping constant, 26.0
$\bar{A}_n, \bar{B}_n, \bar{C}_n, \bar{D}_n$	Coefficients in finite-difference Eq. (III-36)
B_1, B_2, B_3	Wall derivative numerical coefficients defined by Eqs. (IV-4, -5, and -6)
C	Airfoil chord
C^*	Stagnation or attachment line Reynolds number defined by Eq. (96)
C_{f_e}	Local skin-friction coefficient based on inviscid edge conditions
C_{f_∞}	Local skin-friction coefficient based on free-stream conditions
$C_{L_{max}}$	Maximum lift coefficient
C_{L_u}	Sectional lift coefficient
C_p	Constant pressure specific heat
C_{p_∞}	Surface pressure coefficient defined in Fig. 11
c	Spanwise velocity ratio, $\bar{w}/W_e$
c´	Spanwise velocity ratio gradient, $\partial(\bar{w}/W_e)/\partial\eta$
D	Diameter of circular cylinder
D_1, D_2	Coefficients for finite-difference derivatives defined by Eqs. (III-32) and (III-33)
D_i	Trapezoidal rule integration step size defined by Eq. (III-49)

$\dfrac{dU_e}{dx}$ | Inviscid edge chordwise velocity gradient

E_n — Coefficient in finite-difference Eq. (III-41)

e_n — Coefficient in finite-difference Eq. (III-41)

F_1, F_2, F_3 — Numerical constants in finite-difference Eq. (III-46) as defined in Appendix IV

f — Transformed stream function defined by Eq. (37)

f' — Chordwise velocity ratio, $\bar{u}/U_e$

f'' — Chordwise velocity gradient, $\partial(\bar{u}/U_e)/\partial\eta$

G — Scalar velocity function defined by Eq. (18)

g — Total enthalpy ratio, $\bar{H}/H_e$

g' — Total enthalpy ratio gradient, $\partial(\bar{H}/H_e)/\partial\eta$

H' — Fluctuating total enthalpy

$\bar{H}$ — Mean total enthalpy

H_f — Shape factor

h' — Fluctuating static enthalpy

$\bar{h}$ — Mean static enthalpy

K — Variable grid parameter defined by Eq. (III-34)

k — Thermal conductivity

k_* — Inner law mixing-length constant, 0.435

L — Reference length

ℓ — Density-viscosity product ratio, $\bar{\rho}\mu/\rho_e\mu_e$

ℓ_* — Mixing length

ℓ^* — Modified density-viscosity product ratio for use in momentum equation, defined by Eq. (46)

ℓ^{**} — Modified density-viscosity product ratio for use in energy equation, defined by Eq. (47)

M_e — Local edge Mach number

M_∞ — Free-stream Mach number

N — Total number of grid points

$P_{O,\infty}$	Free-stream stagnation pressure
Pr	Laminar Prandtl number, 0.71
Pr_t	Turbulent Prandtl number, 0.90
$\bar{p}$	Static pressure
p_∞	Free-stream static pressure
$\dot{q}$	Heat flux
$\dot{q}_w$	Wall heat flux
R	Specific gas constant
Re_e	Local Reynolds number based on inviscid edge conditions
$Re_{\infty,C}$	Free-stream Reynolds number based on airfoil chord
$Re_{\infty,D}$	Free-stream Reynolds number based on circular cylinder diameter
St_∞	Local Stanton number based on free-stream conditions
$\bar{T}$	Mean static temperature
T_{aw}	Adiabatic-wall temperature
T_e	Static temperature at outer edge of boundary layer
$\bar{T}_O$	Mean stagnation temperature
$T_{O,\infty}$	Free-stream stagnation temperature
T_w	Wall temperature
T_∞	Free-stream static temperature
U_e	Chordwise velocity component at outer edge of boundary layer
u'	Fluctuating chordwise velocity component
$\bar{u}$	Mean chordwise velocity component
$\bar{u}_{s\ell}$	Streamwise velocity in streamline coordinates
V	Combined normal velocity components according to Eq. (6)
V_∞	Free-stream velocity
v'	Fluctuating normal velocity component

$\bar{v}$	Mean normal velocity component
W	Dependent variable in finite-difference Eq. (III-16)
W_e	Spanwise velocity component at outer edge of boundary layer
w'	Fluctuating spanwise velocity component
$\bar{w}$	Mean spanwise velocity component
$\bar{w}_{s\ell,max}$	Maximum crossflow velocity in streamline coordinates
X	Coordinate along airfoil chord (see Figs. 1 and 2)
x	Chordwise coordinate on airfoil surface (see Figs. 1 and 2)
Y	Coordinate normal to airfoil chord (see Figs. 1 and 2)
y	Coordinate normal to body surface (see Figs. 1 and 2)
y_ℓ	Characteristic thickness of boundary layer in Eq. (25)
z	Spanwise coordinate on airfoil surface (see Figs. 1 and 2)
α	Angle of attack
α_{stall}	Airfoil static stall angle
$\alpha_1, \alpha_2, \alpha_3, \alpha_4$	"Standard form" coefficients for parabolic partial differential equation following Eq. (III-16)
β	Inviscid velocity gradient parameter defined by Eq. (48)
γ	Specific heat ratio, 1.40
δ	Boundary-layer thickness
δ^*	Displacement thickness
ϵ	Eddy viscosity
ϵ_i	Eddy viscosity in inner region
ϵ_o	Eddy viscosity in outer region
ζ	Initial (off wall) $\Delta\eta$ step size defined by Eq. (III-35)
θ	Static temperature ratio, $\bar{T}/T_e$, defined by Eq. (52)
θ'	Static temperature gradient, $\partial(\bar{T}/T_e)/\partial\eta$
θ_m	Momentum thickness

κ	Eddy thermal conductivity
Λ	Sweep or yaw angle
λ	Outer law mixing-length constant, 0.090
μ	Laminar (molecular) viscosity
ξ, η	Transformed coordinates defined by Eqs. (31) and (32)
ρ'	Fluctuating mass density
$\bar{\rho}$	Mean mass density
ρ_e	Mass density at outer edge of boundary layer
ρ_∞	Free-stream mass density
τ	Shear stress
τ_w	Wall shear stress
χ	Crossflow Reynolds number defined by Eq. (97)
ψ	Stream function
Ω	Energy equation term defined by Eq. (49)
Ω'	Energy equation term gradient, $\partial\Omega/\partial\eta$
ω	Local streamline angle
ω_e	Local streamline angle evaluated at outer edge of the boundary layer (see Fig. 2)
ω_s	Local streamline angle evaluated at the body surface (see Fig. 2)

SUBSCRIPTS

aw	Adiabatic wall
C	Chord
e	Outer edge of boundary layer
I	Initial approximation
o	Stagnation or total
o, ∞	Free-stream stagnation or total
s	Surface

sℓ	Streamline coordinates
turb	Turbulent
w	Wall
x	x-direction
z	z-direction
∞	Free stream

SUPERSCRIPTS

      Fluctuation quantity or partial derivative with respect to η, depending on usage

$-$ Quantity averaged with respect to time

SECTION I
INTRODUCTION

The three-dimensional compressible turbulent boundary layer on an infinite yawed airfoil under subsonic or transonic flow conditions is a problem which has received little attention in the literature. Only within recent years, with the development of accurate numerical intergration methods using a digital computer, has even the simplier case of laminar compressible boundary-layer flow over an infinite yawed wing become amenable. (See Ref. 1 for documentation of one such analysis.) Needless to say, the infinite yawed airfoil never occurs in practical applications (e.g., a transport aircraft). The importance of this type flow concerns the trends which it reveals (i.e., the effects of three-dimensional flow on boundary-layer characteristics). In addition, high aspect ratio finite-length swept airfoils may be adequately represented by an infinite yawed wing in regions removed from the wing root and tip; an example of such an airfoil is given in Ref. 2 relative to helicopter rotor applications.

The boundary layer, be it laminar or turbulent, on an infinite yawed wing is three-dimensional in the sense that the velocity and shear-stress profiles are skewed, but quasi-two-dimensional insofar as spanwise derivatives of the pressure, velocity, and temperature are identically zero. For example, there is spanwise flow on the infinite yawed wing but no net boundary-layer "drift" towards the wing tip such as occurs on finite airfoils. An analytical study of the complete three-dimensional turbulent boundary-layer flow over a finite swept airfoil is an extremely difficult problem, with Ref. 3 being the only such analysis currently available (to the author's knowledge). With respect to infinite yawed wing flows, many previous investigations (Refs. 4 through 10) have developed analytical techniques applicable under incompressible conditions for both laminar and turbulent boundary layers. For the case of compressible boundary-layer flow over an infinite yawed airfoil, only the studies of Ref. 1 for laminar flow and Ref. 11 for turbulent flow have been performed.

The present report will examine three-dimensional compressible turbulent boundary-layer flow over an infinite yawed airfoil under subsonic and transonic conditions. The governing turbulent boundary-layer equations are integrated using an implicit finite-difference procedure in conjunction with a scalar eddy viscosity model of three-dimensional turbulence. Comparisons of the present approach with

experimental data are presented in order to establish and ascertain the basic validity and applicability of the current technique under subsonic and transonic flow conditions.

SECTION II
ANALYTICAL ANALYSIS

2.1 OVERVIEW

The present analytical investigation employs a three-dimensional turbulent boundary-layer analysis based on a scalar eddy viscosity model of turbulence for the case of subsonic and transonic flow over an infinite extent yawed airfoil. Full development of the boundary-layer analysis will be presented below; the inviscid analysis utilizes existing well-documented procedures which are described briefly.

2.2 GOVERNING BOUNDARY-LAYER EQUATIONS

The present analysis employs the three-dimensional compressible turbulent boundary-layer equations in terms of time-averaged mean-flow quantities as derived by Vaglio-Laurin (Ref. 12). Assuming the ratio of boundary-layer thickness to local surface curvature to be every-where small, the governing equations of motion, in terms of the ortho-gonal coordinate system x, y, z illustrated in Figs. 1 and 2, Appendix I, reduce to the following (see NOMENCLATURE for terminology):

CONTINUITY

$$\frac{\partial \overline{\rho} \overline{u}}{\partial x} + \frac{\partial \overline{\rho} V}{\partial y} + \frac{\partial \overline{\rho} \overline{w}}{\partial z}^{0} = 0 \tag{1}$$

x-MOMENTUM

$$\overline{\rho} \overline{u} \frac{\partial \overline{u}}{\partial x} + \overline{\rho} V \frac{\partial \overline{u}}{\partial y} + \overline{\rho} \overline{w} \frac{\partial \overline{u}}{\partial z}^{0} = -\frac{\partial \overline{p}}{\partial x} + \frac{\partial}{\partial y} \left[\mu \frac{\partial \overline{u}}{\partial y} - \overline{\rho} \overline{u'v'} \right] \tag{2}$$

y-MOMENTUM

$$\frac{\partial \overline{p}}{\partial y} = 0 \tag{3}$$

2

z- MOMENTUM

$$\bar{\rho}\,\bar{u}\,\frac{\partial \bar{w}}{\partial x} + \bar{\rho}\,V\frac{\partial \bar{w}}{\partial y} + \bar{\rho}\,\bar{w}\,\cancel{\frac{\partial \bar{w}}{\partial z}}^{\,o} = -\cancel{\frac{\partial \bar{p}}{\partial z}}^{\,o} + \frac{\partial}{\partial y}\left[\mu\,\frac{\partial \bar{w}}{\partial y} - \bar{\rho}\,\overline{v'w'}\right] \tag{4}$$

ENERGY

$$\bar{\rho}\,\bar{u}\,\frac{\partial \bar{H}}{\partial x} + \bar{\rho}\,V\frac{\partial \bar{H}}{\partial y} + \bar{\rho}\,\bar{w}\,\cancel{\frac{\partial \bar{H}}{\partial z}}^{\,o} = \frac{\partial}{\partial y}\left[\mu\left(\frac{\partial \bar{H}}{\partial y} + \frac{1-Pr}{Pr}\,\frac{\partial \bar{h}}{\partial y}\right) - \bar{\rho}\,\overline{v'H'}\right] \tag{5}$$

where

$$V = \bar{v} + \frac{\overline{\rho'v'}}{\bar{\rho}} \tag{6}$$

$$\bar{H} = \bar{h} + \frac{\bar{u}^2 + \bar{w}^2}{2} \tag{7}$$

and the usual expressions for the mean and fluctuating parts of the dependent variables are used; e.g.,

$$\rho = \bar{\rho} + \rho' \tag{8}$$

Implicit in Vaglio-Laurin's derivation of the above equations are the following stipulations:

    a.   The rates of change of the mean-flow properties in the x- and z-directions $[\mathcal{O}(1)]$ are smaller than the rates of change in the y-direction $[\mathcal{O}(\delta^{-1})]$ by an order of magnitude.

    b.   Mean squares and products of the turbulent fluctuations are $\mathcal{O}(\delta)$; that is, the turbulent level is small. The terms involving mean squares of the velocity fluctuations are taken to be negligible, which is valid for high Reynolds number flows with a zero or favorable pressure gradient.

    c.   The time-average molecular transports are approximated by those pertaining to the mean flow properties; indeed, even the latter are negligible, except very near the wall, compared with terms involving the turbulent transports.

Also implicit in the above equations is the requirement of an infinite extent body of the yawed cylinder or yawed wing type, which leads to the term $\partial/\partial z = 0$ as discussed in Section I.

3

If subscript w denotes wall and subscript e denotes outer edge of the boundary layer, the associated boundary conditions on the above defined equations are

MOMENTUM

$$y = 0: \bar{u} = \bar{v} = \bar{w} = \overline{u'v'} = \overline{v'w'} = \overline{\rho'v'} = 0$$

$$\text{as } y \to \infty : \bar{u} \to U_e, \bar{w} \to W_e$$

$$\overline{u'v'} \to 0, \overline{v'w'} \to 0, \overline{\rho'v'} \to 0 \tag{9}$$

ENERGY

$$y = 0: \bar{H} = H_w = h_w, \overline{v'H'} = 0 \quad \text{(Prescribed Wall Enthalpy)}$$

$$y = 0: \frac{\partial \bar{H}}{\partial y} = \frac{\partial \bar{h}}{\partial y} = 0, \overline{v'H'} = 0 \text{ (Adiabatic Wall)}$$

$$\text{as } y \to \infty: \bar{H} \to H_e, \overline{v'H'} \to 0 \tag{10}$$

which reflect the requirements of no slip and no mass transfer (suction or blowing) at the wall, as well as a prescribed wall enthalpy or an adiabatic wall. The y-momentum equation (3) reveals that the static pressure variation across the boundary layer is negligible, and hence the static pressure, $\bar{p}(x)$, is regarded as an external input to the boundary-layer analysis from a separate inviscid analysis. The outer edge velocities, U_e and W_e, as well as the outer-edge static enthalpy, h_e, must be determined from the inviscid analysis consistent with the imposed static pressure distribution.

The gas model adopted for the present study is thermally and calorically perfect air having a constant specific heat ratio $\gamma = 1.40$ and obeying the equation of state

$$\bar{p} = \bar{\rho} R \bar{T} \tag{11}$$

where R = 1716 ft^2/sec^2-°R. Under this assumption the static enthalpy, $\bar{h}$, is given by

$$\bar{h} = C_p \bar{T} \tag{12}$$

where C_p = 6006 ft^2/sec^2-°R. The laminar viscosity, μ, is taken to

4

obey Sutherland's law

$$\mu = \frac{2.270 \times 10^{-8} \; T^{3/2}}{T + 198.6} \; \frac{\text{lbf-sec}}{\text{ft}^2} \tag{13}$$

where T must have units of °R. The laminar Prandtl number, Pr, is taken to be a constant value of 0.71 across the entire boundary layer: i.e.,

$$Pr = 0.71 \tag{14}$$

2.3 TURBULENT TRANSPORT MODEL

Before Eqs. (1), (2), (4), and (5) can be solved, expressions must be supplied for the Reynolds stress or turbulent shear terms in the momentum equations and the turbulent flux of total enthalpy in the energy equation. The approach used in the present analysis is to model these terms as functions of the mean-flow variables following Adams (Refs. 13, 14, and 15), whose studies are based on the original analysis by Hunt, Bushnell, and Beckwith (Ref. 11).

The concept that the Reynolds stress in turbulent flow is proportional to a momentum exchange coefficient times the mean-flow velocity gradient normal to the surface is well known and commonly used in turbulent boundary-layer analyses. This concept is based on an assumed analogy between the so-called eddy viscosity and the molecular viscosity. The total shear components in the x- and z-directions are written as

$$\tau_x = \mu \frac{\partial \overline{u}}{\partial y} - \overline{\rho \, u'v'} = \mu \frac{\partial \overline{u}}{\partial y} + \epsilon_x \frac{\partial \overline{u}}{\partial y} \tag{15}$$

$$\tau_z = \mu \frac{\partial \overline{w}}{\partial y} - \overline{\rho \, v'w'} = \mu \frac{\partial \overline{w}}{\partial y} + \epsilon_z \frac{\partial \overline{w}}{\partial y} \tag{16}$$

where the eddy viscosities ϵ_x and ϵ_z might, in general, be different. Applying the Prandtl mixing-length hypothesis in conjunction with the assumption that the eddy viscosity is a scalar function independent of coordinate direction (which means physically that the turbulent shear stress acts in the mean rate of strain direction) results in an eddy viscosity relationship of the form

$$\epsilon = \epsilon_x = \epsilon_z = \overline{\rho} \ell_*^2 \frac{\partial \overline{G}}{\partial y} \tag{17}$$

5

where G is a scalar velocity function defined by

$$\frac{\partial \bar{G}}{\partial y} = \left[\left(\frac{\partial \bar{u}}{\partial y}\right)^2 + \left(\frac{\partial \bar{w}}{\partial y}\right)^2\right]^{1/2} \tag{18}$$

The quantity ℓ_* is termed the mxing length and is some characteristic length related to the size or scales of eddies responsible for the flux of momentum in the y-direction. Under the above model the turbulent shear stress in a three-dimensional turbulent boundary layer may be written in the form

$$\tau_{turb} = \bar{\rho}\ell_*^2\left[\left(\frac{\partial \bar{u}}{\partial y}\right)^2 + \left(\frac{\partial \bar{w}}{\partial y}\right)^2\right] \tag{19}$$

The complete derivation of Eqs. (17), (18), and (19) is given in Refs. 13, 14, and 15.

The expression for the total heat flux in a turbulent boundary layer may be written in terms of the static enthalpy as

$$\dot{q} = \frac{k}{C_p}\frac{\partial \bar{h}}{\partial y} - \bar{\rho}\,\overline{v'h'} = \frac{k}{C_p}\frac{\partial \bar{h}}{\partial y} + \frac{\kappa}{C_p}\frac{\partial \bar{h}}{\partial y} \tag{20}$$

where k is the laminar (molecular) thermal conductivity and κ is the so-called eddy thermal conductivity. Using the definition of the laminar (molecular) Prandtl number

$$Pr = \frac{C_p\mu}{k} \tag{21}$$

and defining, by analogy, a turbulent Prandtl number (based on the use of static enthalpy) as

$$Pr_t = \frac{C_p\epsilon}{\kappa} \tag{22}$$

with ϵ the eddy viscosity discussed previously, the total heat flux expression, Eq. (20), may be written in the form

$$\dot{q} = \mu\left[\frac{1}{Pr} + \frac{\epsilon}{\mu}\frac{1}{Pr_t}\right]\frac{\partial \bar{h}}{\partial y} \tag{23}$$

6

2.4 MIXING-LENGTH MODEL

The turbulent shear stress in a three-dimensional turbulent boundary layer as governed by Eq. (19) is treated herein by the use of a two-layer inner-outer model using Prandtl's mixing-length hypothesis and a modification of van Driest's analysis for the near-wall region. This results in a continuous distribution of the shear stress from the laminar value at the wall, through the fully turbulent region, reaching zero at the outer edge of the boundary layer. The energy transport in a turbulent boundary layer is treated in this work through the incorporation of the eddy conductivity, κ, into the turbulent Prandtl number, Pr_t.

In the manner of Escudier (Ref. 16), Patankar and Spalding (Ref. 17) recommend the following variation of the mixing length, ℓ_*, across the turbulent two-dimensional boundary layer which is adopted for the present three-dimensional case by noting that the scalar properties of a turbulence field are unlikely to be affected by moderate three-dimensionality because turbulence is inherently three-dimensional in nature for even so-called two-dimensional flows:

$$\ell_* = k_* y, \text{ for } 0 < y \leq \lambda y_\ell / k_*$$

$$\ell_* = \lambda y_\ell, \text{ for } \lambda y_\ell / k_* < y \tag{24}$$

where the values for the various numerical constants are taken to be $k_* = 0.435$ and $\lambda = 0.09$. The value of y at the point where the velocity in the boundary layer is equal to 0.99 of the velocity at the boundary-layer outer edge is used to define the distance y_ℓ; i.e.,

$$y_\ell = \left\{ y\text{-value where } \frac{[(\bar{u})^2 + (\bar{w})^2]^{1/2}}{[(U_e)^2 + (W_e)^2]^{1/2}} = 0.99 \right\} \tag{25}$$

By analogy with Stokes' solution for an infinite flat plate undergoing simple harmonic motion parallel to itself in an infinite fluid, van Driest (Ref. 18) concluded that in the vicinity of a wall the total shear stress in a turbulent two-dimensional fluid should be of the form

$$\tau = \mu \frac{\partial \bar{u}}{\partial y} + \bar{\rho} k_*^2 y^2 \left[1 - \exp\left(\frac{-y\sqrt{\tau_w \bar{\rho}}}{\mu A_*} \right) \right]^2 \left(\frac{\partial \bar{u}}{\partial y} \right)^2 \tag{26}$$

7

which results in an exponential damping of the turbulent part of the shear stress as the wall is approached and yields exactly the laminar shear stress form, $\tau = \mu(\partial \bar{u}/\partial y)$, at the wall. Although Eq. (26) was originally developed for incompressible flow, it can be applied to compressible flow by application of the suggestion by Patankar and Spalding (Ref. 17) that the <u>local</u> value of shear stress be used instead of the wall value as originally recommended by van Driest (Ref. 18). Hence, by analogy of Eq. (26) with Eqs. (18) and (19), the relationship for the three-dimensional near-wall shear stress as used in the present analysis is

$$\tau = \mu \frac{\partial \bar{G}}{\partial y} + \bar{\rho} \, k_*^2 y^2 \left[1 - \exp\left(\frac{-y\sqrt{\tau\bar{\rho}}}{\mu A_*} \right) \right]^2 \left(\frac{\partial \bar{G}}{\partial y} \right)^2 \tag{27}$$

where the constant A_* is taken to be 26.0 following the original van Driest proposal (Ref. 18). Note that the damping term in Eq. (27) reflects the application of the <u>local</u> <u>total</u> shear stress as opposed to the wall shear stress of Eq. (26), as discussed previously.

Based on Eqs. (17), (18), (24), and (27), the eddy viscosity expression for the inner region is

$$\epsilon_i = \bar{\rho} k_*^2 y^2 \left[1 - \exp\left(\frac{-y\sqrt{\tau\bar{\rho}}}{\mu A_*} \right) \right]^2 \frac{\partial \bar{G}}{\partial y} \tag{28}$$

and for the outer region is

$$\epsilon_o = \bar{\rho} \lambda^2 y_\ell^2 \frac{\partial \bar{G}}{\partial y} \tag{29}$$

with the constants k_*, A_*, λ, and y_ℓ defined previously. The constraint used to define the end of the inner region and the beginning of the outer region is the continuity of the eddy viscosity. From the wall outward, the expression for the inner eddy viscosity applies until $\epsilon_i = \epsilon_o$, from which point the outer eddy viscosity is used. A schematic of this variation in terms of the mixing length follows.
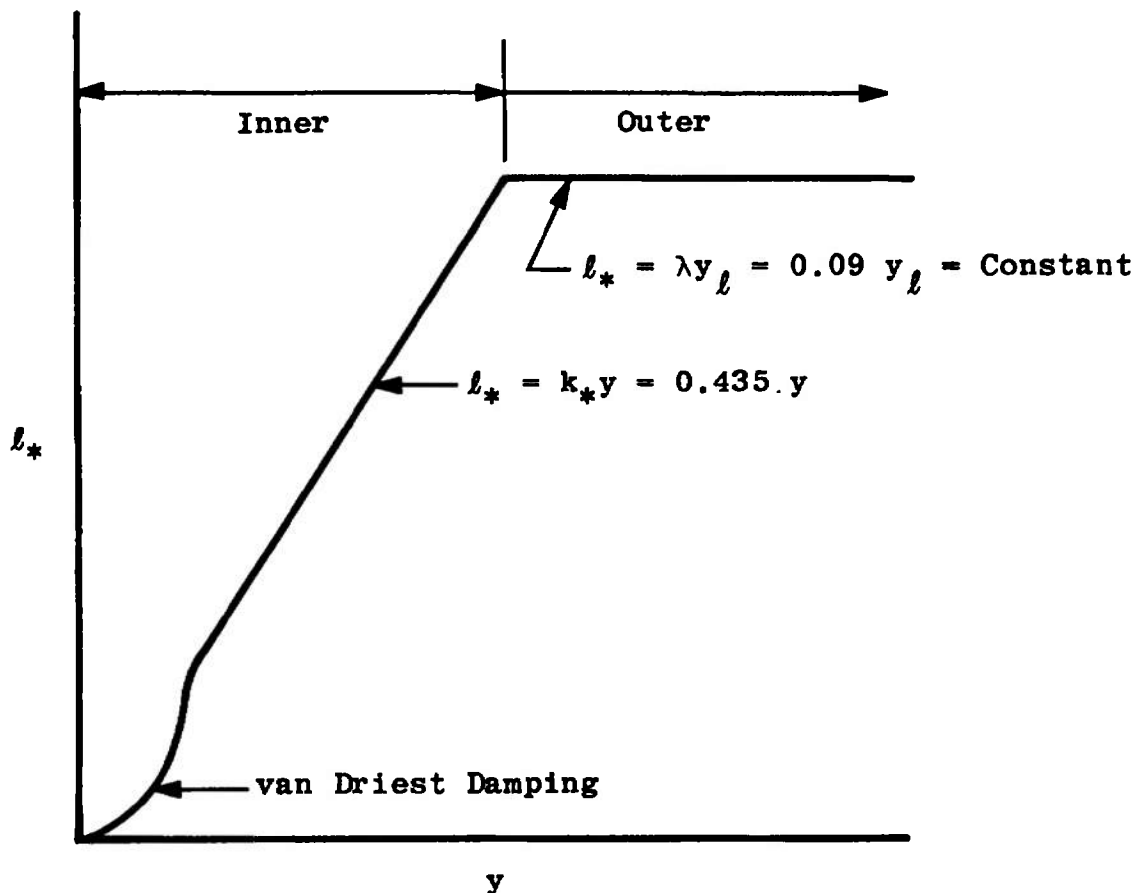
The turbulent Prandtl number (based on the static enthalpy defini-
tion of the turbulent heat flux) as given by Eq. (22) is physically a meas-
ure of the ratio of the turbulent transport of momentum to the turbulent
transport of heat. For the present work, the turbulent Prandtl number
defined by Eq. (22) is taken to remain constant at the value 0.90 across
the entire boundary layer as recommended by Patankar and Spalding
(Ref. 17) for two-dimensional turbulent boundary layers.

For the case of purely laminar flow in the present analysis, the
inner and outer eddy viscosities defined by Eqs. (28) and (29) are both
set identically equal to zero so that the governing turbulent boundary-
layer equations reduce to their laminar counterpart.

9

2.5 ALTERNATE FORM OF ENERGY EQUATION

To apply the eddy viscosity-eddy thermal conductivity model discussed above to the present work, the energy equation (5) must be rewritten to replace the total turbulent energy flux $\bar{\rho}\,\overline{v'H'}$ in terms of static quantities. By following the steps outlined on pages 176-183 in Dorrance (Ref. 19), one can see that the energy equation (5) may be written in the equivalent form

$$\bar{\rho}\,\bar{u}\frac{\partial\bar{H}}{\partial x} + \bar{\rho}\,\bar{V}\frac{\partial\bar{H}}{\partial y} + \bar{\rho}\,\bar{w}\frac{\partial\bar{H}}{\partial z} = \frac{\partial}{\partial y}\left\{\frac{\mu}{Pr}\left(1+\frac{\epsilon}{\mu}\frac{Pr}{Pr_t}\right)\frac{\partial\bar{H}}{\partial y}\right.$$
$$\left.+ \mu\left[\frac{Pr-1}{Pr}+\frac{\epsilon}{\mu}\frac{Pr_t-1}{Pr_t}\right]\left[\bar{u}\frac{\partial\bar{u}}{\partial y}+\bar{w}\frac{\partial\bar{w}}{\partial y}\right]\right\} \quad (30)$$

based on the definitions of the scalar eddy viscosity and the turbulent Prandtl number given in Section 2.3 of the present report. Equation (30) is to be regarded as the three-dimensional analog of Eq. (7-31) on page 182 in Dorrance (Ref. 19) for a two-dimensional turbulent boundary layer. Implicit in the derivation of Eq. (30) is the neglect of terms involving mean squares of the velocity fluctuations, which is consistent with Vaglio-Laurin's derivation of the governing equations as discussed previously in Section 2.2.

2.6 COORDINATE TRANSFORMATION

To facilitate numerical integration of the governing boundary-layer equations (1), (2), (4), and (30), it is convenient to transform them to a coordinate system that removes the mathematical singularity at x = 0 and stretches the coordinate normal to the surface, as is usually done in two-dimensional laminar flow analyses. The coordinate transformation used in the present work is the well-known Illingworth-Levy (Ref. 19, p. 30) transformation. The new independent variables introduced are

$$\xi(x) = \int_0^x \rho_e\mu_e U_e dx \quad (31)$$

$$\eta(x,y) = \frac{\rho_e U_e}{\sqrt{2\xi}}\int_0^y \frac{\bar{\rho}}{\rho_e}\,dy \quad (32)$$

10

so that the transformed streamwise and normal derivatives become

$$\frac{\partial}{\partial x} = \rho_e \mu_e U_e \frac{\partial}{\partial \xi} + \frac{\partial \eta}{\partial x} \frac{\partial}{\partial \eta} \tag{33}$$

$$\frac{\partial}{\partial y} = \frac{\bar{\rho} U_e}{\sqrt{2\xi}} \frac{\partial}{\partial \eta} \tag{34}$$

Define a so-called stream function, $\psi(x, y)$, in such a manner as to identically satisfy the continuity equation (1); i.e.,

$$\overline{\rho u} = \frac{\partial \psi}{\partial y} \tag{35}$$

$$\bar{\rho} v = -\frac{\partial \psi}{\partial x} \tag{36}$$

and introduce a nondimensional stream function $f(\xi, \eta)$ such that

$$\psi(\xi,\eta) = \sqrt{2\xi} \, f(\xi,\eta) \tag{37}$$

so that the governing boundary-layer equations (2), (4), and (30) become, in the transformed (ξ, η) coordinates:

x-MOMENTUM

$$(\ell^* f'')' + ff'' + \beta[\theta - (f')^2] = 2\xi \left[f' \frac{\partial f'}{\partial \xi} - f'' \frac{\partial f}{\partial \xi} \right] \tag{38}$$

z-MOMENTUM

$$(\ell^* c')' + fc' = 2\xi \left[f' \frac{\partial c}{\partial \xi} - c' \frac{\partial f}{\partial \xi} \right] \tag{39}$$

ENERGY

$$\left(\frac{\ell^{*}}{Pr} g \right)' + fg' + \Omega' = 2\xi \left[f' \frac{\partial g}{\partial \xi} - g' \frac{\partial f}{\partial \xi} \right] \tag{40}$$

with the new dependent variables

$$f'(\xi,\eta) = \frac{\bar{u}}{U_e} \tag{41}$$

11

$$c\,(\xi,\eta) \;=\; \frac{\overline{w}}{w_e} \tag{42}$$

$$g\,(\xi,\eta) \;=\; \frac{\overline{H}}{H_e} \tag{43}$$

The following definitions apply to the above equations:

$$\theta \;=\; \frac{\rho_e}{\overline{\rho}} \;=\; \frac{\overline{T}}{T_e} \tag{44}$$

$$\ell \;=\; \frac{\overline{\rho}\,\overline{\mu}}{\rho_e \mu_e} \tag{45}$$

$$\ell^* \;=\; \ell\Big[1 + \frac{\epsilon}{\mu}\Big] \tag{46}$$

$$\ell^{**} \;=\; \ell\Big[1 + \frac{\epsilon}{\mu}\frac{Pr}{Pr_t}\Big] \tag{47}$$

$$\beta_1 \;=\; \frac{2\xi}{U_e}\frac{d\,U_e}{d\xi} \tag{48}$$

$$\Omega \;=\; \ell\Big[\frac{\epsilon}{\mu}\big(1 - \frac{1}{Pr_t}\big) + \big(1 - \frac{1}{Pr}\big)\Big]\Big[\frac{U_e^2}{H_e}\,f'f'' + \frac{w_e^2}{H_e}\,cc'\Big] \tag{49}$$

where the inviscid x-momentum equation evaluated on the body surface,

$$\frac{d\overline{p}}{dx} + \rho_e U_e \frac{d\,U_e}{dx} \;=\; 0 \tag{50}$$

has been used to relate the inviscid velocity, U_e, to the imposed inviscid static pressure, $\overline{p}$. In the transformed governing equations, primes denote partial differentiation with respect to the η-coordinate; i.e.,

$$\left.\begin{array}{l} f' = \dfrac{\partial f}{\partial \eta} \\[2mm] f'' = \dfrac{\partial^2 f}{\partial \eta^2} \end{array}\right\} \tag{51}$$

An expression for the static temperature ratio, θ, of Eq. (44) can be found by application of Eq. (7) to yield

$$\theta = \frac{\overline{T}}{T_e} = \frac{\overline{h}}{h_e} = \frac{\overline{H} - \left(\frac{\overline{u}^2 + \overline{w}^2}{2}\right)}{h_e} \tag{52}$$

which, using Eqs. (41), (42), and (43), can be written in the form

$$\theta = \frac{H_e}{h_e} g - \frac{1}{2}\left[\frac{U_e^2}{h_e}(f')^2 + \frac{W_e^2}{h_e}(c)^2\right] \tag{53}$$

The physical boundary conditions given by Eqs. (9) and (10) become, in terms of the transformed variables,

MOMENTUM

$$\left.\begin{array}{l} f(\xi,\eta = 0) = 0 \\[2mm] f'(\xi,\eta = 0) = 0 \\[2mm] c(\xi,\eta = 0) = 0 \\[2mm] \lim_{\eta \to \infty} f'(\xi,\eta) = 1 \\[2mm] \lim_{\eta \to \infty} c(\xi,\eta) = 1 \end{array}\right\} \tag{54}$$

ENERGY

$$\left.\begin{array}{ll} g(\xi,\eta = 0) = \dfrac{H_w}{H_e} = \dfrac{h_w}{H_e} = g_w & \text{(Prescribed Wall Enthalpy)} \\[3mm] g'(\xi,\eta = 0) = 0 & \text{(Adiabatic Wall)} \\[3mm] \lim_{\eta \to \infty} g(\xi,\eta) = 1 & \end{array}\right\} \tag{55}$$

2.7 BOUNDARY-LAYER PARAMETERS

Given the numerical solution to the governing equations of motion (Eqs. (38), (39), and (40)) following the integration procedure of Appendix III, the associated local boundary-layer parameters at a given body

13

station may be determined as follows. The local convective heat flux at the body surface (y = 0) is given by the well-known Fourier law,

$$\dot{q}_w = -k_w \left(\frac{\partial \overline{T}}{\partial y} \right)_w = \frac{-k_w}{c_p} \left(\frac{\partial \overline{h}}{\partial y} \right)_w \tag{56}$$

which can be written in the equivalent form

$$\dot{q}_w = -\frac{\mu_w}{Pr} \left(\frac{\partial \overline{H}}{\partial y} \right)_w \tag{57}$$

making use of Eqs. (7) and (21) with

$$\left(\frac{\partial \overline{H}}{\partial y} \right)_w = \left(\frac{\partial \overline{h}}{\partial y} \right)_w + \left[\overset{\circ}{\cancel{\overline{u}}} \frac{\partial \overline{u}}{\partial y} + \overset{\circ}{\cancel{\overline{w}}} \frac{\partial \overline{w}}{\partial y} \right]_w \tag{58}$$

through application of $\overline{u}$ = 0 and $\overline{w}$ = 0 at the wall, as given by Eq. (9). In terms of the transformed (ξ, η) coordinates, Eq. (57) becomes

$$\dot{q}_w = \frac{-\ell_w \rho_e \mu_e U_e H_e}{Pr\sqrt{2\xi}} \ g'(\xi, \eta = 0) \tag{59}$$

where

$$\ell_w = \frac{\overline{\rho}_w \mu_w}{\rho_e \mu_e} \tag{60}$$

In a similar manner, the local wall shearing stress in the x- and z-directions may be written in terms of the transformed coordinates as

$$\tau_{w,x} = \mu_w \left(\frac{\partial \overline{u}}{\partial y} \right)_w = \frac{\ell_w \rho_e \mu_e U_e^2}{\sqrt{2\xi}} \ f''(\xi, \eta = 0) \tag{61}$$

$$\tau_{w,z} = \mu_w \left(\frac{\partial \overline{w}}{\partial y} \right)_w = \frac{\ell_w \rho_e \mu_e U_e W_e}{\sqrt{2\xi}} \ c'(\xi, \eta = 0) \tag{62}$$

Physical height in the boundary layer is determined from the y-transformation relationship, Eq. (34), as

$$y = \frac{\sqrt{2\xi}}{\rho_e U_e} \int_o^{\eta} \theta \, d\eta \tag{63}$$

For the case of three-dimensional boundary-layer flow, two lengths characterizing mass-flow defect may be defined in terms of the profiles of the two velocity components in the x- and z-directions

$$\delta_x^* = \int_o^{\infty} \left(1 - \frac{\overline{\rho}\,\overline{u}}{\rho_e U_e}\right) dy \tag{64}$$

$$\delta_z^* = \int_o^{\infty} \left(1 - \frac{\overline{\rho}\,\overline{w}}{\rho_e W_e}\right) dy \tag{65}$$

In terms of the transformed (ξ, η) coordinates, the above two mass-flow defect lengths may be written as

$$\delta_x^* = \frac{\sqrt{2\xi}}{\rho_e U_e} \int_o^{\infty} (\theta - f') \, d\eta \tag{66}$$

$$\delta_z^* = \frac{\sqrt{2\xi}}{\rho_e U_e} \int_o^{\infty} (\theta - c) \, d\eta \tag{67}$$

As shown by Moore (Ref. 20, p. 7), Eq. (64) is the proper definition of the boundary-layer displacement thickness for flow over an infinite extent yawed body (airfoil or cylinder); i.e., δ_x^* defined by Eq. (64) properly describes the extent to which the nonviscous flow is deflected by the boundary layer on an infinite yawed airfoil.

In a similar manner, the momentum thicknesses in the x- and z-directions may be written as

$$\theta_{m,x} = \int_o^{\infty} \frac{\overline{\rho}\,\overline{u}}{\rho_e U_e} \left(1 - \frac{\overline{u}}{U_e}\right) dy \tag{68}$$

$$= \frac{\sqrt{2\xi}}{\rho_e U_e} \int_o^{\infty} f'(1 - f') \, d\eta \tag{69}$$

15

and

$$\theta_{m,z} = \int_0^\infty \frac{\overline{\rho}\,\overline{w}}{\rho_e\,W_e}\left(1 - \frac{\overline{w}}{W_e}\right) dy$$

$$= \frac{\sqrt{2\xi}}{\rho_e\,U_e}\int_0^\infty c(1-c)\,d\eta \tag{70}$$

Along the stagnation or attachment line of a blunt-nosed infinite extent yawed airfoil where $\xi = 0$ since $x = 0$ (see Fig. 1 for clarification), the above equations reduce to the following limiting forms (under the restriction that $U_e \approx \left[\dfrac{d\,U_e}{dx}\right]_{x=0} x$ near $x = 0$ so that

$\xi \approx \dfrac{1}{2}\,\rho_e\,\mu_e\left[\dfrac{d\,U_e}{dx}\right]_{x=0} x^2$ near $x = 0$):

$$[\dot{q}_w]_{x=0} = \frac{-\ell_w\,H_e}{Pr}\sqrt{\rho_e\mu_e\left[\frac{d\,U_e}{dx}\right]_{x=0}}\;g'(\xi,\eta = 0) \tag{71}$$

$$[\tau_{w,x}]_{x=0} = 0$$

$$[\tau_{w,z}]_{x=0} = \ell_w\,\overline{W}_e\sqrt{\rho_e\mu_e\left[\frac{d\,U_e}{dx}\right]_{x=0}}\;c'(\xi,\eta = 0) \tag{72}$$

$$[y]_{x=0} = \sqrt{\frac{\mu_e}{\rho_e\left[\frac{d\,U_e}{dx}\right]_{x=0}}}\int_0^\eta \theta\,d\eta \tag{73}$$

$$[\delta_x^*]_{x=0} = \sqrt{\frac{\mu_e}{\rho_e\left[\frac{d\,U_e}{dx}\right]_{x=0}}}\int_0^\infty (\theta - f')\,d\eta \tag{74}$$

$$[\delta_z^*]_{x=0} = \sqrt{\frac{\mu_e}{\rho_e\left[\frac{d\,U_e}{dx}\right]_{x=0}}}\int_0^\infty (\theta - c)\,d\eta \tag{75}$$

$$[\theta_{m,x}]_{x=0} = \sqrt{\frac{\mu_e}{\rho_e\left[\frac{d\,U_e}{dx}\right]_{x=0}}}\int_0^\infty f'(1 - f')\,d\eta \tag{76}$$

16

$$[\theta_{m,z}]_{x=0} = \sqrt{\frac{\mu_e}{\rho_e\left[\dfrac{d\,U_e}{dx}\right]_{x=0}}} \int_0^\infty c(1-c)\,d\eta \qquad (77)$$

Furthermore, the pressure gradient parameter, β, defined by Eq. (48) assumes the value $\beta \equiv 1$ on the stagnation or attachment line under the above restriction on U_e and ξ near x = 0.

Various quantities of interest are defined as follows:

FREE-STREAM REYNOLDS NUMBER BASED ON CHORD LENGTH C

$$Re_{\infty,C} = \frac{\rho_\infty V_\infty C}{\mu_\infty} \qquad (78)$$

LOCAL UNIT REYNOLDS NUMBER BASED ON INVISCID
EDGE CONDITIONS

$$[Re_e/ft]_x = \frac{\rho_e U_e}{\mu_e} \qquad (79)$$

$$[Re_e/ft]_z = \frac{\rho_e W_e}{\mu_e} \qquad (80)$$

LOCAL MOMENTUM THICKNESS REYNOLDS NUMBER BASED ON
INVISCID EDGE CONDITIONS

$$Re_{e,\theta_{m,x}} = \frac{\rho_e U_e \theta_{m,x}}{\mu_e} \qquad (81)$$

$$Re_{e,\theta_{m,z}} = \frac{\rho_e W_e \theta_{m,z}}{\mu_e} \qquad (82)$$

FREE-STREAM MACH NUMBER

$$M_\infty = \frac{V_\infty}{\sqrt{\gamma R T_\infty}} \qquad (83)$$

LOCAL MACH NUMBER BASED ON INVISCID EDGE CONDITIONS

$$M_{e,x} = \frac{U_e}{\sqrt{\gamma R T_e}} \qquad (84)$$

17

$$M_{e,z} = \frac{W_e}{\sqrt{\gamma R T_e}} \tag{85}$$

LOCAL ANGULAR DIRECTION OF A STREAMLINE RELATIVE TO THE Z-AXIS DIRECTION

$$\omega = \arctan\left[\frac{U_e f'(\xi,\eta)}{W_e c(\xi,\eta)}\right] \tag{86}$$

which becomes at the outer edge

$$\omega_e = \arctan\left[\frac{U_e}{W_e}\right] \tag{87}$$

and at the body surface

$$\omega_s = \arctan\left[\frac{U_e f''(\xi,\eta=0)}{W_e c'(\xi,\eta=0)}\right] \tag{88}$$

LOCAL STANTON NUMBER BASED ON FREE-STREAM CONDITIONS

$$St_\infty = \frac{-\dot{q}_w}{\rho_\infty V_\infty C_p (T_{o,\infty} - T_w)} \tag{89}$$

LOCAL SKIN-FRICTION COEFFICIENT BASED ON FREE-STREAM CONDITIONS

$$C_{f_{\infty,x}} = \frac{\tau_{w,x}}{\frac{1}{2}\rho_\infty V_\infty^2} \tag{90}$$

$$C_{f_{\infty,z}} = \frac{\tau_{w,z}}{\frac{1}{2}\rho_\infty V_\infty^2} \tag{91}$$

LOCAL SKIN-FRICTION COEFFICIENT BASED ON INVISCID EDGE CONDITIONS

$$C_{f_{e,x}} = \frac{\tau_{w,x}}{\frac{1}{2}\rho_e U_e^2} \tag{92}$$

$$C_{f_{e,z}} = \frac{\tau_{w,z}}{\frac{1}{2}\rho_e W_e^2} \tag{93}$$

LOCAL BOUNDARY-LAYER SHAPE FACTOR

$$H_{f,x} = \frac{\delta_x^*}{\theta_{m,x}} \qquad (94)$$

$$H_{f,z} = \frac{\delta_z^*}{\theta_{m,z}} \qquad (95)$$

2.8 BOUNDARY-LAYER TRANSITION CORRELATION PARAMETERS

As discussed by Cumpsty and Head (Ref. 6) the attachment line flow on an infinite swept wing resembles fully developed pipe or channel flow much more closely than normal boundary-layer flow in that the attachment line boundary layer is constant in thickness (and indeed in all its properties) with downstream distance; see Fig. 3 for illustration. In particular, the attachment line boundary layer, be it laminar or turbulent, can be specified by the value of a single nondimensional parameter, C^*, defined as (see Ref. 5 for clarification)

$$C^* = \left(\frac{\rho_e W_e^2}{\mu_e \frac{dU_e}{dx}} \right)_{x=0} \qquad (96)$$

with the nomenclature defined as in Fig. 4.

The experimental work of Cumpsty and Head (Ref. 6) shows quite clearly that the attachment line laminar boundary layer appears very stable with respect to small disturbances. To produce a turbulent attachment line flow, there must be a sufficient disturbance and the parameter C^* must be large enough. Assuming a sufficient disturbance (for example, a tripping device such as a trip wire), the attachment line boundary layer has the properties of a fully turbulent flow for values of C^* greater than 1.4×10^5. Without external disturbance, the laminar attachment line boundary layer exhibits no instability characteristics for values of C^* as large as 3.7×10^5. Furthermore, at $C^* = 3.1 \times 10^5$ disturbances decay from a trip wire almost large enough to produce immediate transition to a fully turbulent flow. These results strongly suggest that, at large values of C^* in conjunction with a tripping device only slightly smaller than a "critical" size, the attachment line flow will revert to a laminar condition; for a tripping device just above the critical size there appears to be an immediate transition to

19

fully turbulent flow with the downstream flow essentially independent of the nature of the disturbance. The criterion proposed by Gaster (Ref. 21) appears applicable and accurate for estimating the critical size of the tripping device.

Assuming that the attachment line boundary layer has not been tripped as discussed above, natural transition will occur (under high Reynolds number conditions) at some downstream chordwise location because of the three-dimensional nature of the swept-wing boundary-layer flow. Briefly, three-dimensional crossflow has an adverse effect on laminar boundary-layer stability in that a system of stream-wise vortices contained within the boundary layer may be formed, apparently because of the inflection point in the rotated crossflow velocity profile illustrated in Fig. 5, which is unstable to small disturbances. This vortex formation apparently signals the onset to three-dimensional crossflow-induced transition of the boundary layer from laminar to turbulent flow. A complete discussion of this phenomenon relative to subsonic swept-wing flows may be found in a report by Owen and Randall (Ref. 22); supersonic flows have been examined by Chapman (Ref. 23) and hypersonic flows by Adams (Ref. 24). Application to hypersonic lifting bodies at incidence (such as the Space Shuttle) have been reported by Adams and Martindale (Ref. 25).

The exact location at which the above-discussed vortex system will originate cannot be determined from classical boundary-layer stability theory for three-dimensional flows such as that presented by Gregory, Stuart, and Walker (Ref. 26). Instead, the abrupt formation of these vortices and also the development of complete turbulence, i.e., transition, in a three-dimensional boundary layer can apparently be correlated with a so-called maximum local crossflow Reynolds number, x, defined (Refs. 22, 23, and 24) as

$$\chi = \frac{\rho_e \, \overline{w}_{s\ell,max} \, \delta}{\mu_e} \tag{97}$$

where $\overline{w}_{s\ell,max}$ is the maximum crossflow velocity in the streamline coordinates of Fig. 5, and δ is the boundary-layer thickness defined as the normal distance from the surface where the total resultant velocity

$$\sqrt{\overline{u}^2 + \overline{w}^2}$$

20

reaches 0.995 of the total resultant inviscid edge velocity

$$\sqrt{U_e{}^2 + W_e{}^2} \; ;$$

ρ_e and μ_e are the values of density and viscosity, respectively, evaluated at the inviscid edge conditions. Owen and Randall (Ref. 22) found the critical value of crossflow Reynolds number for vortex formation and for crossflow-induced transition to be 125 and 175, respectively, based on the leading edge of swept wings at subsonic speeds. The work by Chapman (Ref. 23) on swept cylinders at supersonic speeds (free-stream Mach numbers up to seven) indicates that

$$X < 100 \longrightarrow \text{Laminar Boundary Layer}$$
$$100 \lesssim X \lesssim 200 \longrightarrow \text{Vortex Formation and Transitional Boundary Layer}$$
$$X > 200 \longrightarrow \text{Turbulent Boundary Layer}$$

which means that the crossflow stability criterion of Owen and Randall may apparently be expected to apply without change on cylindrical leading edges for both subsonic and supersonic flows. Chapman's work further showed that the amount of crossflow needed to induce crossflow instability downstream of the leading edge was very small - on the order of one to five percent of the inviscid edge velocity for the conditions observed. This means physically that transition may occur extremely near the leading edge of a swept blunt-nosed airfoil because of the small amount of crossflow needed to cause crossflow-induced transition at small values of the local crossflow Reynolds number, X.

It should be noted that the above-discussed crossflow-induced transition phenomenon and stability criterion have been verified under subsonic flight conditions on various aircraft as discussed in the Appendix of Ref. 22.

2.9 NUMERICAL SOLUTION OF THE GOVERNING BOUNDARY-LAYER EQUATIONS

In the present study of infinite extent yawed airfoil boundary-layer flows, numerical solution of the governing nonlinear, parabolic, partial differential equations (Eqs. (38), (39), and (40)) is performed by obtaining linear finite-difference equivalents of the equations and solving these using an iterative, marching, implicit finite-difference integration technique involving inversion of tridiagonal matrices. Full details of this numerical approach are given in Appendix III.

The digital computer code is written in FORTRAN 63 for use on a CDC 1604-B digital computer. Solution time (including on-line input/ output) varies from approximately 30 minutes to one hour for an airfoil divided into 100 to 200 stations. The implicit nature of the present finite-difference approach has not presented any numerical stability problems.

With respect to application of this code, some operational details for various types of analyses are as follows. Given the inviscid flow field over the wing determined as in Section 2.10, one must choose the grid mesh (see Appendix III) and the type of wall boundary condition for the energy equation - adiabatic or prescribed surface temperature. For both subsonic and transonic calculations under either continuous wind tunnel or actual flight conditions, the adiabatic wall option is normally used since this is the physically correct boundary condition for this type of flow. However, the surface temperature can be assigned a constant value over the entire wing if one is interested in heat-transfer phenomena; an example of this type analysis will be given in Section 3.3 relative to Space Shuttle reentry applications. In the present report, unless otherwise specifically stated (as in Section 3.3), all calculations have been performed using an adiabatic-wall boundary condition.

2.10 INVISCID FLOW FIELD

The inviscid flow-field quantities needed for input to the present boundary-layer analysis (such as U_e, W_e, $\bar{p}$, etc.) are herein determined via application of classical sweep theory for sweptback wings (Ref. 27, pp. 415-416). Briefly, sweep theory applied to an infinite yawed wing having sweep angle Λ (see Figs. 1 and 2) is based upon the fact that the spanwise (z-direction) component of the free-stream flow, namely $V_\infty \sin \Lambda$, does not influence the pressure distribution on the wing; only the chordwise (x-direction) component, $V_\infty \cos \Lambda$, is significant for determination of the inviscid flow governing the surface pressure distribution. This means that well-established two-dimensional analysis techniques can be applied for determination of infinite yawed wing inviscid flow fields in the chordwise (x) direction. For subsonic (incompressible) flows, the surface pressure distribution on a specified NACA airfoil section can be derived from the tabular data presented in Appendix I of Abbott and von Doenhoff (Ref. 28). For transonic (compressible) flows, the surface pressure distribution on a specified airfoil section can be determined from transonic small-disturbance theory using the digital computer codes of Refs. 29, 30, 31, and 32 for

22

numerical solution (via relaxation procedures) of the transonic small-disturbance equation written in terms of the velocity potential. In either case, the airfoil ordinates for NACA airfoil sections can be obtained from tabulated values in the Appendixes of Ref. 28. An alternate approach for either subsonic or transonic conditions is an experimentally determined surface pressure distribution; such may require numerical smoothing before input since numerical differentiation of the pressure distribution is used to determine the local static pressure gradient which is one of the parameters required in the boundary-layer calculation.

With the surface pressure distribution determined from one of the above approaches, all inviscid surface quantities at any chordwise (x) location along the airfoil can be determined through application of an isentropic expansion from the stagnation or attachment line conditions to the desired x-location pressure. Constancy of total energy is used to determine the x-direction component of velocity, $U_e(x)$, knowing the value of the static temperature, $T_e(x)$, from an isentropic expansion and the fact that $W_e(x)$ remains constant at the value $W_e(x) = V_\infty \sin \Lambda$ from sweep theory. An alternate procedure useful for subsonic flows where the inviscid surface velocity in the x-direction, $U_e(x)$, is known (from Ref. 28, for example) is as follows: Knowing the local value of $U_e(x)$, as well as $W_e(x) = V_\infty \sin \Lambda$ from sweep theory, the local value of the static temperature, $T_e(x)$, can.be determined from constancy of total energy. The local static pressure can then be determined through application of an isentropic expansion from the stagnation or attachment line conditions to the local x-direction static temperature. These techniques comprise a subroutine for determination of the inviscid edge conditions required in the numerical solution of the boundary-layer equations via the digital computer code described in Section 2.9.

SECTION III
RESULTS AND DISCUSSION

Presentation of results from the present analysis technique for three-dimensional turbulent boundary-layer flow on infinite yawed bodies will be given in this section. Included are stagnation or attachment line flows as well as infinite extent yawed airfoils under both subsonic and transonic flow conditions. Comparisons with other analytical analyses and experimental measurements are presented in order to ascertain the validity and applicability of the current approach.

3.1 STAGNATION OR ATTACHMENT LINE FLOW

Certainly one of the simplest of all infinite yawed body flows is the classical yawed cylinder case, which is directly applicable to the stagnation or attachment line flow on a blunt-nosed infinite extent swept airfoil. Cumpsty and Head (Ref. 5) have considered this problem in detail for the case of subsonic (incompressible) turbulent attachment line flow on a blunt-nosed infinite extent swept wing. Their results can be expressed in terms of a single parameter, C^*, discussed previously in Section 2.8 and defined by Eq. (96) as

$$C^* = \left(\frac{\rho_e \bar{w}_e^2}{\mu_e \frac{dU_e}{dx}}\right)_{x=0}$$

with the nomenclature as in Fig. 4. Note that C^* may be considered as a stagnation or attachment line Reynolds number based solely on local inviscid conditions; all effects of sweep, leading-edge radius, and free-stream velocity are absorbed into the inviscid flow parameters.

Presented in Figs. 6, 7, and 8 are comparisons of stagnation or attachment line calculations using the present analysis technique relative to experimental measurements under subsonic flow conditions as reported by Cumpsty and Head (Ref. 6). In all three figures circles denote experimental measurements of the spanwise (z) direction boundary-layer flow with a 0.064-in.-diam trip wire wrapped around the leading edge about 18 in. from the upstream tip of the wing; the inverted triangles denote experimental measurements without the trip wire. As discussed previously in Section 2.8, the purpose of the trip wire is to provide a form of upstream disturbance necessary to produce a turbulent flow along the attachment line. Full details of the experimental measurement techniques may be found in Ref. 6.

The important point to observe from Figs. 6 and 7 is that there is no experimental evidence of any instability (i.e., tendency to undergo boundary-layer transition) for the attachment line flow without the trip wire. However, addition of the trip wire causes an almost instantaneous transition from laminar to fully turbulent flow for values of C^* greater than about 0.6×10^5 to 0.8×10^5. The present numerical calculations are in reasonable agreement with experiment for both laminar and turbulent flow conditions; in addition, the present calculations are in good agreement with the approximate integral-type approach by Cumpsty and Head (Ref. 5), as can be seen by comparing the results in Figs. 6 and 7 with Fig. 4 of Ref. 6. Further observe that the

24

present turbulent calculation procedure automatically reduces to a laminar flow calculation for small values of the C^* parameter (values of C^* less than about 0.2×10^5) with a sort of calculated transition region between C^* values of 0.2×10^5 and about 0.5×10^5. This interesting behavior can be directly traced to the fact that the present eddy viscosity model evaluated on the stagnation or attachment line is of the form

$$[\epsilon]_{x=0} \propto \sqrt{C^*}$$

as can be seen from consideration of Eqs. (28) or (29) evaluated at $x = 0$ using Eqs. (18), (33), and (73) as well as $\xi \approx 1/2 \, \rho_e \mu_e (dU_e/dx)_{x=0} \, x^2$ near $x = 0$.

A comparison of the spanwise (z-direction) local skin-friction coefficient on the stagnation or attachment line based on the present calculation technique is presented in Fig. 8 relative to the experimental measurements (via Preston tubes) reported in Fig. 6 of Cumpsty and Head (Ref. 6). The measurements are based upon Patel's Preston tube calibration using the two-dimensional law of the wall (see Ref. 6 for details). In addition, the measurements correspond to a tripped upstream flow such that the boundary layer should be fully turbulent at the measurement station location. In general, agreement of the present numerical calculation procedure with experiment is good; also shown in Fig. 8 for the sake of comparison is the so-called Method 3 calculation by Cumpsty and Head (Ref. 6). Note again the calculated transition region ($0.2 \times 10^5 < C^* < 0.5 \times 10^5$) between laminar and turbulent flow as shown near the top left-hand corner of Fig. 8.

All of the above-presented results are for the case of stagnation or attachment line boundary-layer flow on a blunt-nosed infinite extent swept wing under low subsonic conditions where the flow is essentially incompressible. To the author's knowledge there has been no work, either analytical or experimental, on the transonic stagnation or attachment line turbulent boundary-layer flow past an infinite extent swept wing or a yawed circular cylinder. Since compressibility effects become of importance under transonic conditions, it would be of great value to conduct a joint analytical/experimental investigation of transonic turbulent boundary layers on, say, yawed circular cylinders of varying sweep angle so as to assess the applicability of the C^* similarity parameter under nonsubsonic flow conditions.

3.2 INFINITE EXTENT YAWED AIRFOIL UNDER SUBSONIC CONDITIONS

The case of subsonic incompressible turbulent boundary-layer flow over an infinite yawed airfoil has been examined in many previous investigations; e. g., see Refs. 4, 7, 8, 9, and 10. The important finding from these studies is that quite small departures from the situation of the infinite swept wing can produce appreciable differences in boundary-layer parameters. This remarkable sensitivity appears to be directly traceable to small spanwise pressure gradients which invalidate the infinite yawed body assumption of zero spanwise gradients. The possibility of this occurrence must be kept in mind when one compares theory with experiment for so-called infinite yawed airfoil flows.

3.2.1 Comparison with Other Analytical Techniques

Both Nash (Ref. 8) and Bradshaw (Ref. 9) have developed numerical calculation techniques for the three-dimensional turbulent boundary layer on infinite swept wings based on a kinetic-energy-of-turbulence approach. Reasonable agreement with experiment has been reported for both methods. A more recent investigation by Nash and Tseng (Ref. 10) using the kinetic-energy-of-turbulence approach (in conjunction with the assumption that the turbulent shear stress acts in the direction of the mean rate of strain) is concerned with high Reynolds number incompressible flow over a 35-deg infinite swept wing having a symmetrical, 12-percent-thick NACA 65_1A012 airfoil section in the chordwise direction. Calculations were performed for the upper surface of the wing at two angles of incidence - corresponding to two-dimensional lift coefficients of 0. 15 and 0. 50 - and for two values of the free-stream chord Reynolds number, namely $Re_{\infty,C}$ = 6. 14 x 10^7, which corresponds to a full-scale condition for a large transport aircraft, and $Re_{\infty,C}$ = 0. 82 x 10^7, which corresponds to a typical wind tunnel scale for an aircraft model or to full scale for a helicopter rotor.

In order to assess the present calculation technique using an eddy viscosity approach relative to the kinetic-energy-of-turbulence analysis by Nash and Tseng (Ref. 10), turbulent boundary-layer calculations have been performed for the upper surface of the above-described NACA 65_1A012 airfoil at 35-deg sweep with a sectional lift coefficient of 0. 50 and a free-stream chord Reynolds number of $Re_{\infty,C}$ = 6. 14 x 10^7. The inviscid flow field is determined as in Section 2. 10 in the present report (i.e., surface pressure distribution is derived from simple sweep theory using the two-dimensional, potential-flow velocity distribution

26

tabulated on p. 370 of Ref. 28). A plot of the resulting inviscid surface velocity distribution may be found in Fig. 2 of Nash and Tseng (Ref. 10); this figure shows an adverse pressure gradient over almost the entire airfoil with only the leading-edge region in a favorable pressure gradient. In order to be consistent with the analysis by Nash and Tseng (Ref. 10), the leading edge of the airfoil is herein taken to be turbulent.

As shown in Fig. 9, agreement between the present infinite yawed wing calculation, based on a scalar eddy viscosity model of turbulence, and the more elaborate kinetic-energy-of-turbulence analysis of Nash and Tseng (Ref. 10) is excellent. Recall from Section 2.7 that it is the chordwise (x-direction) component of the displacement thickness, δ_x^*, which has physical meaning for infinite yawed wing flows, which explains the choice of δ_x^* for comparison in Fig. 9. Another important point is that the present analysis technique actually integrates the governing turbulent boundary-layer equations in the near-wall region using the van Driest modification of the eddy viscosity; Nash and Tseng (Ref. 10) match their outer numerical solution onto an inner-layer solution which takes the form of some variation of the universal inner law. As discussed by Nash in Ref. 33, a generalized version of Townsend's inner law (Ref. 34) is used with modifications which permit departures from collateral flow through the inner layer as well as small deviations from the strict linearity of the variation of shear stress with normal distance from the wall. It is believed that the small discrepancy in both chordwise and spanwise skin-friction coefficients presented in Fig. 9 may be a function of the assumed inner law for the Nash and Tseng analysis.

Further comparison of the present scalar eddy viscosity approach relative to the Nash and Tseng kinetic-energy-of-turbulence analysis is given in Fig. 10 relative to the surface streamline direction, ω_s, as defined in Fig. 2. Agreement between the two methods is excellent, with the choice of the inner law as discussed in the previous paragraph being of importance relative to the Nash and Tseng results. Note from Fig. 10 that the three-dimensional turbulent boundary layer is nearly collateral with the inviscid outer-edge flow over the forward half of the wing; this correspondence is caused by the extreme thinness of the high Reynolds number turbulent boundary layer in this region. Over the rear of the wing, as the boundary layer becomes thicker due to its upstream growth, the adverse pressure gradient causes a rapid increase in boundary-layer crossflow, which is reflected as an increasing difference between the surface and outer-edge streamline angles in Fig. 10.

The most favorable comparisons presented above indicate that the current scalar eddy viscosity model of three-dimensional turbulent boundary-layer flow over an infinite yawed wing yields almost identical results to the three-dimensional kinetic-energy-of-turbulence analysis by Nash (Refs. 8 and 33) as applied in Nash and Tseng (Ref. 10). Hence it must be concluded that the present scalar eddy viscosity model employing a mixing-length hypothesis and the kinetic-energy-of-turbulence hypothesis (Refs. 8, 9, 10, and 33) are equally satisfactory for numerical calculation of infinite yawed wing turbulent boundary-layer flows under adverse pressure gradient situations which are of interest for transport aircraft applications. Similar conclusions have been reached by Sivasegaram and Whitelaw (Ref. 35), who compared the Patankar-Spalding mixing-length approach (Ref. 17) to the Bradshaw-Ferriss-Atwell kinetic-energy-of-turbulence approach (Ref. 36) for the case of two-dimensional supersonic turbulent boundary layers in favorable, zero, and adverse pressure gradient flows both with and without heat-transfer effects.

3.2.2 Comparison with Experiment

Probably the most complete and best-documented set of experimental data for subsonic flow over an infinite yawed airfoil is that reported by Altman and Hayter (Ref. 37) some twenty years ago. This experimental investigation was conducted in the Ames Aeronautical Laboratory 7- by 10-ft subsonic wind tunnel using both swept and unswept NACA 63_1-012 section airfoils. The unswept wing, having a chord of 4 ft, was mounted vertically and spanned the 7-ft dimension of the wind tunnel (see Fig. 2 of Ref. 37 for clarification). The swept wing, having a sweep angle of 45 deg and a chord of 2.5 ft perpendicular to the leading edge, was mounted horizontally and spanned the 10-ft dimension of the wind tunnel (see Fig. 3 of Ref. 37 for clarification). Detailed boundary-layer velocity profiles were measured along the mid-span section at 30, 40, 50, 60, 70, 80, and 90 percent of the stream-wise chord on both wings. In addition, the flow direction within the boundary layer was determined for the swept wing. These measurements were made for section lift coefficients of 0, 0.32, 0.46, 0.74, and 1.00 based on the component of velocity normal to the leading edge. In conjunction with the above-described profile measurements, the distribution of surface pressure over both wings was also measured; for the swept wing the spanwise distribution of surface pressure was measured along constant-chord lines at 5, 15, 30, 50, and 80 percent of the chord. The tests of the swept wing were conducted at a dynamic pressure of 150 psf and those on the unswept wing at a dynamic pressure

28

of 29.5 psf. The free-stream Reynolds number based on the airfoil chord and the component of free-stream velocity normal to the leading edge was approximately 3.8×10^6 for both wings.

A comparison of experimental and theoretical chordwise pressure distributions on the upper surface of the NACA 63_1-012 airfoil at 45-deg sweep in presented in Fig. 11 for two values of the sectional lift coefficient, C_{L_u}, namely 0.0 and 0.74. The theoretical distribution is based upon application of classical sweep theory (as previously discussed in Section 2.10) using the surface velocity distribution tabulated in Table I, which is taken directly from p. 337 of Abbott and von Doenhoff (Ref. 28). As is obvious from Fig. 11, classical sweep theory is in excellent agreement with experiment over the entire airfoil for both values of the sectional lift coefficient. Further comparisons of sweep theory relative to experiment for the airfoil of current interest may be found in Ref. 38.

Before examining the three-dimensional turbulent boundary-layer results for the swept airfoil, it would be well to first ascertain the validity of the present analysis under two-dimensional conditions of zero sweep and zero lift. Presented in Fig. 12 is a comparison of calculated chordwise turbulent boundary-layer parameters (displacement thickness δ_x^*, momentum thickness $\theta_{m,x}$, and shape factor $H_{f,x}$) relative to experimental measurements for zero sweep and zero yaw as given in Fig. 7 of Ref. 37. Instantaneous transition from laminar to turbulent flow is taken to occur at 20 percent of the chord, which corresponds to the location of artifically induced (roughness) transition in the experiments of Ref. 37 under zero-lift conditions. Agreement between the present analysis technique and experiment is excellent for this two-dimensional condition. Further illustration of the applicability and validity of the present turbulent boundary-layer model may be seen in Fig. 13, which compares a calculated turbulent boundary-layer velocity profile with experimental probe measurements (see Fig. 6 of Ref. 37) for the 50-percent chord location on the zero sweep - zero yaw airfoil.

Turn now to three-dimensional flow situations. Figure 14 shows the calculated chordwise (x-direction) turbulent boundary-layer parameters (displacement thickness δ_x^*, momentum thickness $\theta_{m,x}$, and shape factor $H_{f,x}$) relative to experimental measurements as given in Fig. 7 of Ref. 37 for the case of 45-deg sweep and zero lift. Instantaneous transition from laminar to turbulent flow is taken to occur at 20-percent chord, which corresponds to the location of artifically induced

(roughness) transition in the experiments of Ref. 37 under zero-lift conditions. Agreement between the present analysis technique and experiment is excellent for this yawed wing at zero-lift flow. A comparison of calculated chordwise ($\bar{u}/U_e$) and spanwise ($\bar{w}/W_e$) turbulent boundary-layer velocity profiles at the 50-percent chord location is given in Fig. 15 relative to experimental measurements reported in Fig. 6 of Ref. 37 for the 45-deg sweep condition at zero lift. Note from Fig. 15 that the chordwise and spanwise velocity profiles are almost identical, which is a direct consequence of the almost constant surface pressure distribution between about 10-percent chord and the 50-percent chord location of present interest (see the C_{L_u} = 0.0 curve given in Fig. 11 for clarification).

A two-dimensional turbulent calculation in the chordwise direction would predict the chordwise components of the boundary-layer flow correctly if the so-called principle of independence held, as it does in the case of incompressible laminar boundary-layer flow over infinite yawed cylinders and wings. According to the principle of independence, the shear-stress component in a particular direction depends only on the resolved velocity profile in that direction. The failure of the principle of independence in the turbulent case has received wide coverage in the literature, and it is now well known that a chordwise two-dimensional calculation does not predict the correct behavior of the turbulent boundary layer on a yawed flat plate. (See pp. 54 through 56 of Ref. 39 for a good discussion of this point.) As can be seen from a review of Sections 2.3, 2.4, and 2.5 in the present report, the scalar eddy viscosity model of turbulence as used herein does not admit the principle of independence since, for example, the chordwise shear stress, τ_x, as given by Eq. (15) is a function of both the chordwise and spanwise velocity profiles through the eddy viscosity relationship given by Eqs. (17) and (18); the same is true for the spanwise shear stress, τ_z, given by Eq. (16). Practical examples illustrating the effects of sweep on the present airfoil at zero-lift flow situation are given in Figs. 16 and 17. Note from Fig. 16 that the influence of sweep (and hence three-dimensionality) is to increase the magnitude of the chordwise turbulent boundary-layer properties at a given chordwise location. Further observe from Fig. 17 that the influence of sweep is to increase the chordwise turbulent boundary-layer thickness at the 50-percent chord location. Similar findings have been reported by Ashkenas and Riddell (Ref. 40) for turbulent boundary-layer flow over yawed and unyawed flat plates.

As discussed previously in this section, the laminar boundary layer was tripped to turbulent flow at 20-percent chord location for both the yawed and the zero-yaw flows. This means that natural transition did not occur under the experimental flow conditions of present interest. Recall from Section 2.8 that natural boundary-layer transition on yawed wings appears to be governed by a three-dimensional crossflow instability phenomenon which can be correlated with a so-called maximum local crossflow Reynolds number, X, defined by Eq. (97); all of the work to date on crossflow-dominated natural transition indicates that

$$X < 100 \longrightarrow \text{Laminar Boundary Layer}$$

$$100 \leqq X \leqq 200 \longrightarrow \text{Vortex Formation and Transitional Boundary Layer}$$

$$X > 200 \longrightarrow \text{Turbulent Boundary Layer}$$

As shown in Fig. 18 the calculated crossflow Reynolds number, X, distribution for the present flow situation (NACA 63_1-012 airfoil at 45-deg sweep with $Re_{\infty,C} = 5.37 \times 10^6$) attains a maximum value of approximately 120 at a chordwise location of $X/C = 0.27$. As shown in the above discussion, crossflow-dominated natural transition should not occur on the present wing; this is in agreement with the experimental observations of Ref. 37. It should be further noted from Fig. 18 that the physical chordwise location of the artificial roughness used to promote boundary-layer transition coincides fairly closely with the chordwise location of maximum crossflow Reynolds number, X, where it is to be expected that the three-dimensional laminar boundary layer is most unstable with respect to external disturbances. The author believes that, generally, boundary-layer trips on yawed wings should be placed to correspond with the chordwise location of maximum crossflow Reynolds number, X, in order to promote effective tripping.

All of the above results and discussion have been for the zero-lift airfoil under both yawed and unyawed conditions. For transport aircraft applications the important area of interest to the aerodynamicist is the upper surface of swept lifting airfoils relative to adverse pressure gradient effects on the three-dimensional turbulent boundary layer. The present 45-deg sweep NACA 63_1-012 airfoil at angle of attack such that the sectional lift coefficient, C_{L_u}, equals 0.74 is an excellent example of this type of flow. Reference to Fig. 11 presented previously shows that the pressure gradient over the entire upper surface of the

airfoil is adverse with a particularly large gradient in the leading-edge region. Comparisons of calculated and experimental turbulent boundary-layer parameters (displacement thickness, δ^*, momentum thickness, θ_m, and shape factor, H_f) for both the chordwise (x-direction) and spanwise (z-direction) components of flow over the upper surface of the airfoil are given in Fig. 19. Boundary-layer transition from laminar to turbulent flow is taken to occur near the leading edge of the airfoil in accord with the experimental results of Ref. 37. As can be seen from Fig. 19, agreement between the present analysis technique and experiment is, in general, good over the entire airfoil with the largest discrepancy in the chordwise displacement thickness near the trailing edge. The chordwise and spanwise turbulent boundary-layer velocity profiles at the 50-percent chord location are presented in Fig. 20 for the current yawed lifting airfoil condition. The calculated spanwise velocity profile, $\bar{w}/W_e$, is in excellent agreement with experiment; the calculated chordwise velocity profile, $\bar{u}/U_e$, is somewhat different from the experimental profile in the near-wall region but is in excellent agreement near the outer edge of the boundary layer. Adverse pressure gradient effects on both the chordwise and spanwise turbulent boundary-layer velocity profiles become apparent upon examination of Figs. 21 and 22, which are for the 50-percent chord and trailing-edge locations, respectively, on the upper surface of the present lifting swept airfoil. The spanwise profile remains typical of a zero pressure gradient turbulent flow, whereas the chordwise profile clearly illustrates the retarding effects of the chordwise adverse pressure gradient. Corresponding calculated eddy viscosity distributions across the turbulent boundary layer at the above two locations (50- and 100-percent chord) are given in Fig. 23. Also indicated on this figure are inner and outer regions which correspond to the particular form of equation used for the eddy viscosity relationship, namely Eq. (28) for the inner region calculation and Eq. (29) for the outer region calculation. As is obvious from Fig. 23, the turbulence levels in the outer region of the boundary layer are quite large.

Comparisons of calculated streamline direction, ω, within the three-dimensional turbulent boundary layer at various chordwise locations on the upper surface of the above-discussed swept lifting airfoil are given in Fig. 24 relative to experimental measurements (via a directional rake) reported in Fig. 16 of Ref. 37. Agreement between the present analysis technique and experiment is reasonably good, with the largest discrepancy in the inner region of the boundary layer near the wall. This behavior can be traced directly to the difference between calculated and experimental chordwise (x-direction) velocity

distributions near the wall as discussed previously in connection with
Fig. 20. The physical reason for this near-wall disagreement may well
be the small spanwise pressure gradient over the swept lifting airfoil
under experimental conditions as discussed in Ref. 37. Recall from
the beginning of Section 3.2 that small spanwise pressure gradients can
cause large departures from the true infinite swept-wing situation, re-
sulting in appreciable differences relative to boundary-layer parameters.

3.3 INFINITE EXTENT YAWED AIRFOIL UNDER TRANSONIC CONDITIONS

To the author's knowledge the case of transonic compressible
boundary-layer flow over an infinite yawed airfoil has not been consid-
ered in any previous investigation, either analytical or experimental.
The recent report by Nash and Scruggs (Ref. 3) describes the calcula-
tion of the three-dimensional compressible turbulent boundary layer on
the supercritical finite swept wing of the NASA modified F8 transonic
research aircraft using the kinetic-energy-of-turbulence method of
Nash (Refs. 2, 8, and 33) extended to compressible flow via the Crocco
relationship for temperature (which restricts the analysis to adiabatic-
wall flows). No comparisons with experiment, either wind tunnel or
flight, are presented in Ref. 3 since such data are classified. This
particular area of transonic research is currently undergoing much ef-
fort for transonic transport applications and hence will not be further
considered in the present report. Instead, the following treatment of
hot-wall transonic boundary-layer flow will be pursued because of its
direct applicability to the design of ground test experiments for cor-
rect simulation of aerodynamic phenomena to be encountered during
transonic and subsonic flight of lifting entry vehicles such as the NASA
Space Shuttle.

With the advent of maneuverable reentry vehicles such as the Space
Shuttle, a new problem involving heat transfer from hot aerodynamic
surfaces has evolved. During entry into the atmosphere, the Shuttle
will be subjected to large heat loads which depend upon the geometric
configuration as well as the attitude of the vehicle during reentry.
Some of this entry heat load will inevitable soak into the structure and
aerodynamic surfaces. After the hypersonic reentry phase of the
flight, the Shuttle will slow to subsonic speeds and maneuver for a con-
ventional aircraft landing. It has been estimated (see Ref. 41) that the
Shuttle wings may reach soak temperatures on the order of 1000°R,
which is some 2.5 times the local free-stream stagnation temperature
under subsonic flight conditions. Thus, during the transonic

AEDC-TR-73-112

maneuvering and subsonic landing phase of Shuttle reentry, the heated
aerodynamic surfaces will be (literally) injecting heat into a high Rey-
nolds number turbulent boundary layer. The important question rela-
tive to transonic testing of Shuttle vehicles becomes, "What are the
aerodynamic effects of high rates of heat transfer from the surface to
a transonic, turbulent boundary layer, and must we simulate this hot-
wall environment in ground testing of Shuttle configurations?" Of par-
ticular interest is the effect of a hot wall on the three-dimensional
transonic turbulent boundary-layer which will be herein considered
through examination of infinite yawed airfoil flows. To the author's
knowledge, the present analysis technique is the only available method
which allows calculation of infinite yawed airfoil flows including flow
compressibility and surface heat-transfer effects. In this connection
the current method, slightly modified with respect to the inviscid flow-
field input to the boundary layer, has been applied under supersonic
and hypersonic conditions with excellent results. (See Ref. 25 for com-
plete documentation relative to Space Shuttle configurations.)

In order to provide some insight into the above-defined problem
area, to which little or no attention has been given in previous studies,
infinite yawed wing calculations based on the present analysis techni-
que have been performed for the upper surface of the Douglas Aircraft
Company (DAC) 30-deg-sweep airfoil given in Fig. 15 of Ref. 1. Free-
stream conditions used in the calculations are as follows:

$$M_\infty = 0.815$$

$$Re_{\infty,C} = 1.05 \times 10^8$$

$$T_{0,\infty} = 489°R, \quad T_\infty = 432°R$$

$$P_{0,\infty} = 325 \text{ psia}, \quad p_\infty = 210 \text{ psia}$$

$$C = 1.0 \text{ ft}$$

These values are representative of the proposed AEDC high Reynolds
number transonic tunnel (HIRT) as described in Ref. 42. The above-
defined free-stream Mach number/chord Reynolds number combination
is very close to actual flight values quoted in Fig. 3 of Ref. 43 for the
McDonnell Douglas Astronautics Company (MDAC) Shuttle Orbiter at
an altitude of 42,500 ft. In all of the calculated results to be presented
below, hot-wall (surface temperature of 1000°R) results typical of ac-
tual Shuttle entry conditions will be compared with adiabatic-wall results
since an adiabatic-wall condition represents conventional transonic test-
ing in continuous wind tunnels such as the AEDC Propulsion Wind Tun-
nel (16T) and Aerodynamic Wind Tunnel (4T).

Presented in Fig. 25 are the inviscid flow parameters over the up-
per surface of the DAC airfoil. As can be seen from the figure, the
chordwise (x-direction) inviscid flow is supercritical (local x-direction
Mach number exceeds the sonic or critical value), whereas the span-
wise (z-direction) inviscid flow remains subsonic throughout. For the
present study the chordwise inviscid supercritical flow is not allowed
to terminate via a shock wave but is forced to recompress smoothly
over the aft section of the airfoil with a continually increasing adverse
pressure gradient; this is done in order to assess the effects of con-
tinuous adverse pressure gradient on three-dimensional transonic tur-
bulent boundary-layer flow. Note in Fig. 25 that the airfoil chord
length is one foot, which is representative of allowable model size in
the proposed AEDC HIRT facility.

Figure 26 presents the calculated distribution for the ratio of the
adiabatic-wall temperature to the free-stream total temperature. Note
that this ratio ranges from 0.975 to 0.995 with a distribution which fol-
lows in trend the surface pressure distribution of the previous figure.
The hot-wall condition (T_W = 1000°R) yields a wall temperature ratio
($T_W/T_{O,\infty}$) of 2.043, which remains constant over the entire airfoil.

Figures 27 through 31 illustrate the results of the hot- (1000°R)
versus adiabatic-wall calculations of present interest. As can be seen
from Fig. 27, three-dimensional turbulent boundary-layer separation
(defined as the chordwise surface location where the surface flow angle,
ω_S, is identically zero following Refs. 39 and 44) occurs at 93-percent
chord for the hot-wall case and 99-percent chord for the adiabatic-wall
condition; note that over the entire aft half of the airfoil the adiabatic-
wall surface flow angle is always larger than the corresponding x-
location hot-wall value. The chordwise (x-direction) and spanwise (z-
direction) components of the three-dimensional turbulent skin-friction
coefficient are presented in Fig. 28, with the important point being
that the hot wall reduces the local x-direction skin friction by some 20
to 40 percent over the corresponding location x-direction adiabatic wall
value. Similarly, the z-direction hot-wall skin friction is reduced
some 20 to 25 percent over the entire airfoil as compared with the cor-
responding location z-direction adiabatic-wall value. Needless to say,
this significant decrease in local skin friction due to the heated wall
can result in appreciable reduction of integrated skin-friction drag on
the airfoil. The corresponding calculated three-dimensional turbulent
boundary-layer parameters (H_f, δ^*, θ_m) for both the x- and z-directions
are presented in Figs. 29 through 31. Note from Fig. 29 the sizable in-
crease in the shape factors $H_{f,x}$ and $H_{f,z}$ caused by the heated wall as

compared with the adiabatic wall. The reason for this behavior can be seen from Figs. 30 and 31 where, in general, the hot wall increases the displacement thicknesses δ_x^* and δ_z^* over the entire airfoil but decreases the momentum thicknesses $\theta_{m,x}$ and $\theta_{m,z}$ over the majority of the airfoil. Recalling from Section 2.7 that it is the x-direction displacement thickness, δ_x^*, which has physical meaning relative to infinite yawed wing boundary-layer interaction with the inviscid flow, Fig. 30 shows that the hot wall increases the magnitude of δ_x^* some 50 percent over the entire airfoil as compared with the corresponding x-location adiabatic-wall value.

The calculated surface heat-transfer rate as reflected through the Stanton number, St_∞, defined by Eq. (89) is given in Fig. 32 for the present hot-wall condition. As shown on the figure, the local heat flux, $\dot{q}_w$, is positive (denoting heat flow from the airfoil to the flow) while the wall temperature is greater than the stagnation temperature ($T_w/T_{0,\infty} = 2.043$) which together combine to yield a positive value for the Stanton number. Note the high rate of heat transfer in the leading-edge region with essentially a constant heat-transfer rate over the midsection of the airfoil and a decrease in the heating rate as the trailing edge is approached. Recall that three-dimensional boundary-layer separation occurred at 93-percent chord.

Hot-wall effects on the three-dimensional turbulent boundary-layer velocity and temperature profiles are illustrated in Figs. 33 and 34 relative to the adiabatic-wall results at a common chordwise location, namely 90-percent chord. This particular location is chosen to permit examination of turbulent boundary-layer structure having an upstream adverse pressure gradient history. As is obvious from Fig. 33, the hot wall tends to retard the chordwise velocity profile, $\bar{u}/U_e$, more than does the adiabatic wall; this results in earlier boundary-layer separation under hot-wall conditions, as noted earlier. The spanwise velocity profile, $\bar{w}/W_e$, is not strongly affected by the hot wall except in the near-wall region, where the van Driest damping term given by Eq. (27) becomes important. The most important hot-wall effects on turbulent boundary-layer structure are seen in Fig. 34 with respect to both the static temperature ratio, $\bar{T}/T_e$, and stagnation temperature ratio, $\bar{T}_0/T_{0,\infty}$. Due to the constancy of static pressure across the boundary layer, the static temperature ratio, $\bar{T}/T_e$, is the inverse of the static density ratio, $\bar{\rho}/\rho_e$, through the perfect gas equation of state, $\bar{p} = \bar{\rho}R\bar{T}$. Hence the hot-wall case under present examination results in appreciable density variation across the turbulent boundary layer as compared with the adiabatic-wall condition. This density variation

becomes directly reflected in the eddy viscosity distribution across the boundary layer as can be seen from Eqs. (28) and (29).

All of the above-presented results clearly indicate that hot-wall effects can indeed have a significant influence on transonic aerodynamics. The recent experimental investigation of Ref. 41 conducted in the Texas A & M University 7- by 10-ft subsonic wind tunnel using an electrically heated NACA 0012-64 airfoil reveals that both the maximum lift coefficient, $C_{L_{max}}$, and the stall angle of the airfoil, α_{stall}, are reduced as the wing-to-free-stream temperature ratio, T_w/T_∞, is increased under subsonic conditions; e.g.:

T_w/T_∞	$C_{L_{max}}$	α_{stall}
1.0	1.6	17.0
2.0	1.2	---
2.2	---	12.5

Hence, simulation of the hot wall/cold free-stream environment using electrically heated models appears necessary in ground testing under subsonic and transonic conditions for Space Shuttle applications, especially for aerodynamic drag and stall characteristics. More work, both analytical and experimental, is definitely needed to fully explore and understand this relatively new area of hot-wall subsonic and transonic aerodynamics for application to lifting bodies such as the Space Shuttle. Especially desirable for future studies are turbulent boundary-layer structure measurements in two- and three-dimensional subsonic and transonic flows under controlled hot-wall conditions.

SECTION IV
CONCLUDING SUMMARY

The present report has documented a three-dimensional compressible turbulent boundary-layer analysis applicable to yawed airfoil flows of infinite extent under subsonic and transonic conditions. The boundary-layer analysis has been based on implicit finite-difference integration of the governing infinite yawed body boundary-layer equations for turbulent flow using a scalar eddy viscosity model of three-dimensional turbulence. Comparisons with other analysis techniques

as well as experimental measurements under subsonic wind tunnel conditions have been presented to establish and ascertain the basic validity and applicability of the current technique for infinite yawed-wing flows.

Ground testing of Space Shuttle configurations under continuous transonic flow conditions with an adiabatic wall may not be totally applicable to actual Shuttle entry where the wing surface temperature may reach soak values on the order of twice the free-stream stagnation temperature because of the hypersonic high heating phase of the reentry trajectory. Numerical calculations presented in this report indicate an appreciable reduction of integrated skin-friction drag on a hot wall ($T_w/T_{0,\infty} \approx 2$) airfoil relative to the same airfoil under adiabatic wall conditions. Airfoil static stall angle and maximum lift coefficient, as well as turbulent boundary-layer parameters, are strongly affected by hot-wall relative to adiabatic-wall conditions. Hence, simulation of the hot wall/cold free-stream environment using electrically heated models appears necessary in ground testing under continuous subsonic and transonic wind tunnel conditions for Space Shuttle applications, especially for aerodynamic drag and stall characteristics determination.

The present work makes no attempt to address the problem of viscous-inviscid interactions at subsonic or transonic speeds. (The term viscous-inviscid interaction is taken here to embrace all flow situations in which the development of the boundary layer and wake has a significant effect on the pressure field.) An excellent discussion of this topic for the case of adiabatic-wall transonic flows may be found in Ref. 45.

REFERENCES

1. Kaups, K. and Keltner, G. "Laminar Compressible Boundary Layer on a Yawed Infinite Wing." Douglas Aircraft Company Report No. LB 32706, March 1967.

2. Hicks, J. G. and Nash, J. F. "The Calculation of Three-Dimensional Turbulent Boundary Layers on Helicopter Rotors." NASA CR-1845, May 1971.

3. Nash, J. F. and Scruggs, R. M. "Three-Dimensional Compressible Boundary-Layer Computations for a Finite Swept Wing." NASA CR-112158, 1972.

4. Cumpsty, N. A. and Head, M. R. "The Calculation of Three-Dimensional Turbulent Boundary Layers. Part I: Flow over the Rear of an Infinite Swept Wing." Aeronaut. Quart., Vol. 18, February 1967, pp. 55-84.

5. Cumpsty, N. A. and Head, M. R. "The Calculation of Three-Dimensional Turbulent Boundary Layers. Part II: Attachment-Line Flow on an Infinite Swept Wing." Aeronaut. Quart., Vol. 18, May 1967, pp. 150-164.

6. Cumpsty, N. A. and Head, M. R. "The Calculation of the Three-Dimensional Boundary Layer. Part III: Comparison of Attachment Line Calculations with Experiment." Aeronaut. Quart., Vol. 20, May 1969, pp. 99-113.

7. Cumpsty, N. A. and Head, M. R. "The Calculation of Three-Dimensional Turbulent Boundary Layers. Part IV: Comparison with Measurements on the Rear of a Swept Wing." Aeronaut. Quart., Vol. 21, May 1970, pp. 121-132.

8. Nash, J. F. "The Calculation of Three-Dimensional Turbulent Boundary Layers in Incompressible Flow." J. Fluid Mech., Vol. 37, Part 4, 1969, pp. 625-642.

9. Bradshaw, P. "Calculation of Three-Dimensional Turbulent Boundary Layers." J. Fluid Mech., Vol. 46, Part 3, 1971, pp. 417-445.

10. Nash, J. F. and Tseng, R. R. "The Three-Dimensional Turbulent Boundary Layer on an Infinite Yawed Wing." Aeronaut. Quart., Vol. 22, November 1971, pp. 346-362.

11. Hunt, J. L., Bushnell, D. M., and Beckwith, I. E. "The Compressible Turbulent Boundary Layer on a Blunt Swept Slab with and without Leading-Edge Blowing." NASA TN D-6203, March 1971.

12. Vaglio-Laurin, R. "Turbulent Heat Transfer on Blunt-Nosed Bodies in Two-Dimensional and General Three-Dimensional Hypersonic Flow." WADC Technical Note 58-301, September 1958. See also J. Aeron. Sci., Vol. 27, No. 1, January 1960, pp. 27-36.

13. Adams, J. C., Jr. "Implicit Finite-Difference Analysis of Compressible Laminar, Transitional, and Turbulent Boundary Layers along the Windward Streamline of a Sharp Cone at Incidence." AEDC-TR-71-235 (AD734535), December 1971.

14. Adams, J. C., Jr. "Finite-Difference Analysis of the Three-Dimensional Turbulent Boundary Layer on a Sharp Cone at Angle of Attack in a Supersonic Flow." AIAA Paper No. 72-186, presented at the AIAA 10th Aerospace Sciences Meeting, San Diego, California, January 1972.

15. Adams, J. C., Jr. "Analysis of the Three-Dimensional Compressible Turbulent Boundary Layer on a Sharp Cone at Incidence in Supersonic and Hypersonic Flow." AEDC-TR-72-66 (AD743003), June 1972.

16. Escudier, M. P. "The Distribution of the Mixing Length in Turbulent Flows Near Walls." Mechanical Eng. Dept. Report TWF/TN/1, Imperial College, London, March 1965.

17. Patankar, S. V. and Spalding, D. B. Heat and Mass Transfer in Boundary Layers. CRC Press, Cleveland, Ohio, 1968.

18. van Driest, E. R. "On Turbulent Flow Near a Wall." J. Aeron. Sci., Vol. 23, No. 11, November 1956, pp. 1007-1011, 1036.

19. Dorrance, W. H. Viscous Hypersonic Flow. McGraw-Hill, Inc., New York, 1962.

20. Moore, F. K. "Displacement Effect of a Three-Dimensional Boundary Layer." NACA TN 2722, June 1952.

21. Gaster, M. "On the Flow Along Swept Leading Edges." Aeronaut. Quart., Vol. 28, May 1967, pp. 165-184.

22. Owen, P. R. and Randall, D. G. "Boundary Layer Transition on a Sweptback Wing." RAE Tech. Memo. No. Aero 277, May 1952.

23. Chapman, G. T. "Some Effects of Leading-Edge Sweep on Boundary Layer Transition at Supersonic Speeds." NASA TN D-1075, September 1961.

24. Adams, J. C., Jr. "Three-Dimensional Laminar Boundary-Layer Analysis of Upwash Patterns and Entrained Vortex Formation on Sharp Cones at Angle of Attack." AEDC-TR-71-215 (AD736880), December 1971.

25. Adams, J. C., Jr. and Martindale, W. R. "Hypersonic Lifting Body Windward Surface Flow-Field Analysis for High Angles of Incidence." AEDC-TR-73-2 (AD756499), February 1973.

26. Gregory, N., Stuart, J. T., and Walker, N. S. "On the Stability of Three-Dimensional Boundary Layers with Application to the Flow Due to a Rotating Disk." Trans. Roy. Soc. (London), Series A, Vol. 248, No. 943, July 1955, pp. 155-159.

27. Shapiro, A. H. The Dynamics and Thermodynamics of Compressible Fluid Flow, Vol. 1. The Ronald Press Company, New York, 1953.

28. Abbott, I. H. and von Doenhoff, A. E. Theory of Wing Sections. Dover Publications, Inc., New York, 1959.

29. Murman, E. M. and Cole, J. D. "Calculation of Plane Steady Transonic Flows." AIAA J., Vol. 9, No. 1, January 1971, pp. 114-121.

30. Steger, J. L. and Lomax, H. "Transonic Flow about Two-Dimensional Airfoils by Relaxation Procedures." AIAA J., Vol. 10, No. 1, January 1972, pp. 49-54.

31. Krupp, J. A. and Murman, E. M. "Computation of Transonic Flows Past Lifting Airfoils and Slender Bodies." AIAA J., Vol. 10, No. 7, July 1972, pp. 880-886.

32. Bailey, F. R. and Steger, J. L. "Relaxation Techniques for Three-Dimensional Transonic Flow About Wings." AIAA J., Vol. 11, No. 3, March 1973, pp. 318-325.

33. Nash, J. F. "An Explicit Scheme for the Calculation of Three-Dimensional Turbulent Boundary Layers." Trans. ASME, J. Basic Engineering, Vol. 94, Series D, No. 1, March 1972, pp. 131-141.

34. Townsend, A. A. "Equilibrium Layers and Wall Turbulence." J. Fluid Mech., Vol. 11, Part 1, 1961, pp. 97-120.

35. Sivasegaram, S. and Whitelaw, J. H. "The Prediction of Turbulent, Supersonic, Two-Dimensional, Boundary-Layer Flows." Aeronaut. Quart., Vol. 22, August 1971, pp. 274-294.

36. Bradshaw, P., Ferriss, D. H., and Atwell, N. P. "Calculation of Boundary-Layer Development Using the Turbulent Energy Equation." J. Fluid Mech., Vol. 28, Part 3, 1967, pp. 593-616.

37. Altman, J. M. and Hayter, N. F. "A Comparison of the Turbulent Boundary-Layer Growth on an Unswept and a Swept Wing." NACA TN 2500, September 1951.

41

38. Dannenberg, R. E. "Measurements of Section Characteristics of a 45° Swept Wing Spanning a Rectangular Low-Speed Wind Tunnel as Affected by the Tunnel Walls." NACA TN 2160, August 1950.

39. Nash, J. F. and Patel, V. C. Three-Dimensional Turbulent Boundary Layers. SBC Technical Books, Scientific and Business Consultants, Inc., Atlanta, Georgia, 1972.

40. Ashkenas, H. and Riddell, F. R. "Investigation of the Turbulent Boundary Layer on a Yawed Flat Plate." NACA TN 3383, April 1955.

41. Macha, J. M., Norton, D. J., and Young, J. C. "Surface Temperature Effect on Subsonic Stall." AIAA Paper No. 72-960, presented at the AIAA 2nd Atmospheric Flight Mechanics Conference, Palo Alto, California, September 11-13, 1972.

42. Starr, R. F. and Schueler, C. J. "Experimental Studies of a Ludwieg Tube High Reynolds Number Transonic Tunnel." AIAA Paper No. 73-212, presented at the AIAA 11th Aerospace Sciences Meeting, Washington, D.C., January 10-12, 1973.

43. Fehrman, A. L. and Masek, R. V. "Study of Uncertainties of Predicting Space Shuttle Thermal Environment." Report MDC E0639, June 1972.

44. Bam-Zelikovich, G. M. "Necessary Condition for Three-Dimensional Boundary Layer Separation." Fluid Dynamics (A translation of Izv. AN SSSR, MZhG), Vol. 5, No. 2, March-April 1970, pp. 267-270.

45. Green, J. E. "A Discussion of Viscous-Inviscid Interactions at Transonic Speeds." RAE TR 72050, May 1972.

46. Blottner, F. G. "Finite Difference Methods of Solution of the Boundary Layer Equations." AIAA J., Vol. 8, No. 2, February 1970, pp. 193-205.

47. Davis, R. T. "Numerical Solution of the Hypersonic Viscous Shock-Layer Equations." AIAA J., Vol. 8, No. 5, May 1970, pp. 843-851.

48. Richtmyer, R. D. and Morton, K. W. Difference Methods for Initial-Value Problems. Interscience Publishers, New York, 1967 (Second Edition).

49. Smith, A. M. O. and Cebeci, T. "Numerical Solution of the Turbulent Boundary-Layer Equations." Douglas Aircraft Division Report 33735, May 1967.

50. Flügge-Lotz, I. and Blottner, F. G. "Computation of the Compressible Laminar Boundary-Layer Flow Including Displacement Thickness Interaction Using Finite-Difference Methods." Stanford University Division of Engineering Mechanics Report No. 131, Stanford, California, January 1962.

51. Conte, S. D. Elementary Numerical Analysis. McGraw-Hill, Inc., New York, 1965.

Infinite-Extent Yawed Body

$$W_e = W_\infty \; ; \; \frac{\partial}{\partial z} (\bar{}) = 0$$

Stagnation or Attachment Line (x = 0)

x, $\bar{u}$; Chordwise Direction

y, $\bar{v}$

z, $\bar{w}$; Spanwise Direction

U_∞

W_∞

Λ

V_∞

(Free-Stream)

D/2
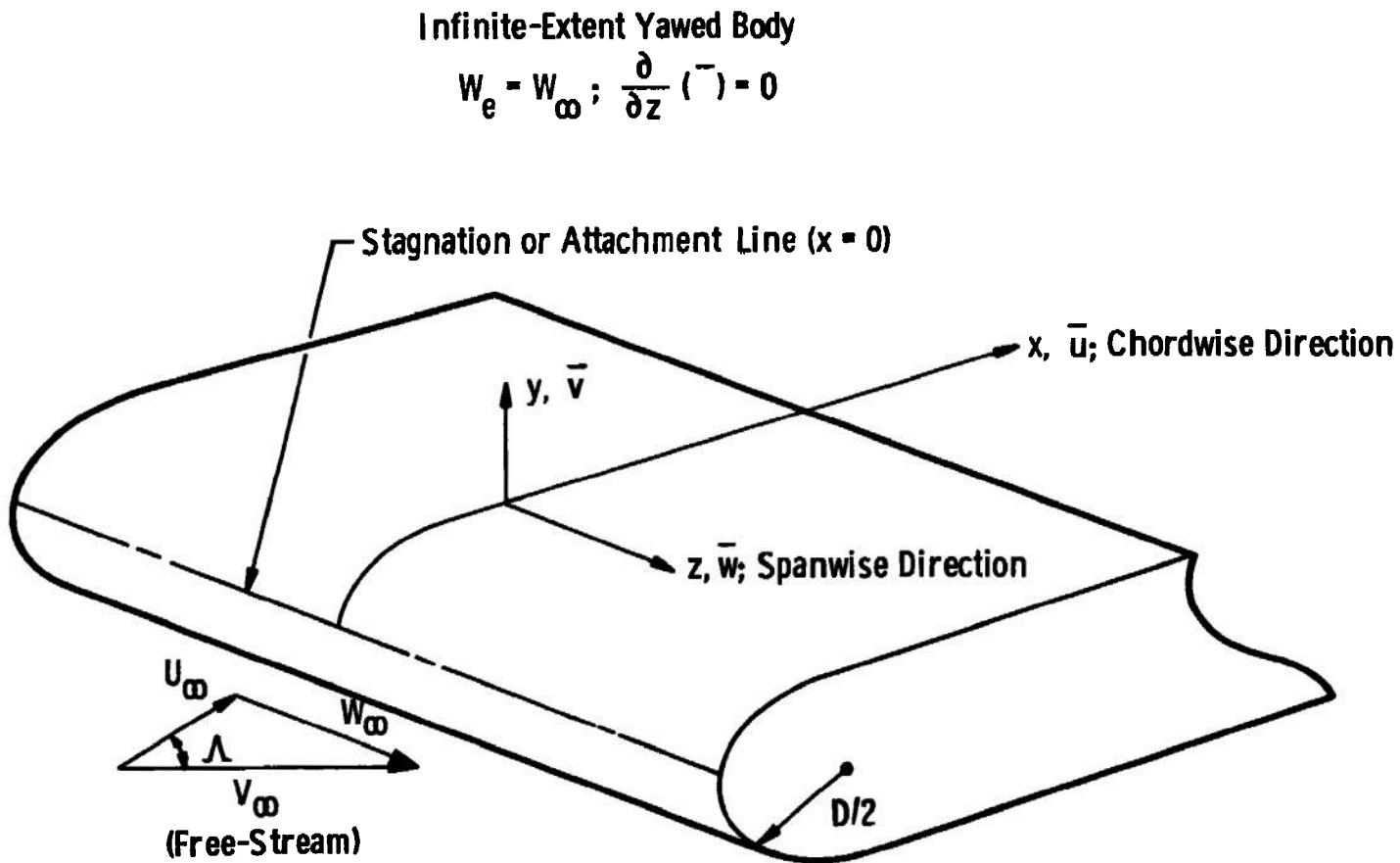
Fig. 1 Infinite Extent Yawed Body Geometry and Nomenclature
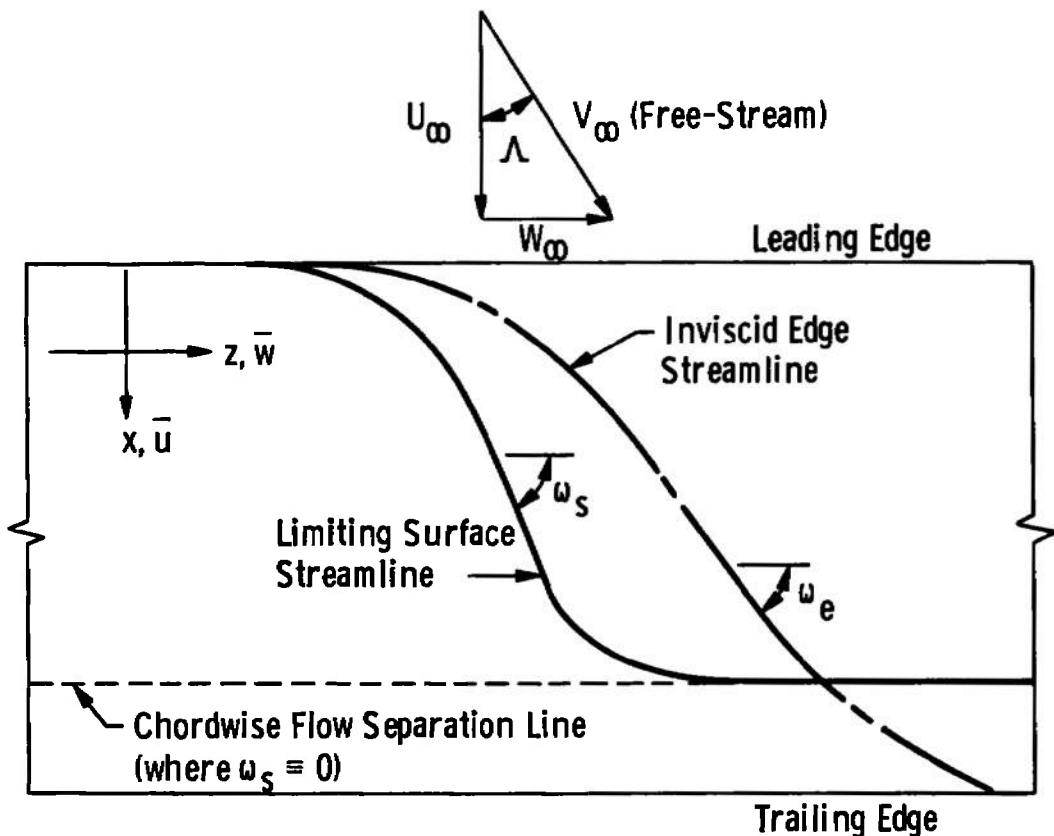
a. Plan View Illustrating Three-Dimensional Boundary-Layer
Separation on an Infinite Yawed Wing
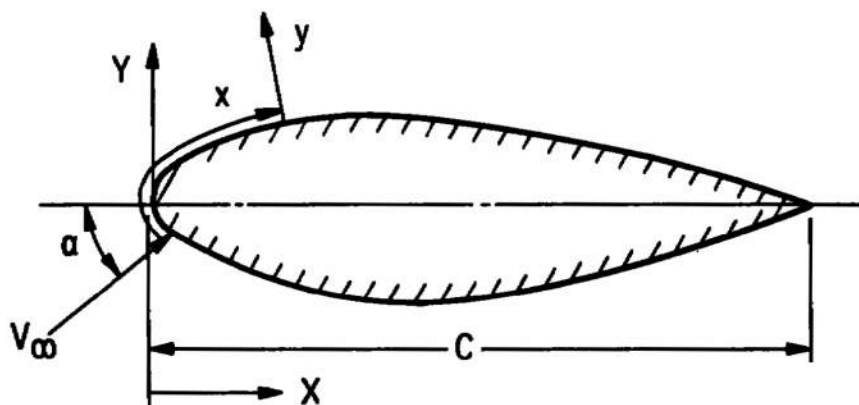
b. Chordwise Section of Wing
Fig. 2 Infinite Yawed Wing Geometry and Nomenclature
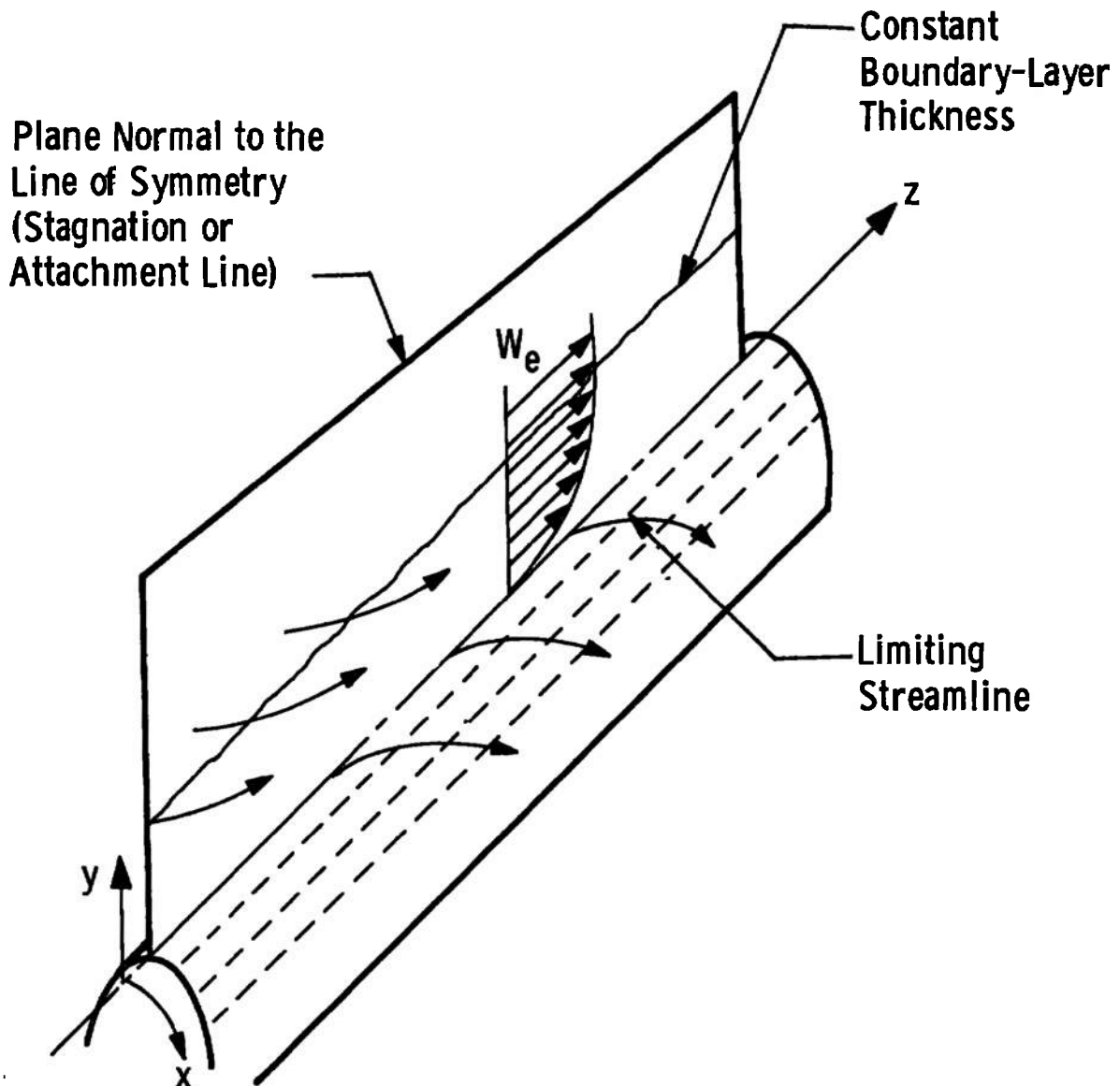
Fig. 3 Schematic of Stagnation or Attachment Line Flow over
an Infinite Extent Yawed Circular Cylinder
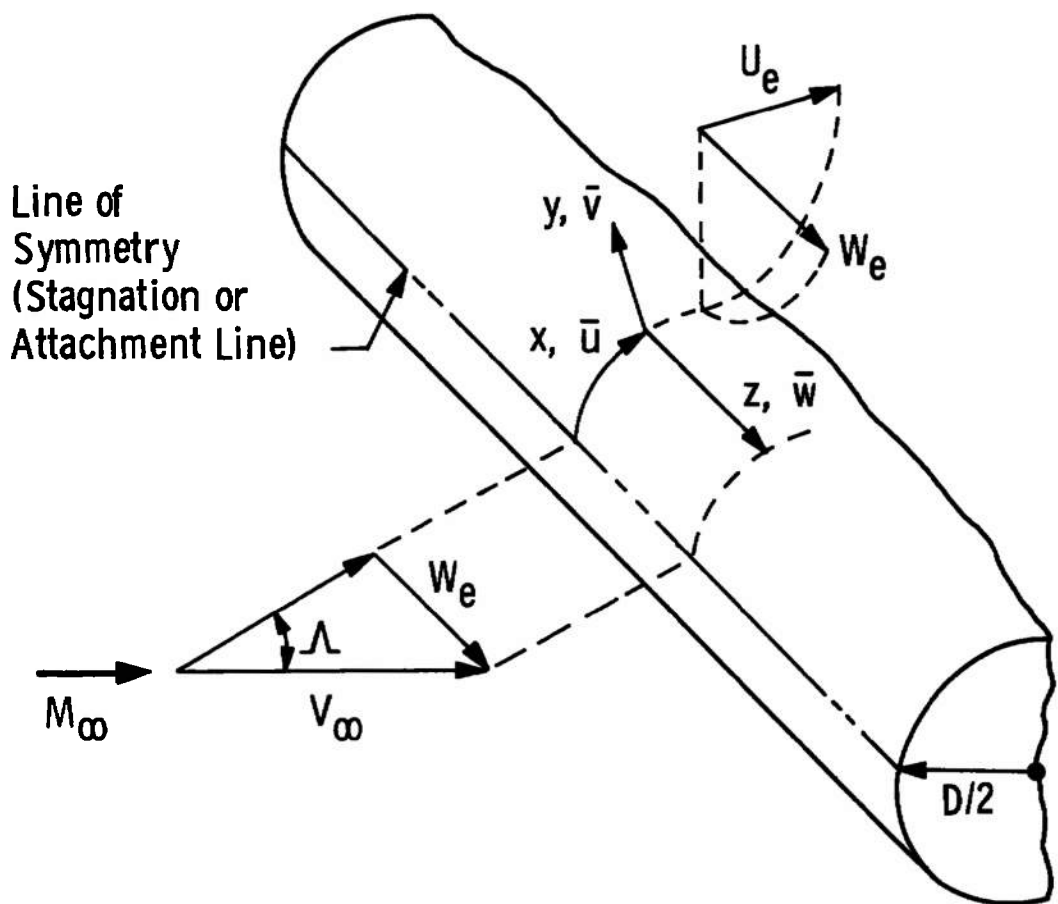
Fig. 4 Coordinate System for Flow over an Infinite Yawed Circular Cylinder
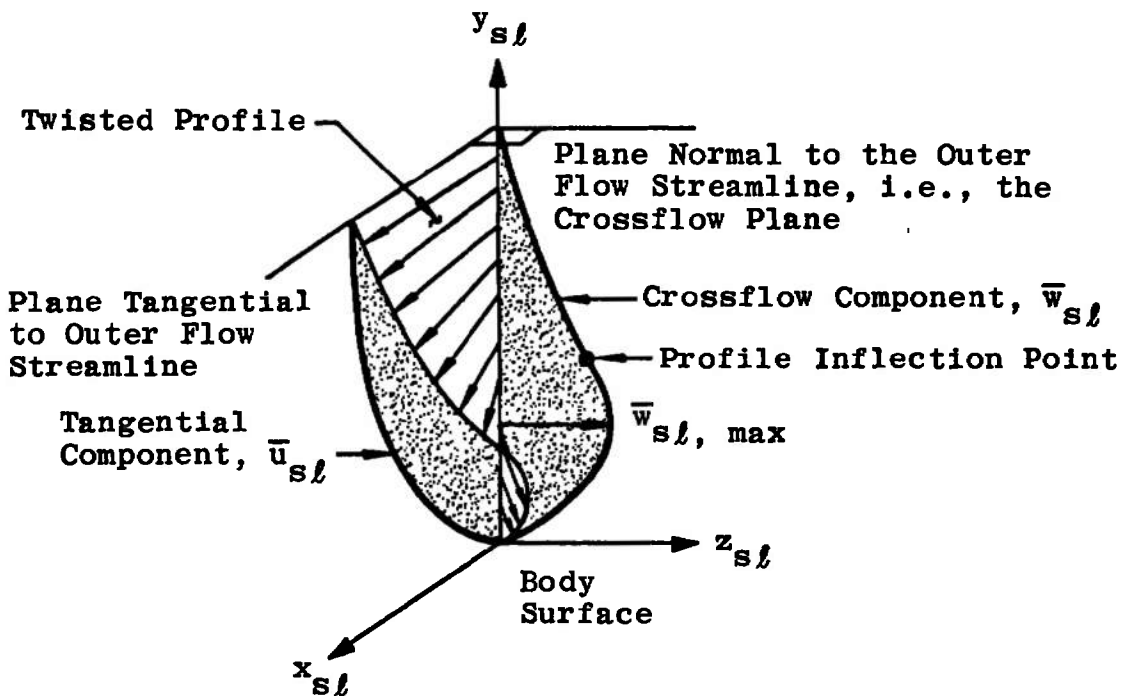
Fig. 5 Three-Dimensional Boundary-Layer Velocity Profiles in Streamline Coordinates
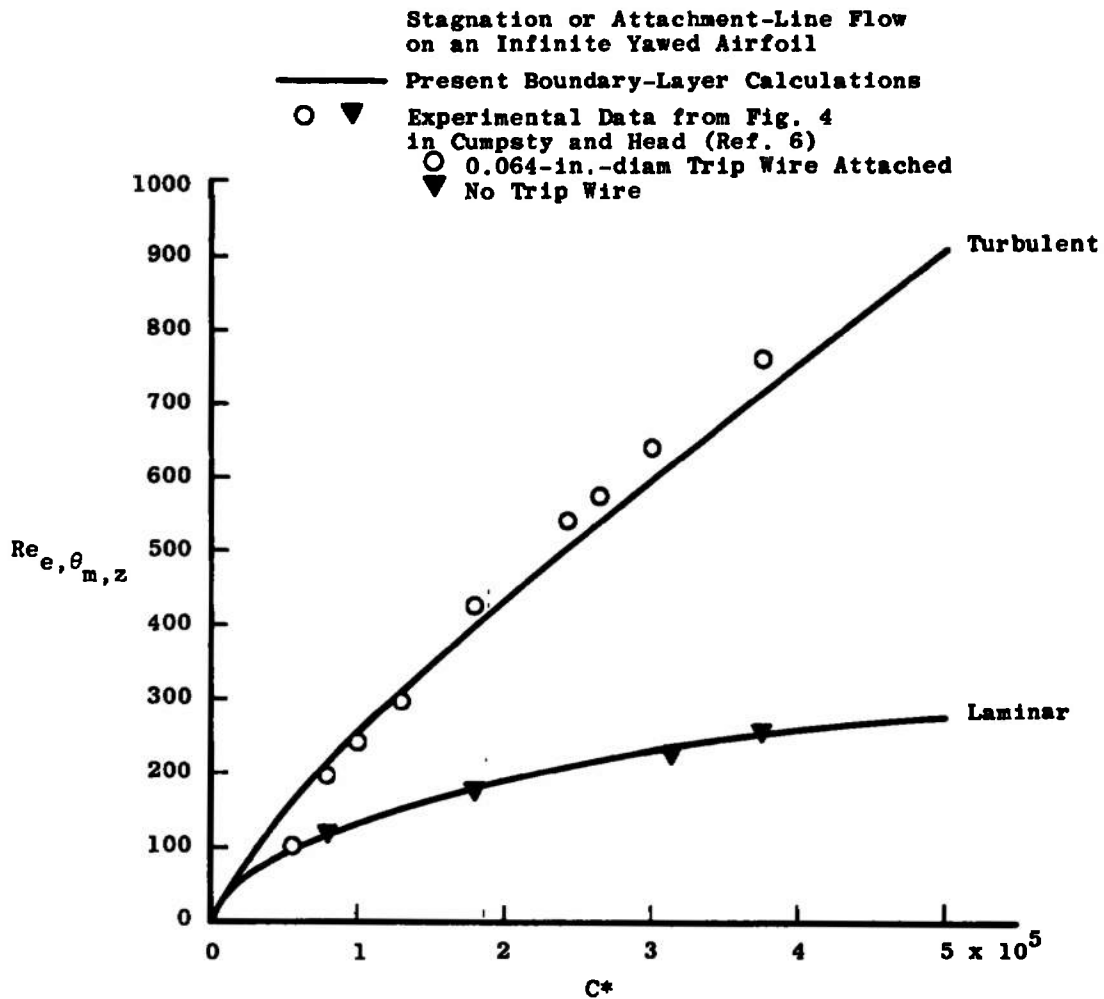
Fig. 6 Variation of Stagnation or Attachment Line $Re_{e,\theta_{m,z}}$ with C*
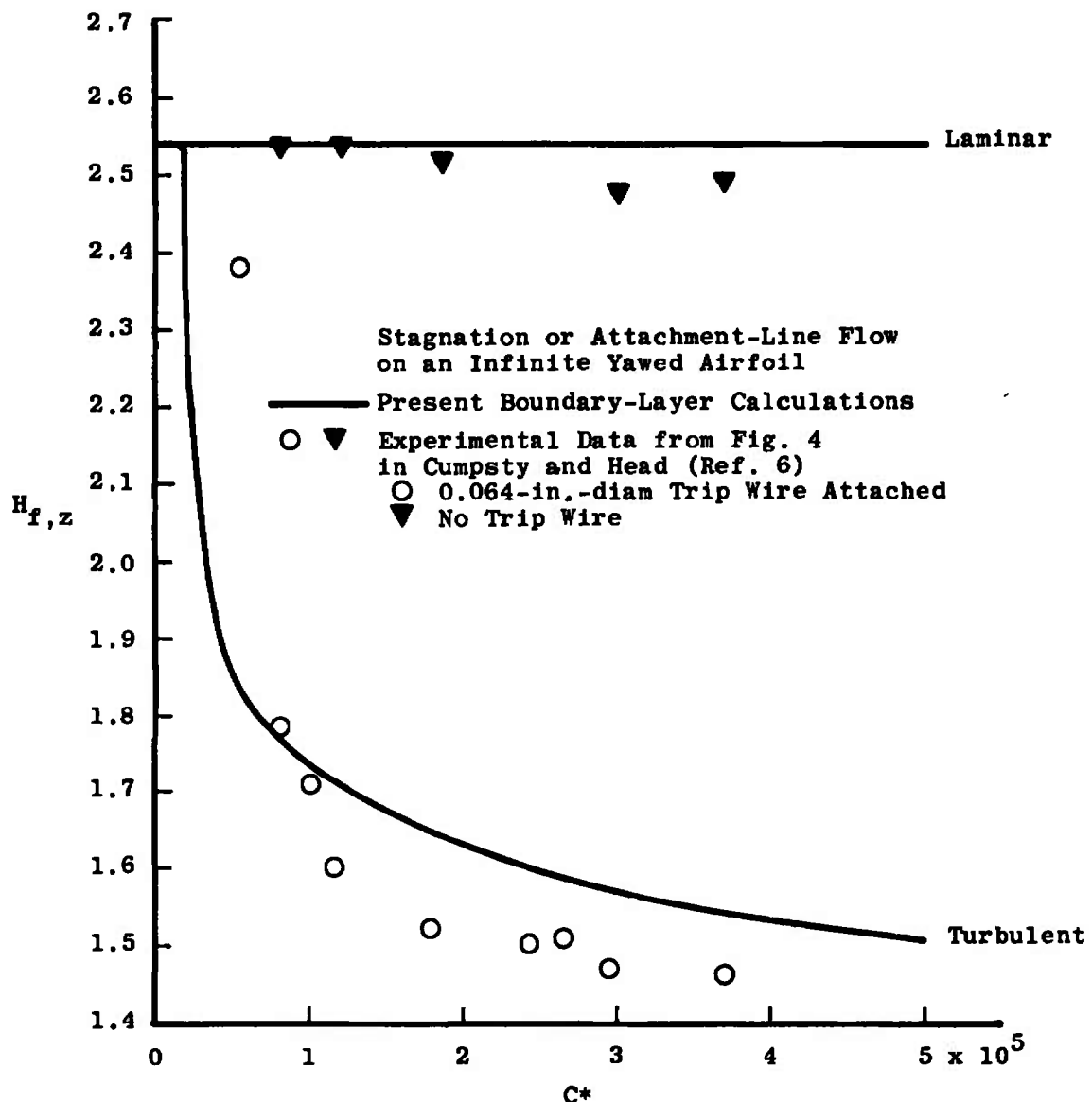
Fig. 7 Variation of Stagnation or Attachment Line $H_{f,z}$ with $C*$
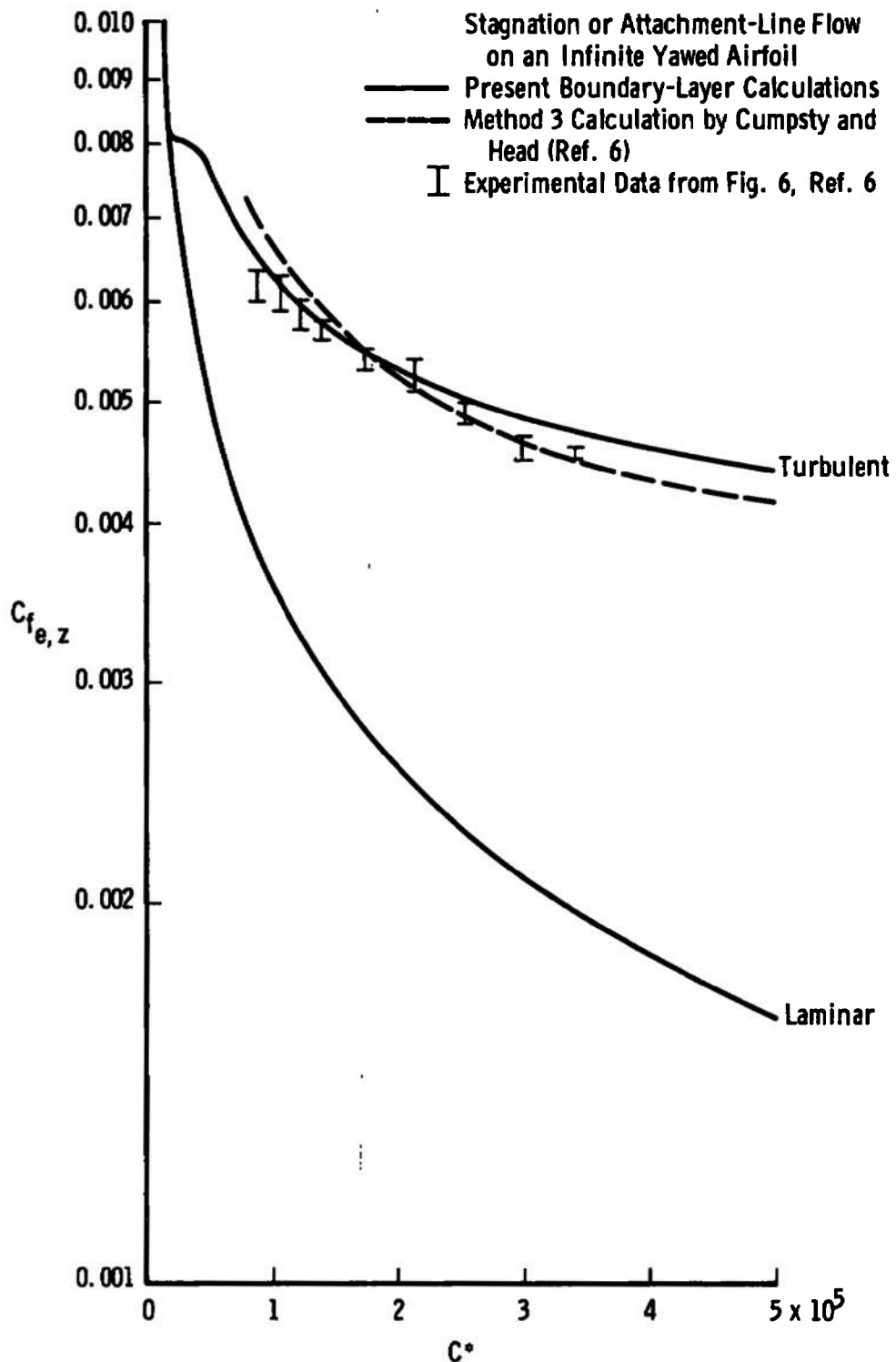
Fig. 8 Variation of Stagnation or Attachment Line $C_{f_{e,z}}$ with C^*

NACA 65$_1$A012 Airfoil at 35-deg Sweep
Re$_{\infty,C}$ = 6.14 x 10^7, Adiabatic Wall,
C$_{L_u}$ = 0.50
——Present Turbulent Boundary-Layer Theory
○◇◁Kinetic-Energy-of-Turbulence Analysis by Nash and Tseng (Ref. 10)
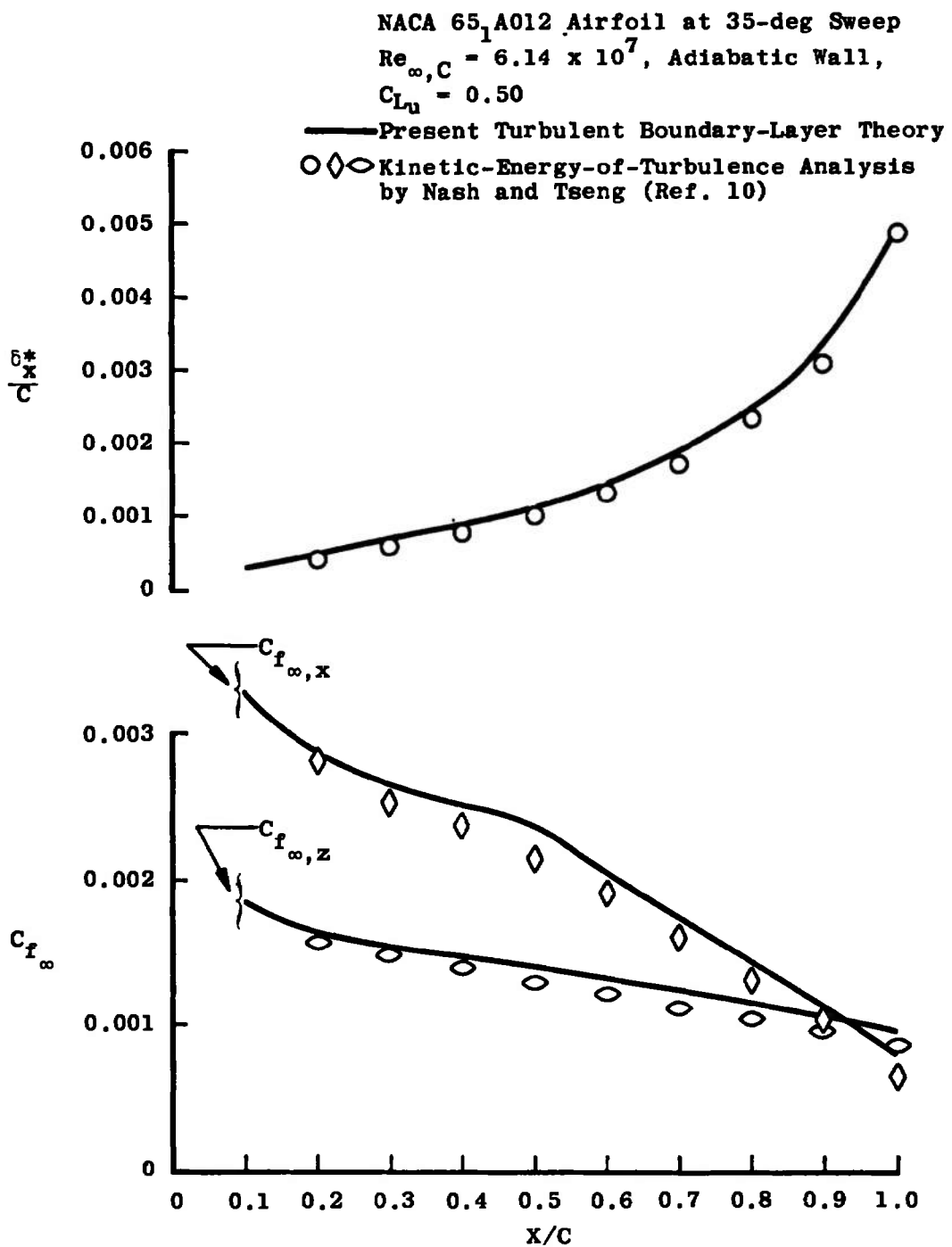
Fig. 9 Comparison of Turbulent Boundary-Layer Parameters with Infinite Yawed Wing Results of Nash and Tseng (Ref. 10)
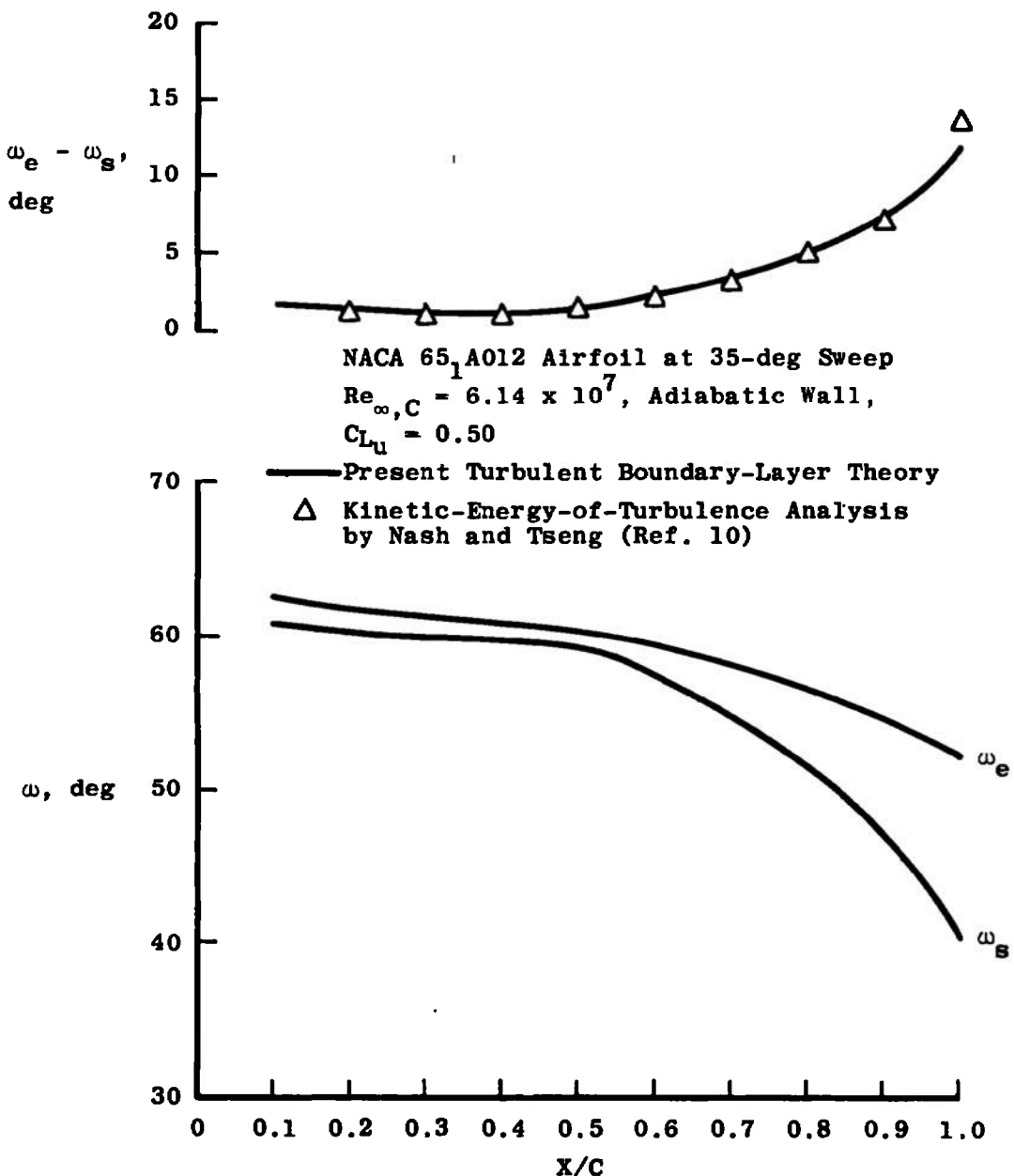
Fig. 10 Comparison of Surface and External Flow Directions with Infinite
Yawed Wing Results of Nash and Tseng (Ref. 10)
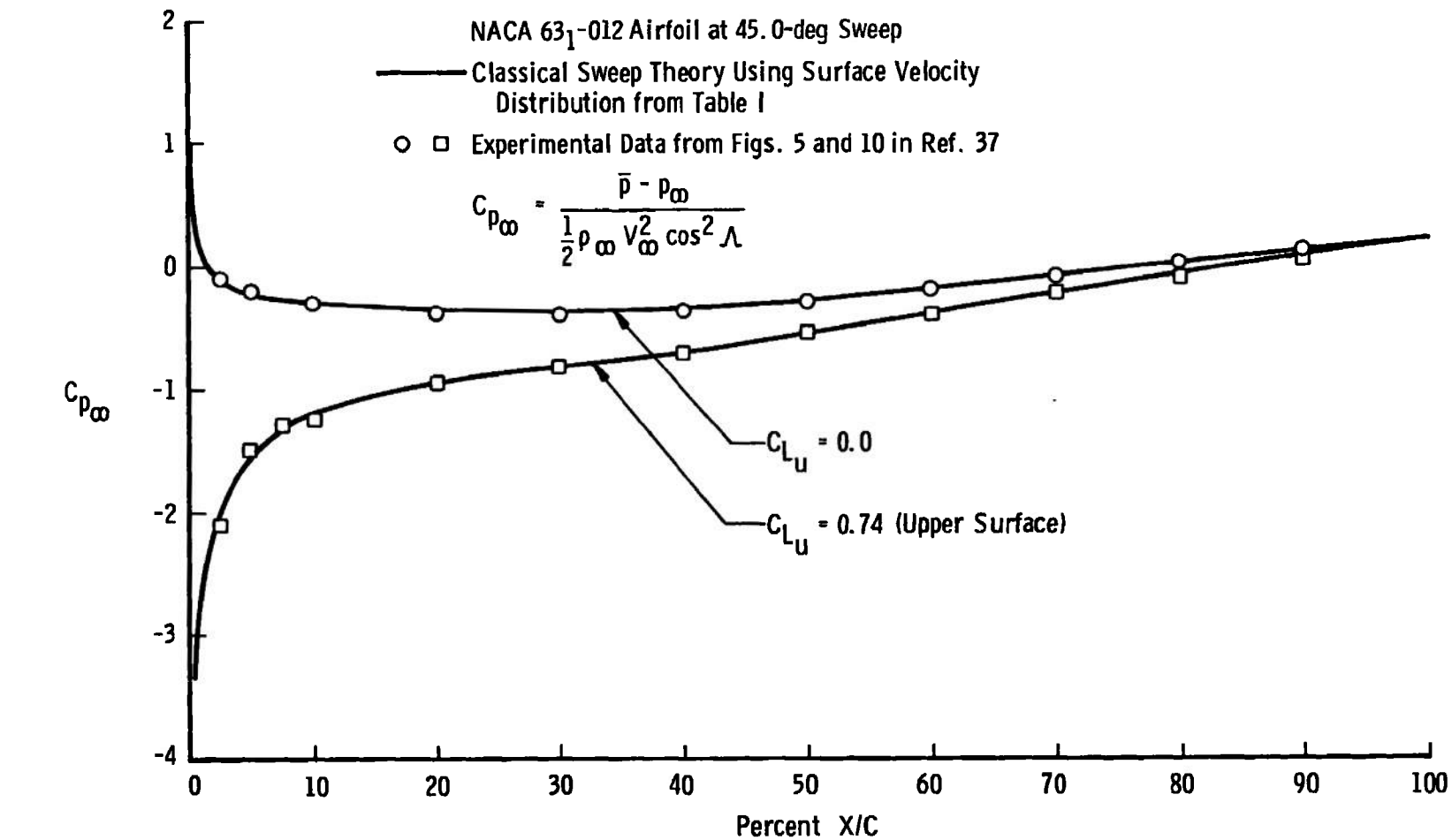
NACA 63_1-012 Airfoil at 45.0-deg Sweep

—— Classical Sweep Theory Using Surface Velocity
   Distribution from Table I

○ □ Experimental Data from Figs. 5 and 10 in Ref. 37

$$C_{p_\infty} = \frac{\bar{p} - p_\infty}{\frac{1}{2}\rho_\infty V_\infty^2 \cos^2 \Lambda}$$

$C_{L_u} = 0.0$

$C_{L_u} = 0.74$ (Upper Surface)

Percent X/C

Fig. 11 Surface Pressure Distribution on an Infinite Yawed Airfoil under Subsonic Conditions

NACA 63_1-012 Airfoil at 0.0-deg Sweep
$Re_{\infty,C} = 3.8 \times 10^6$, Adiabatic Wall

—— Present Turbulent Boundary-Layer Theory

O   Experimental Data from Fig. 7 in Ref. 37
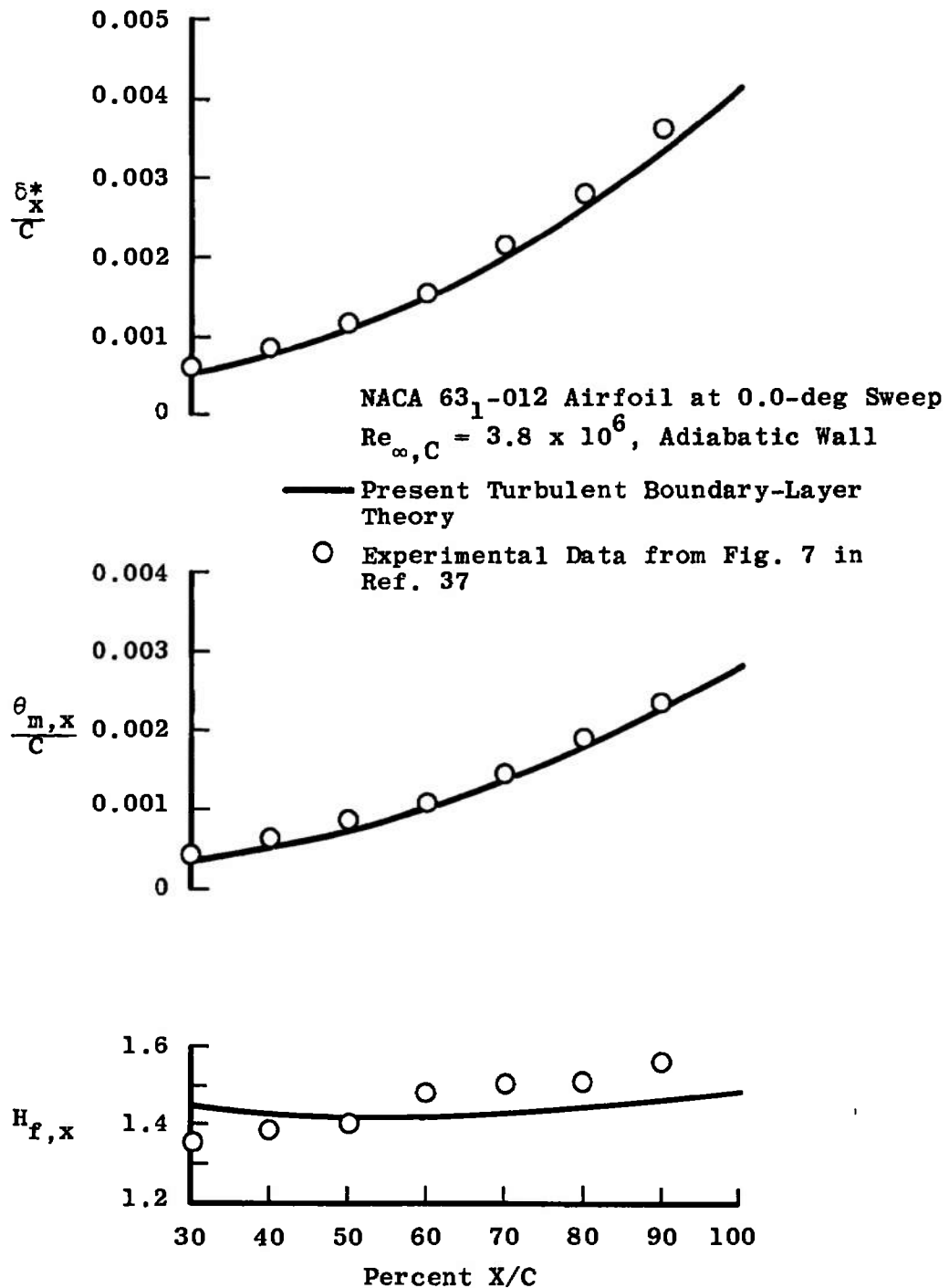
Fig. 12 Turbulent Boundary-Layer Parameters on a Two-Dimensional Airfoil at Zero Lift
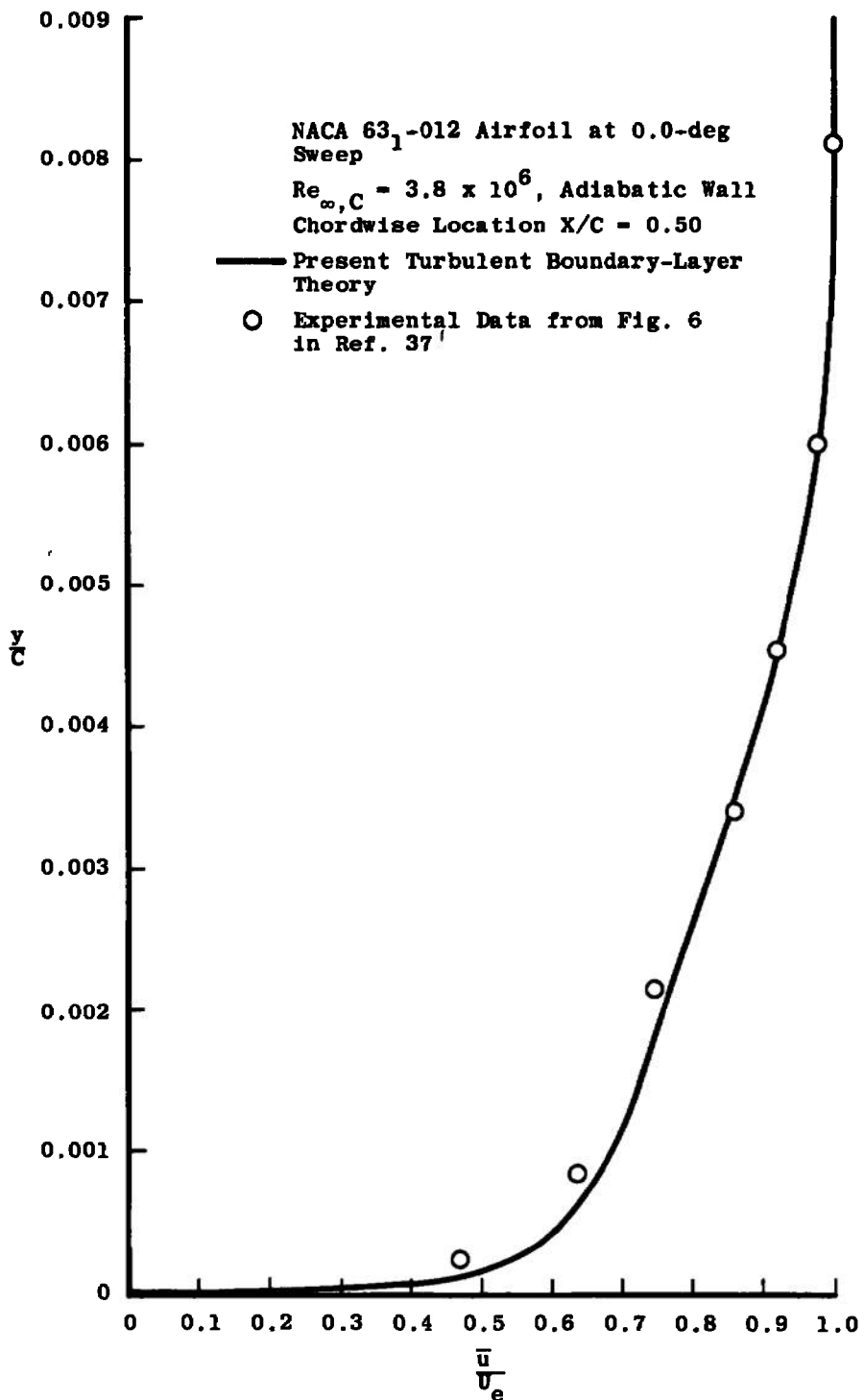
Fig. 13 Turbulent Boundary-Layer Velocity Profile on a Two-Dimensional
Airfoil at Zero Lift

NACA 63_1-012 Airfoil at 45.0-deg Sweep
$Re_{\infty,C} = 5.4 \times 10^6$, Adiabatic Wall
━━━ Present Turbulent Boundary-Layer Theory
△ Experimental Data from Fig. 9 in Ref. 37

Percent X/C
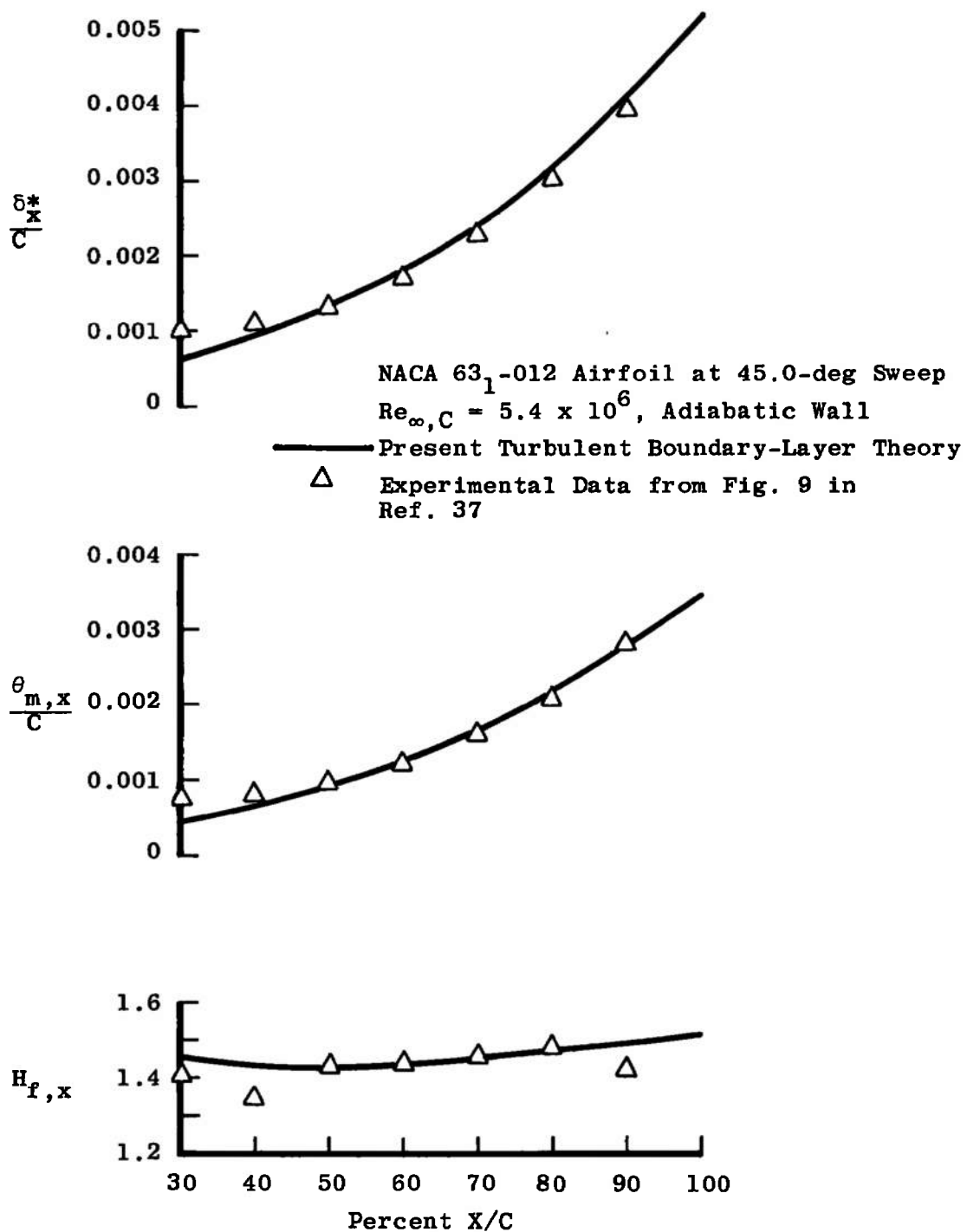
Fig. 14 Turbulent Boundary-Layer Parameters on an Infinite Yawed Airfoil at Zero Lift
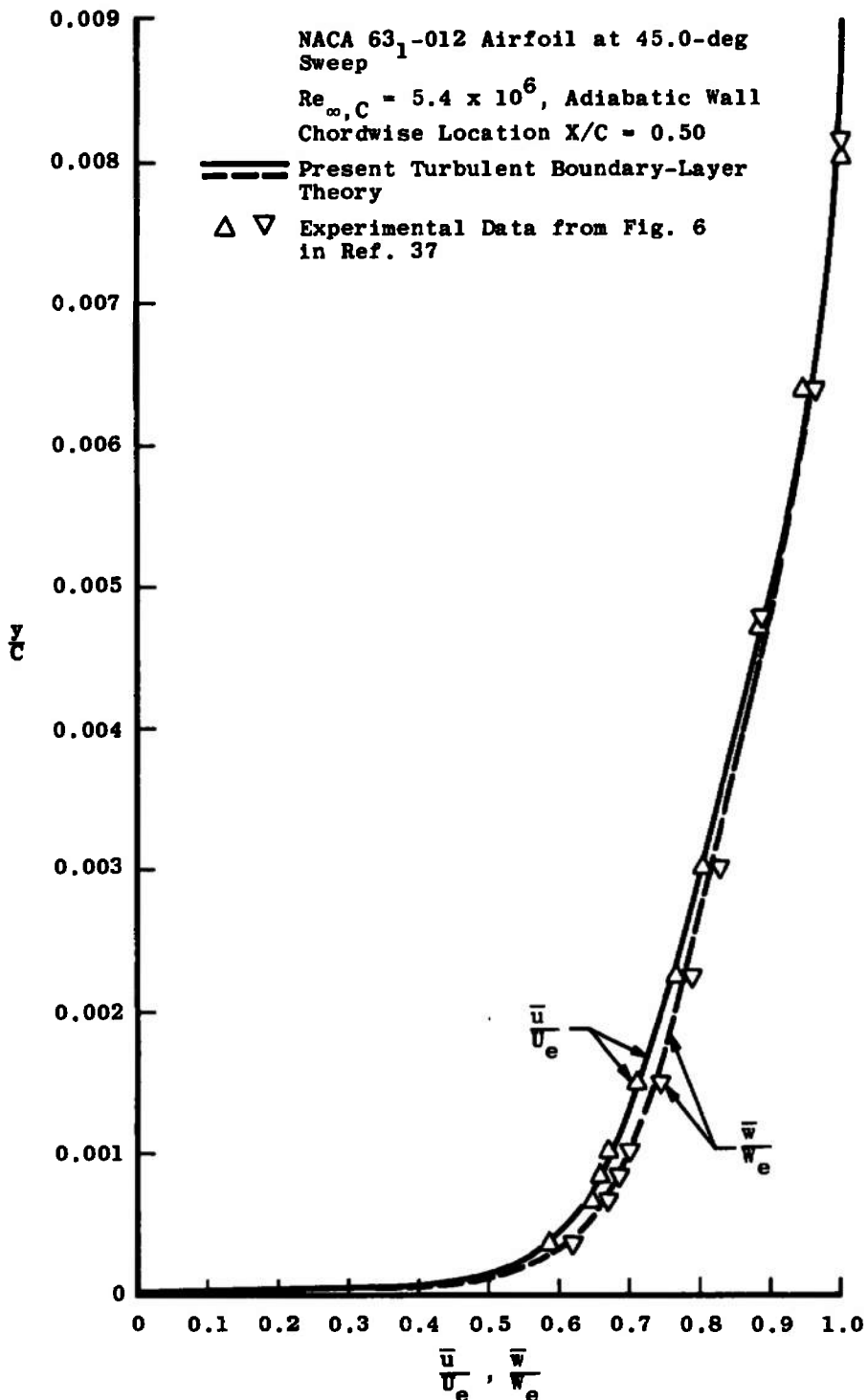
Fig. 15 Turbulent Boundary-Layer Velocity Profiles on an Infinite
Yawed Airfoil at Zero Lift

NACA 63_1-012 Airfoil
———— Present Turbulent Boundary-Layer
Theory at 45.0-deg Sweep from Fig. 14
——— Present Turbulent Boundary-Layer
Theory at 0.0-deg Sweep from Fig. 12
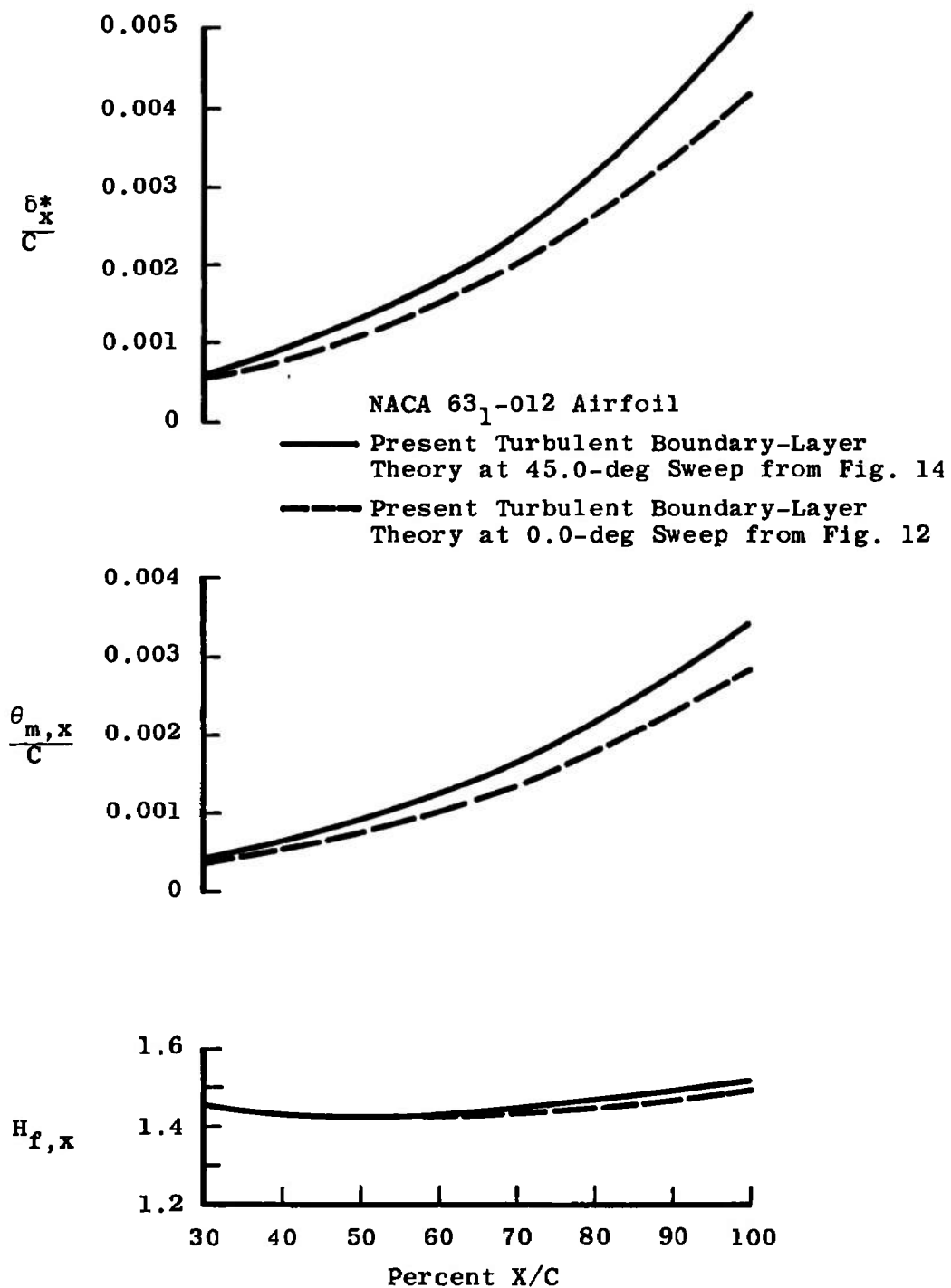
Fig. 16 Comparison of Two-Dimensional and Infinite Yawed Airfoil
Boundary-Layer Parameters
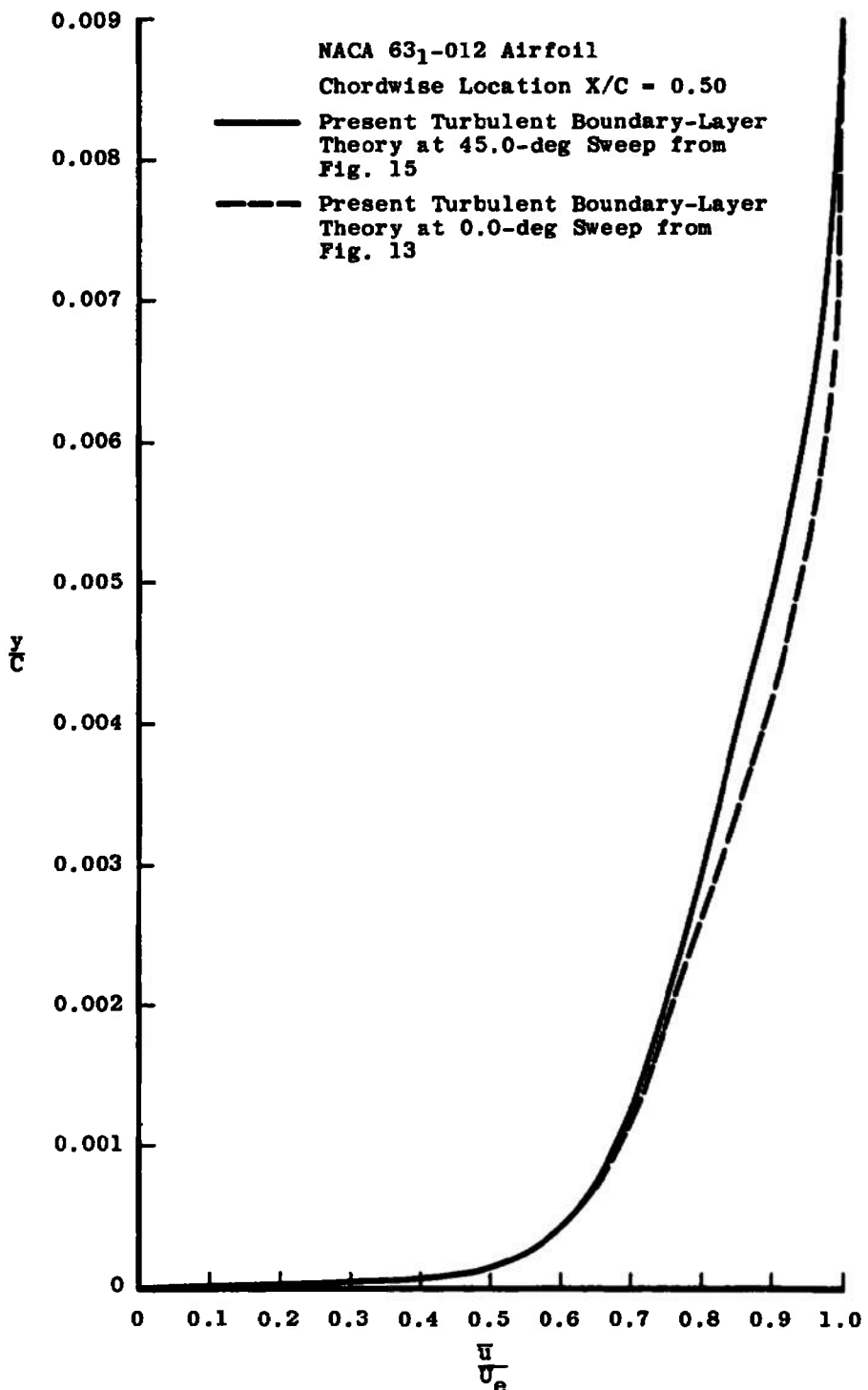
Fig. 17 Comparison of Two-Dimensional and Infinite Yawed Airfoil
Boundary-Layer Velocity Profiles

NACA 63_1-012 Airfoil at 45.0-deg Sweep

$Re_{\infty,C} = 5.4 \times 10^6$, Adiabatic Wall

Laminar Boundary Layer

Location of Artificial
Roughness in Ref. 37

χ

X/C
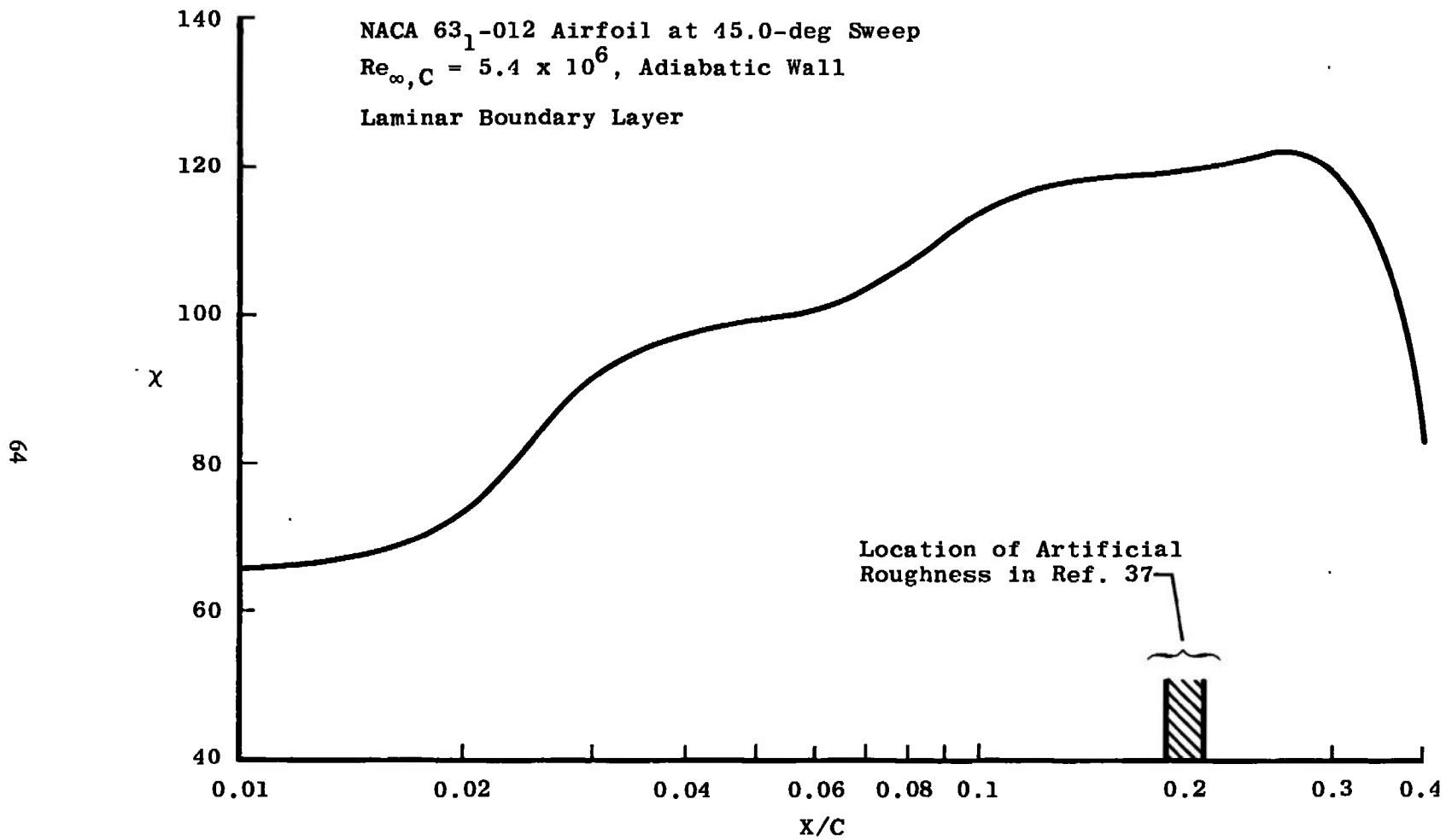
Fig. 18 Crossflow Reynolds Number Distribution on an Infinite Yawed Airfoil at Zero Lift

NACA 63_1-012 Airfoil at 45.0-deg Sweep

$Re_{\infty, C} = 5.4 \times 10^6$, Adiabatic Wall, $C_{L_u} = 0.74$

=== Present Turbulent Boundary-Layer Theory

△ ▽ Experimental Data from Fig. 17 in Ref. 37
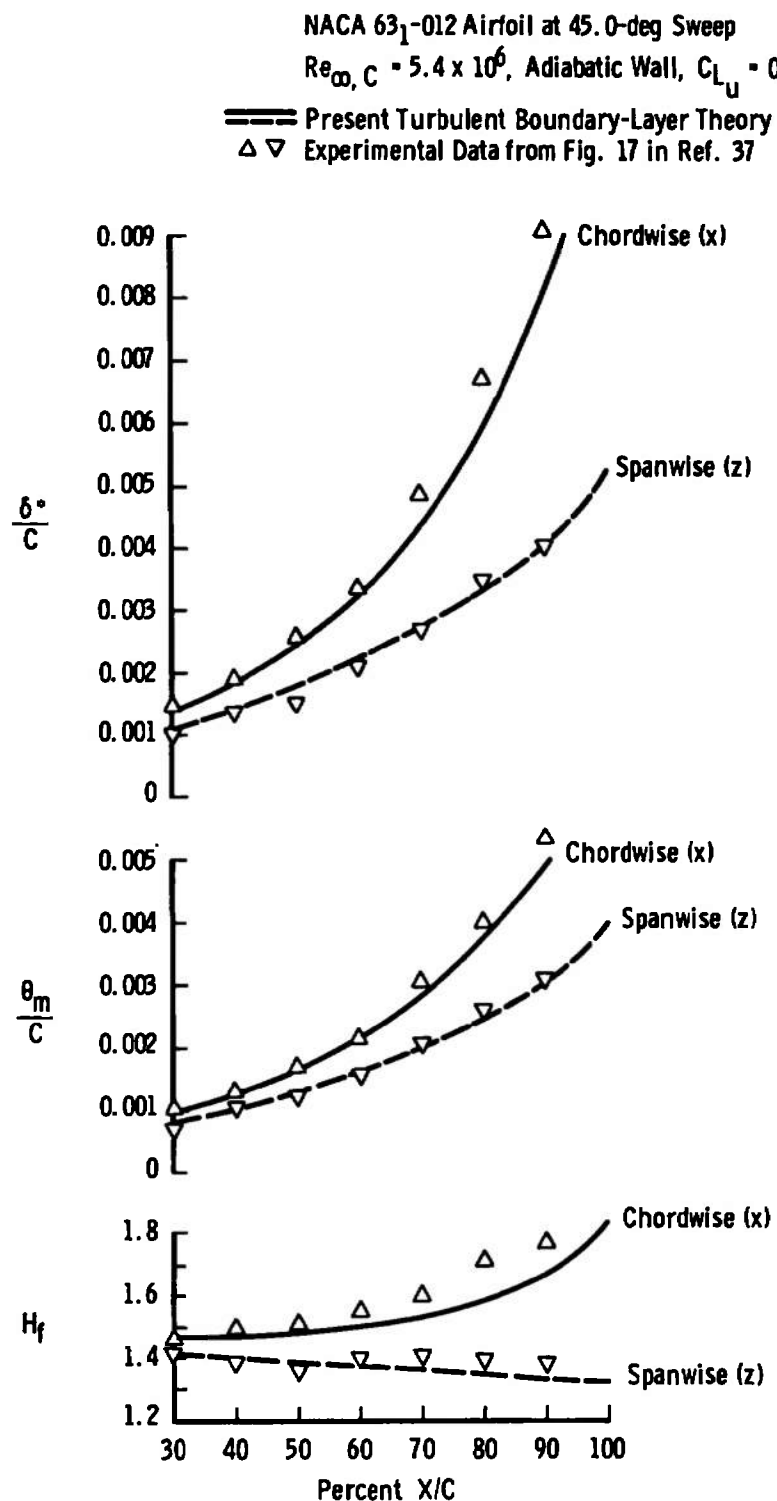
Fig. 19 Turbulent Boundary-Layer Parameters on a Lifting Infinite Yawed Airfoil
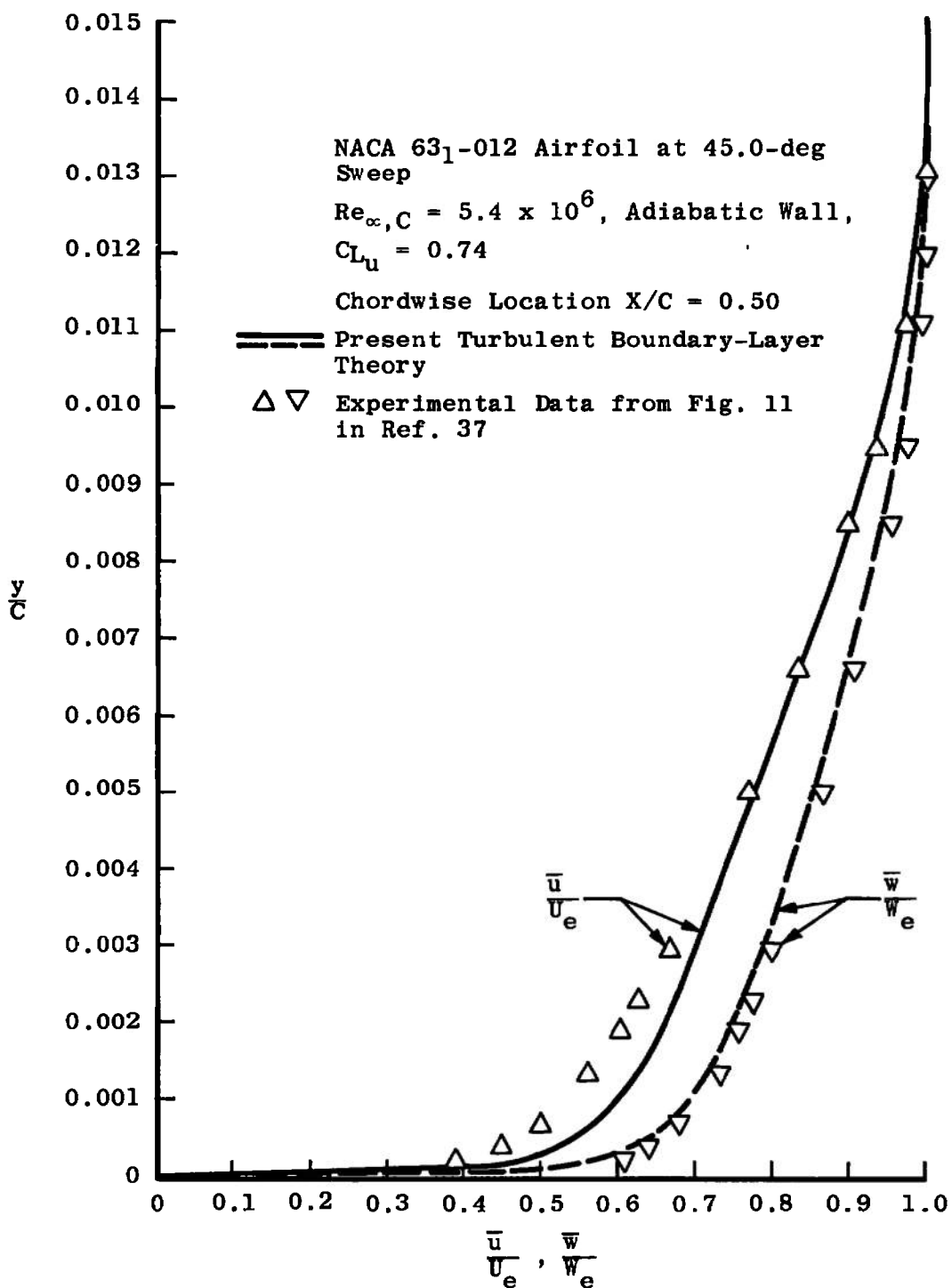
Fig. 20 Turbulent Boundary-Layer Velocity Profiles on a Lifting
Infinite Yawed Airfoil
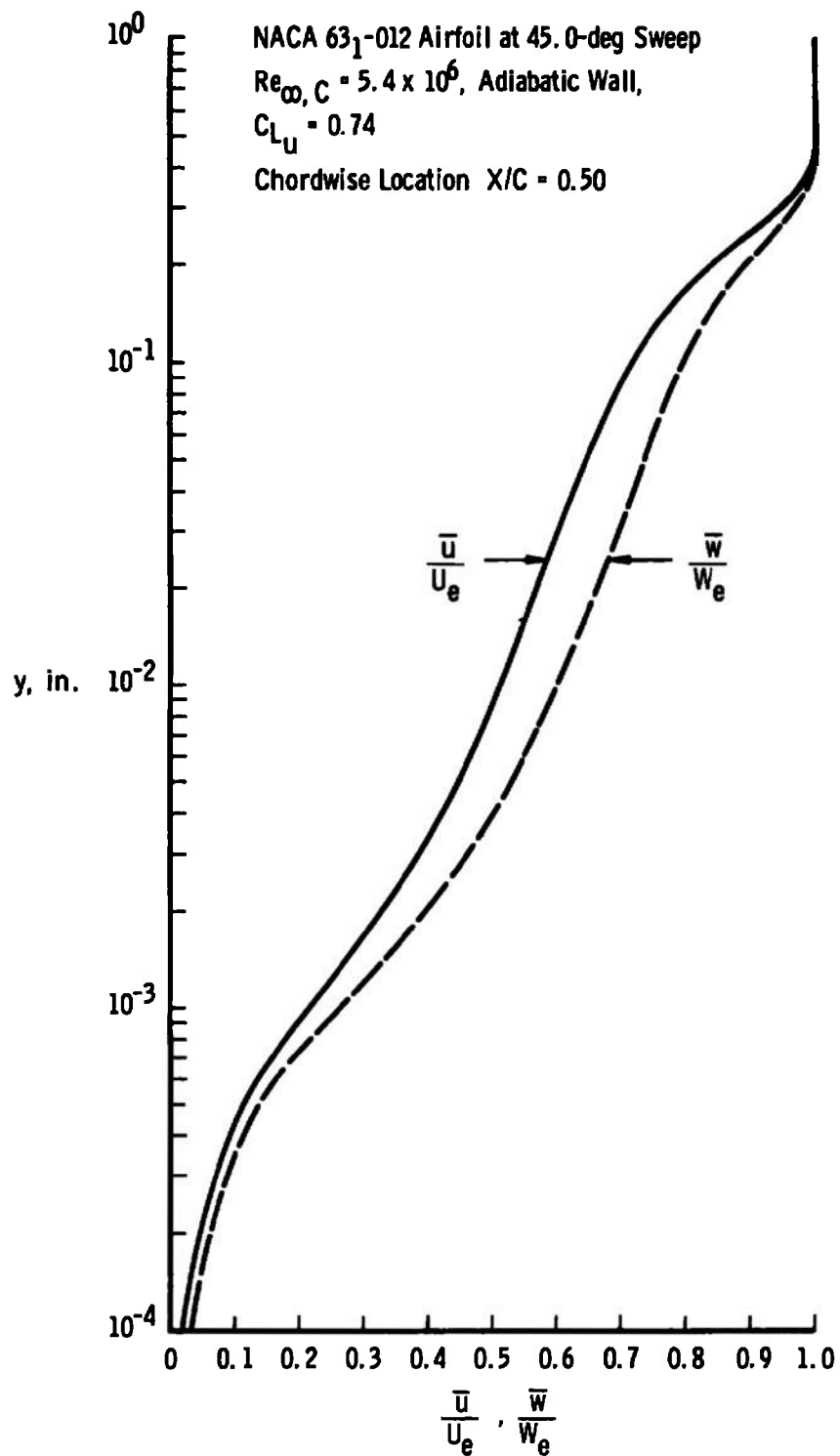
Fig. 21 Semilogarithmic Plot of the Turbulent Boundary-Layer Velocity
Profiles at 50-percent Chord on a Lifting Infinite Yawed Airfoil
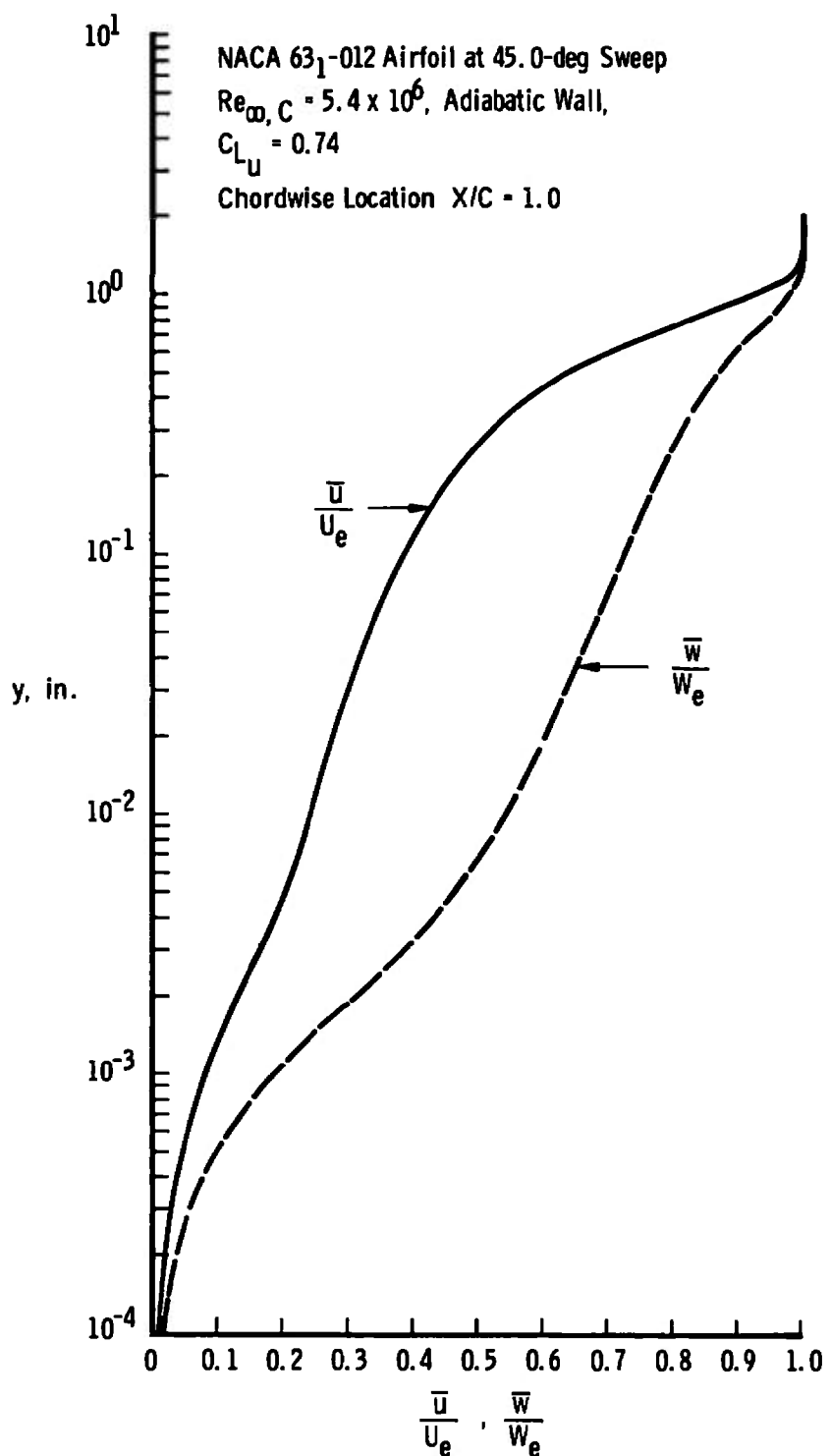
Fig. 22 Semilogarithmic Plot of the Turbulent Boundary-Layer Velocity
Profiles at the Trailing Edge of a Lifting Infinite Yawed Airfoil
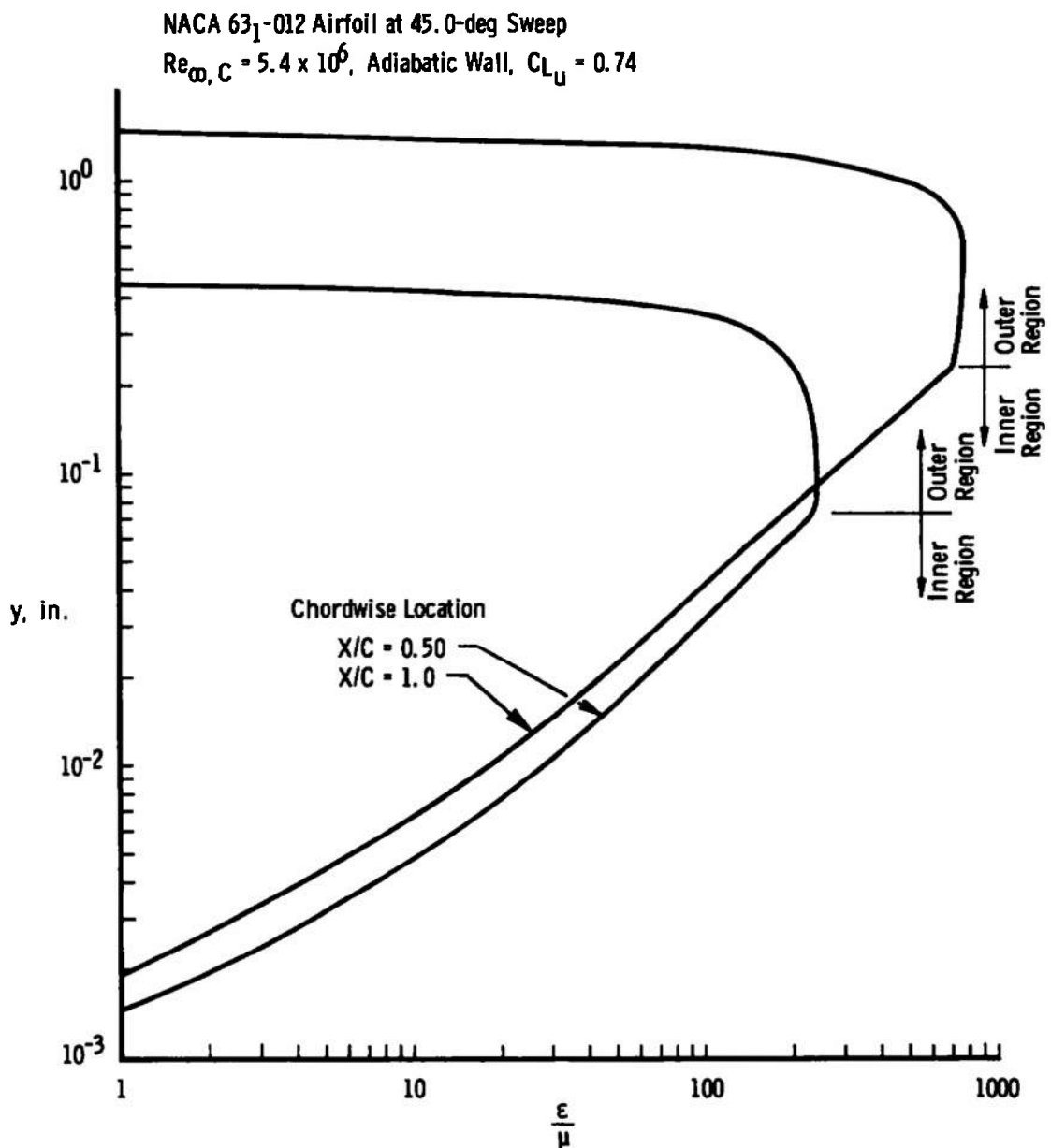
Fig. 23 Eddy Viscosity Distribution across the Turbulent Boundary
Layer on a Lifting Infinite Yawed Wing

NACA 63_1-012 Airfoil at 45.0-deg Sweep
$Re_{\infty,C} = 5.4 \times 10^6$, Adiabatic Wall, $C_{L_u} = 0.74$
━━━━━Present Turbulent Boundary-Layer Theory
△▽□○ Experimental Data from Fig. 16 in Ref. 37
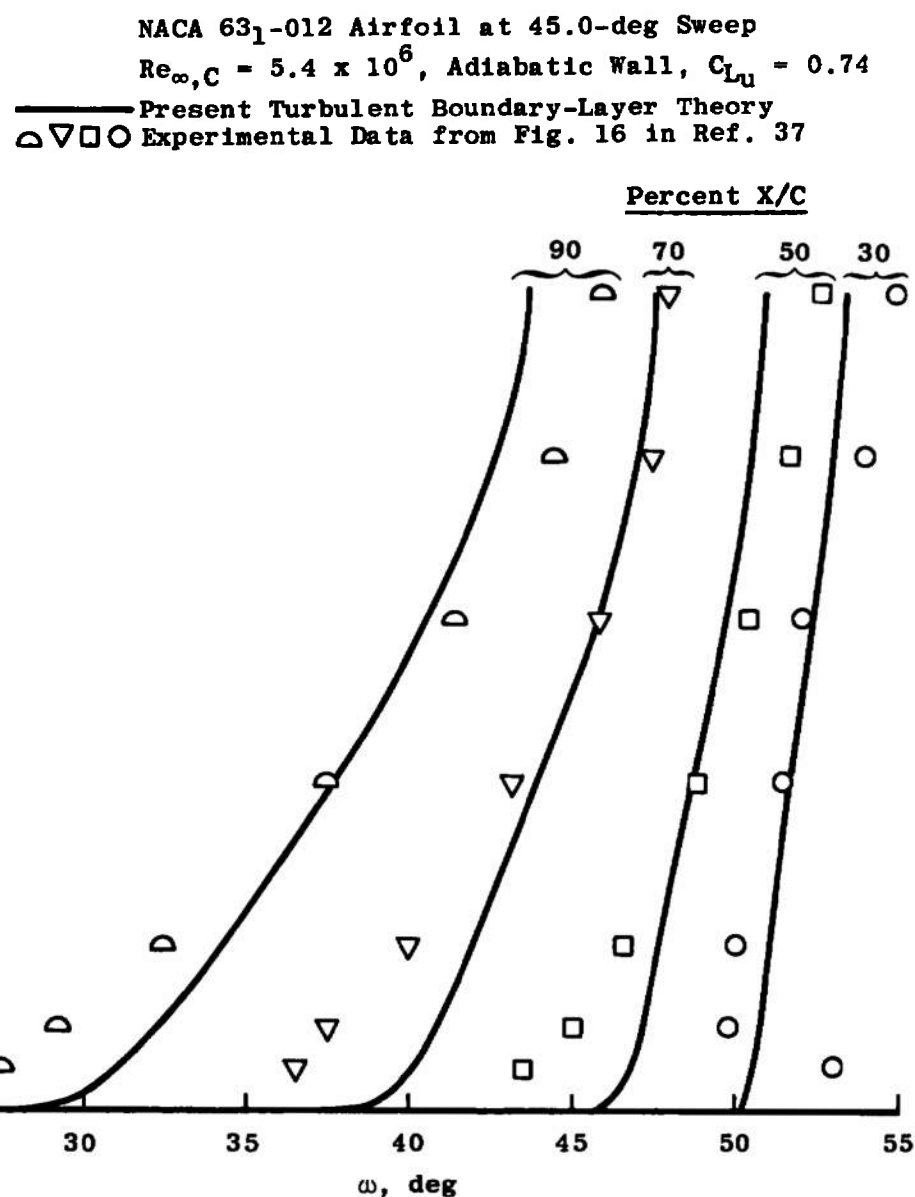
Fig. 24 Streamline Direction across the Turbulent Boundary Layer on a Lifting Infinite Yawed Wing

30°-Sweep DAC Airfoil, C = 1.0 ft
M_∞ = 0.815, p_∞ = 3.024 x 10⁴ lbf/ft², T_∞ = 432°R

Full-Scale HIRT Conditions
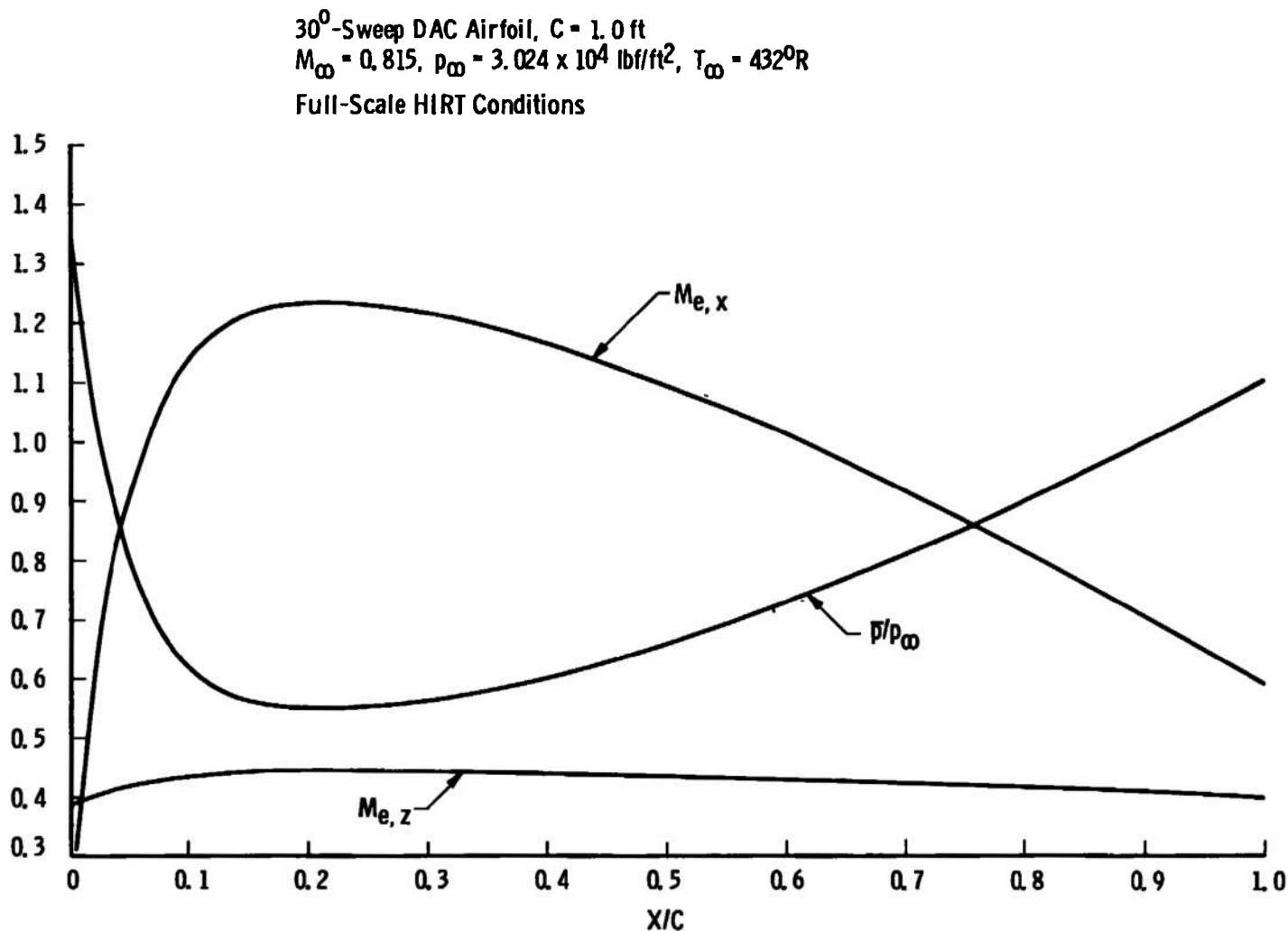
Fig. 25 Inviscid Flow Parameters on the DAC Airfoil under Full-Scale HIRT Conditions
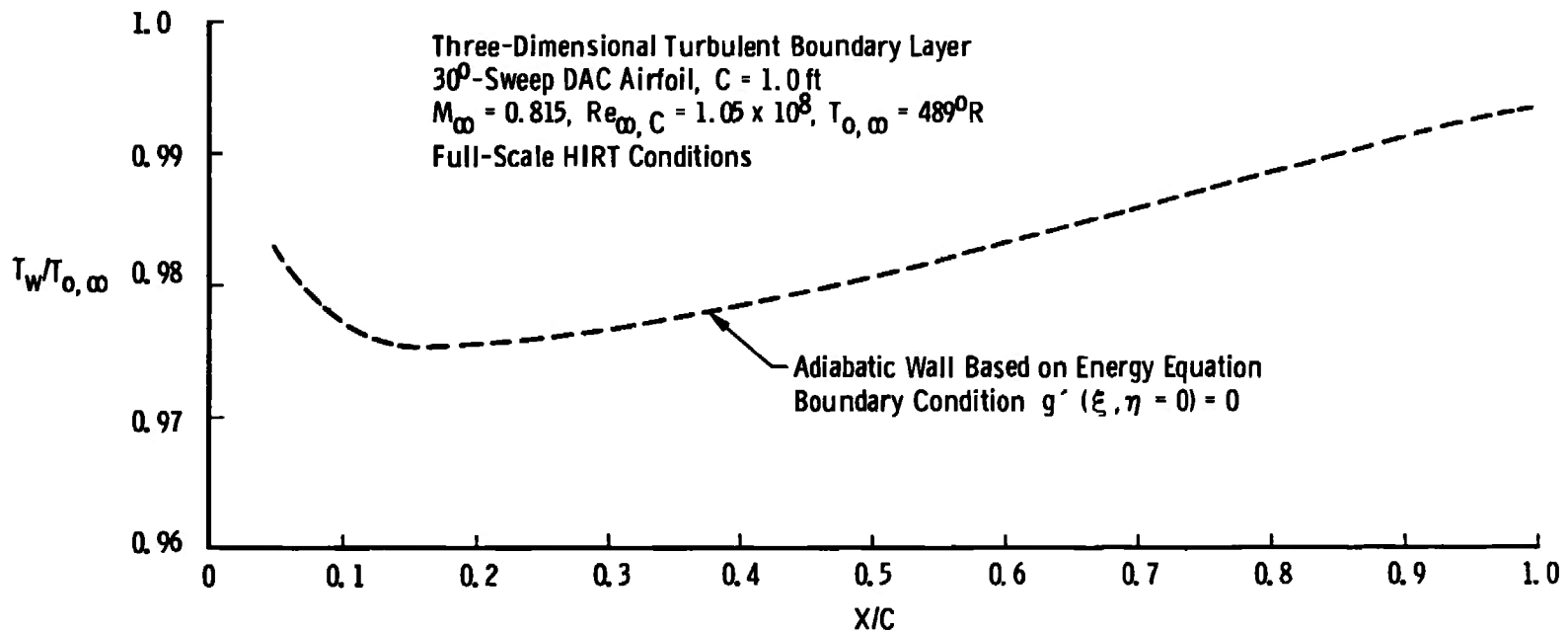
Fig. 26 Adiabatic-Wall Temperature Distribution on the DAC Airfoil under Full-Scale HIRT Conditions
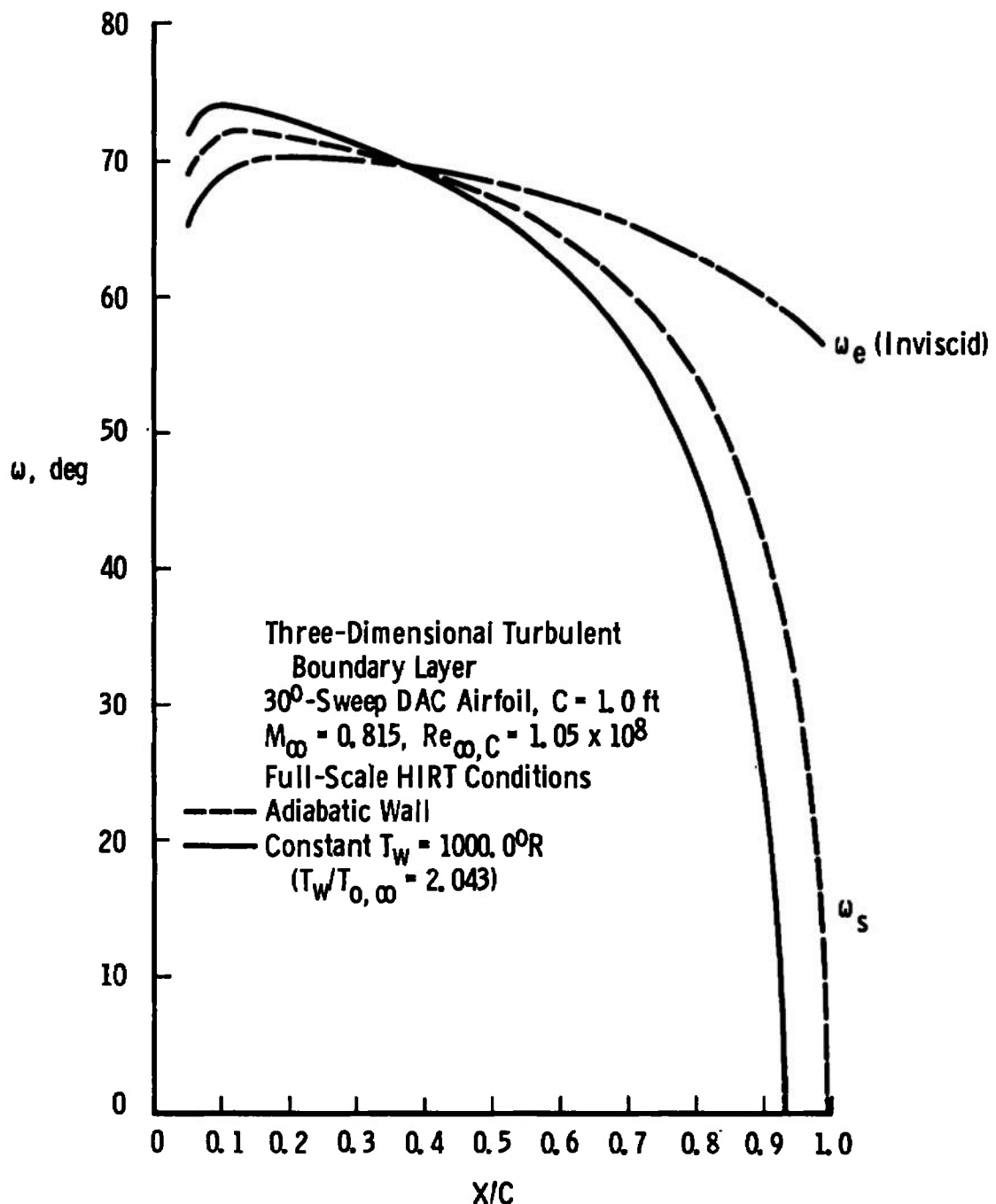
Fig. 27 Hot-Wall Effects on Surface Flow Angle Distribution
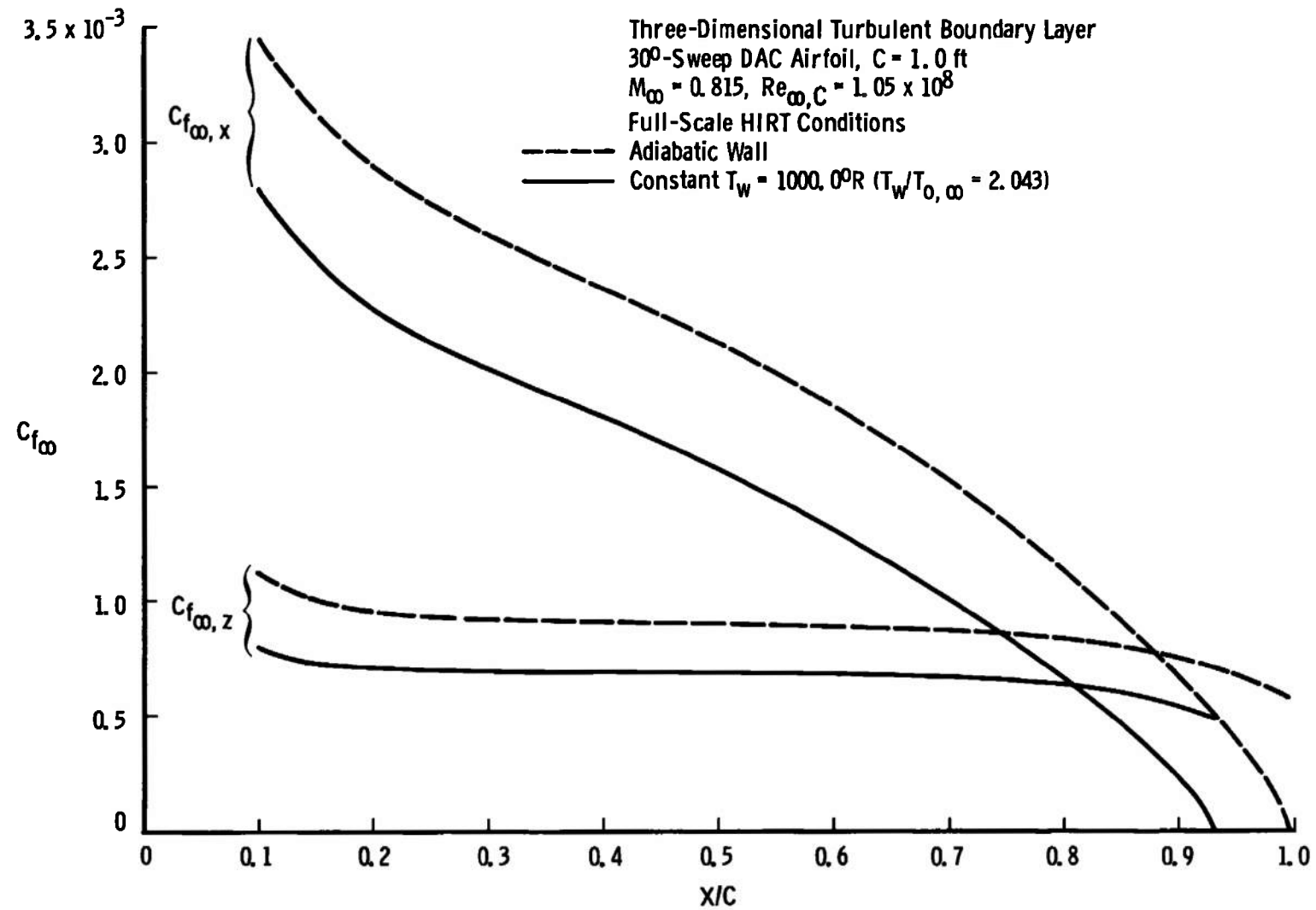
Fig. 28 Hot-Wall Effects on Skin-Friction Coefficient Distributions
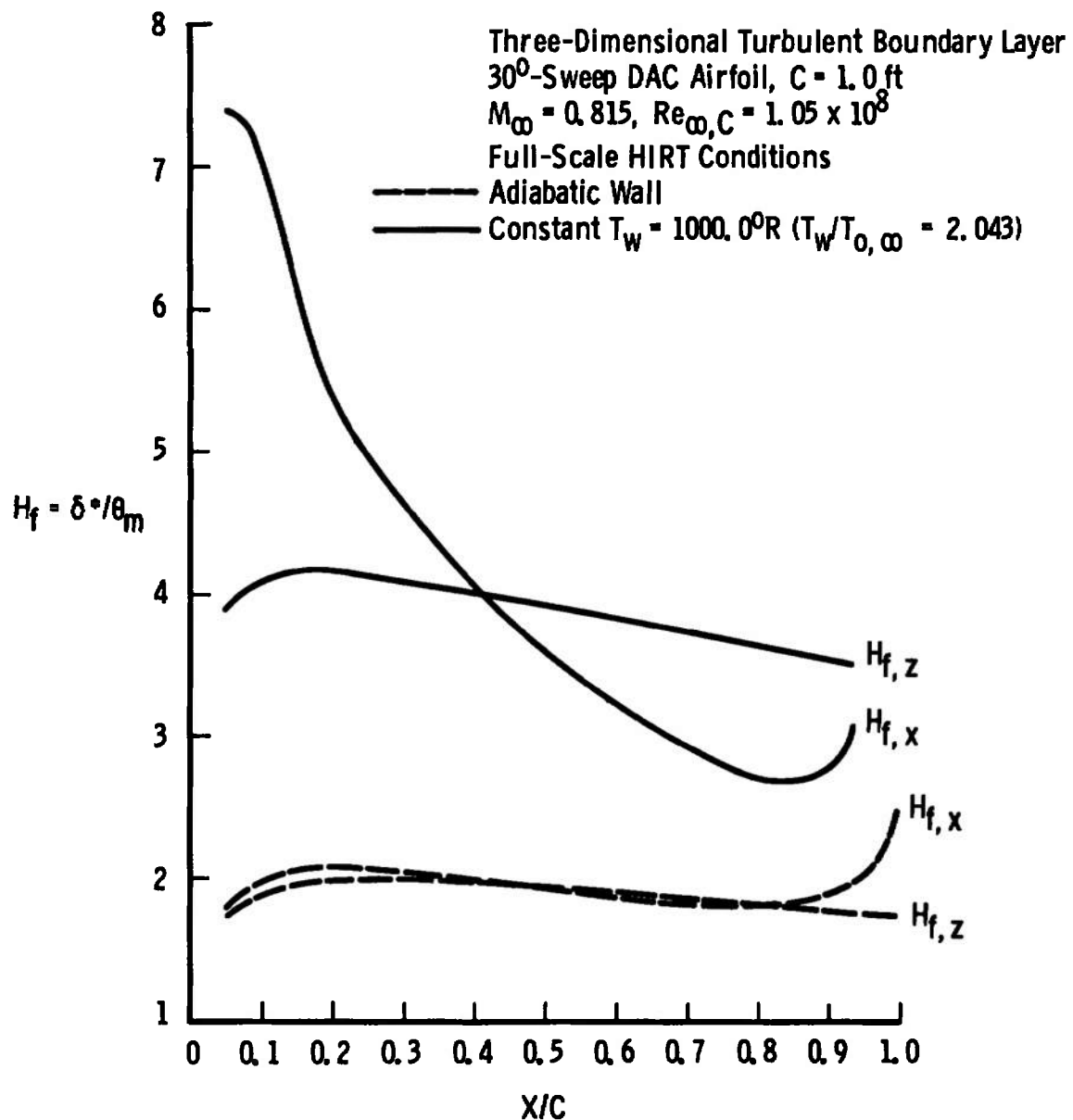
Fig. 29 Hot-Wall Effects on Shape Factor Distributions
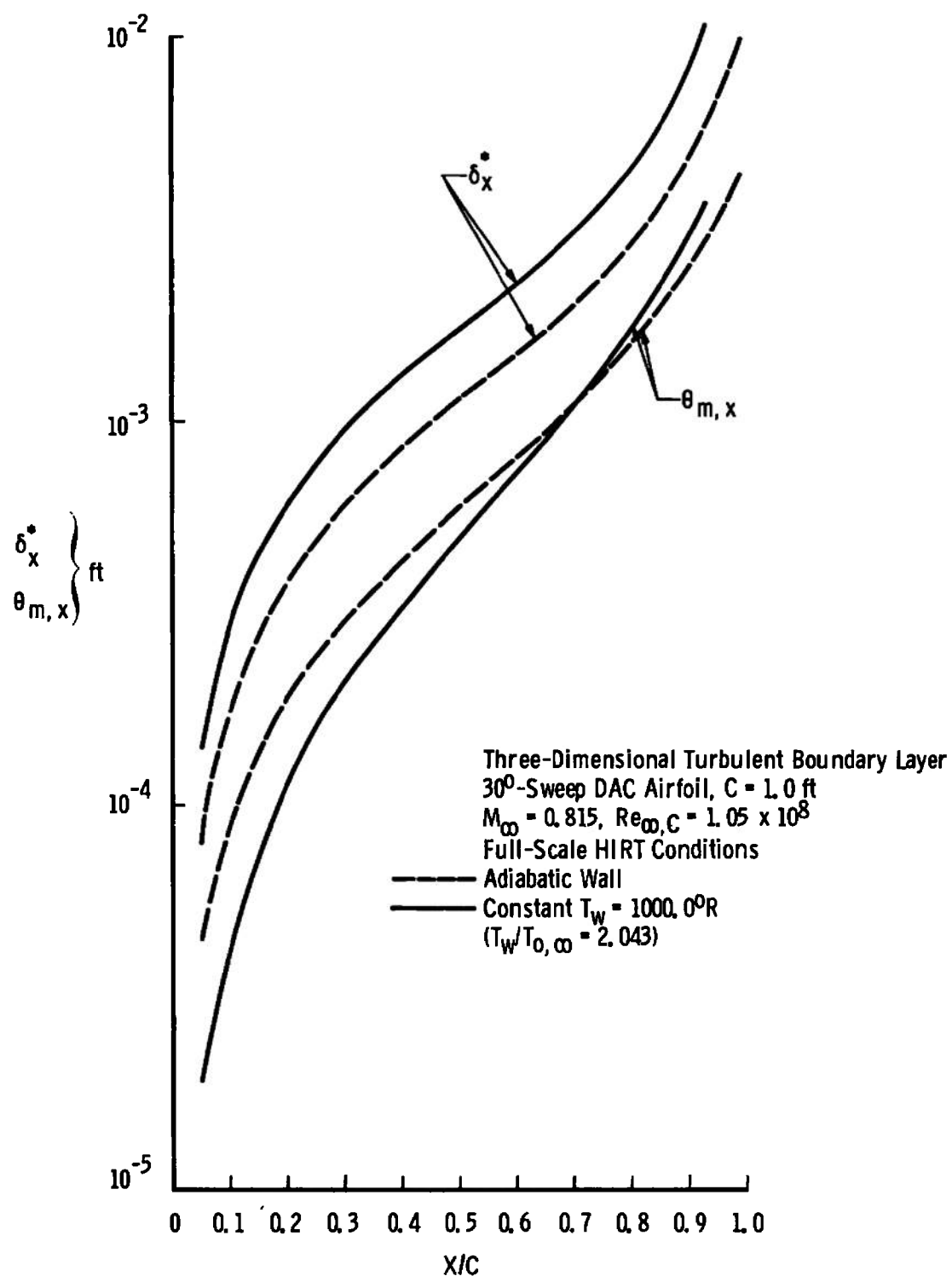
Fig. 30 Hot-Wall Effects on x-Direction Displacement and Momentum
Thickness Distributions
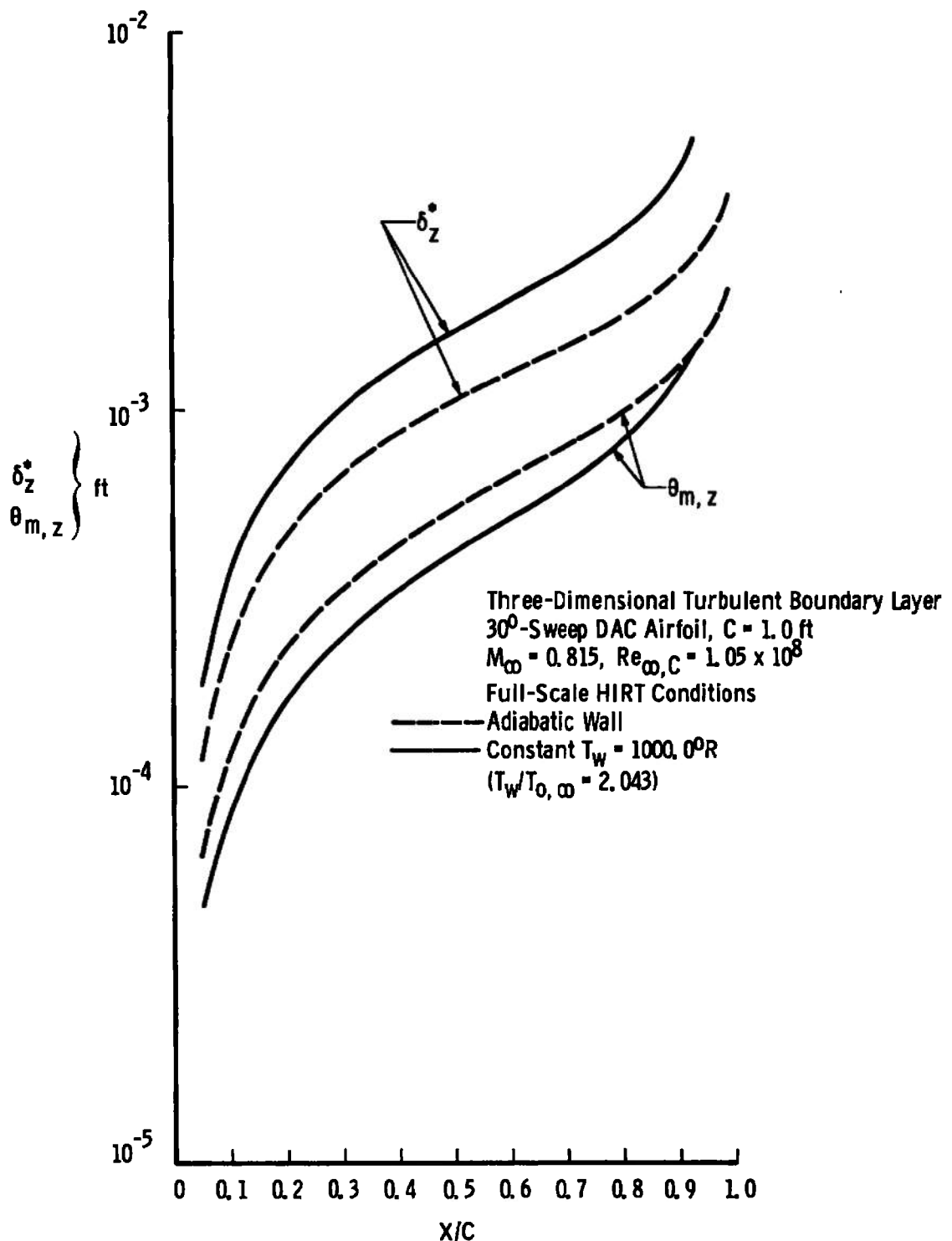
Fig. 31 Hot-Wall Effects on z-Direction Displacement and Momentum
Thickness Distributions

Three-Dimensional Turbulent Boundary Layer

30°-Sweep DAC Airfoil, C = 1.0 ft

$M_\infty = 0.815$, $Re_{\infty,C} = 1.05 \times 10^8$

Full-Scale HIRT Conditions

Constant $T_w = 1000.0^O R$ $(T_w/T_{0,\infty} = 2.043)$

$$St_\infty = \frac{-\dot{q}_w}{\rho_\infty V_\infty C_p (T_{0,\infty} - T_w)}$$
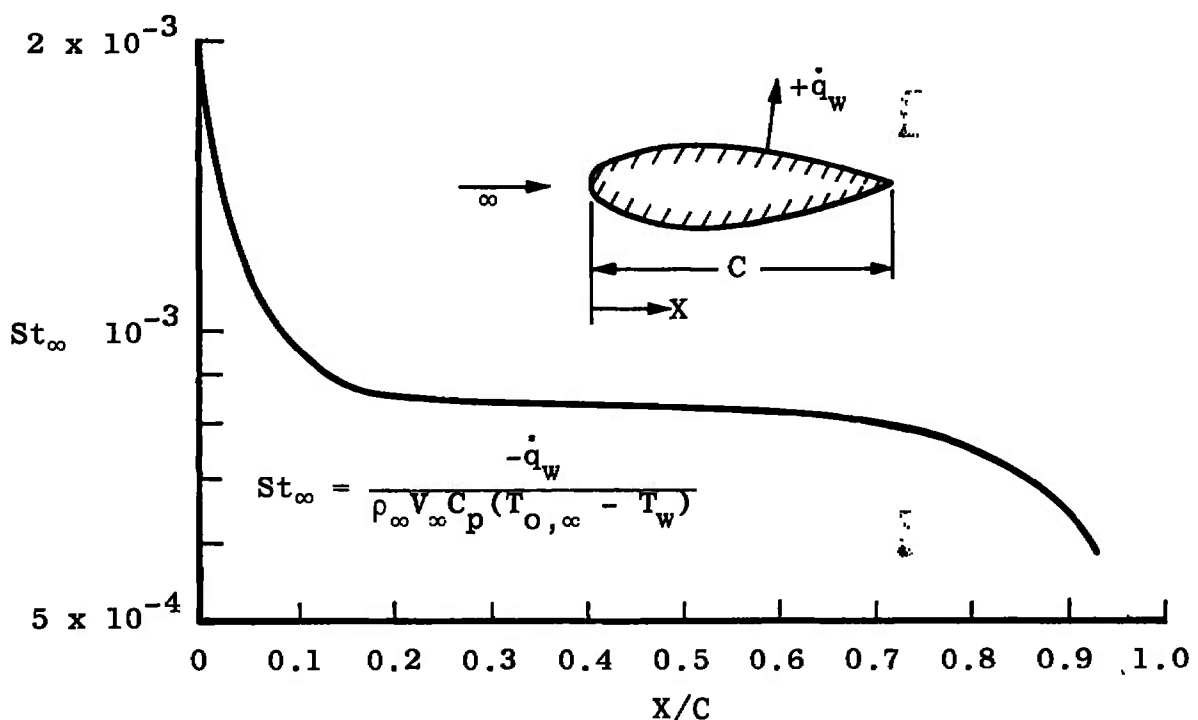
Fig 32 Stanton Number Distribution on the DAC Airfoil under
Hot-Wall Conditions
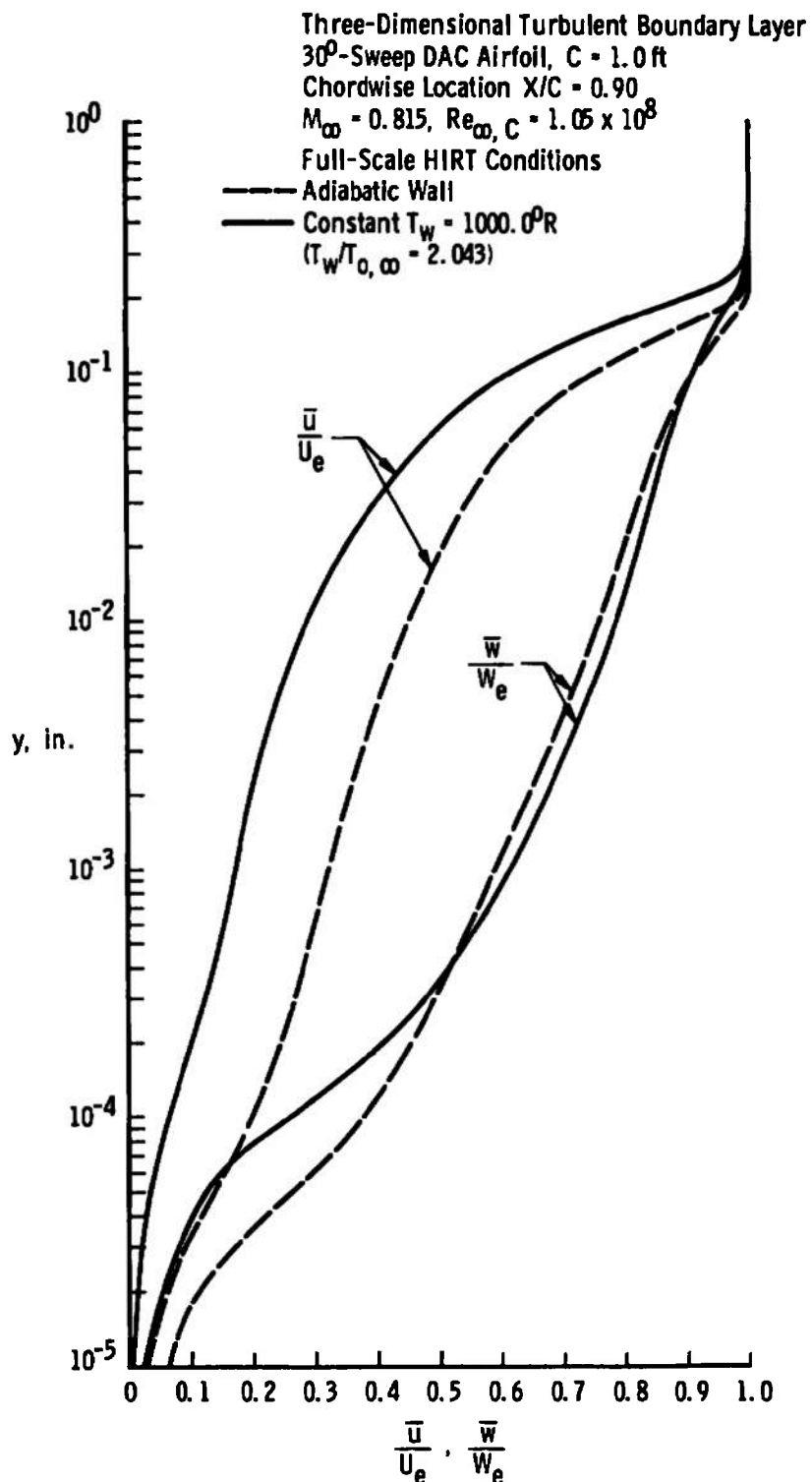
Fig. 33 Hot-Wall Effects on Turbulent Boundary-Layer Velocity Profiles
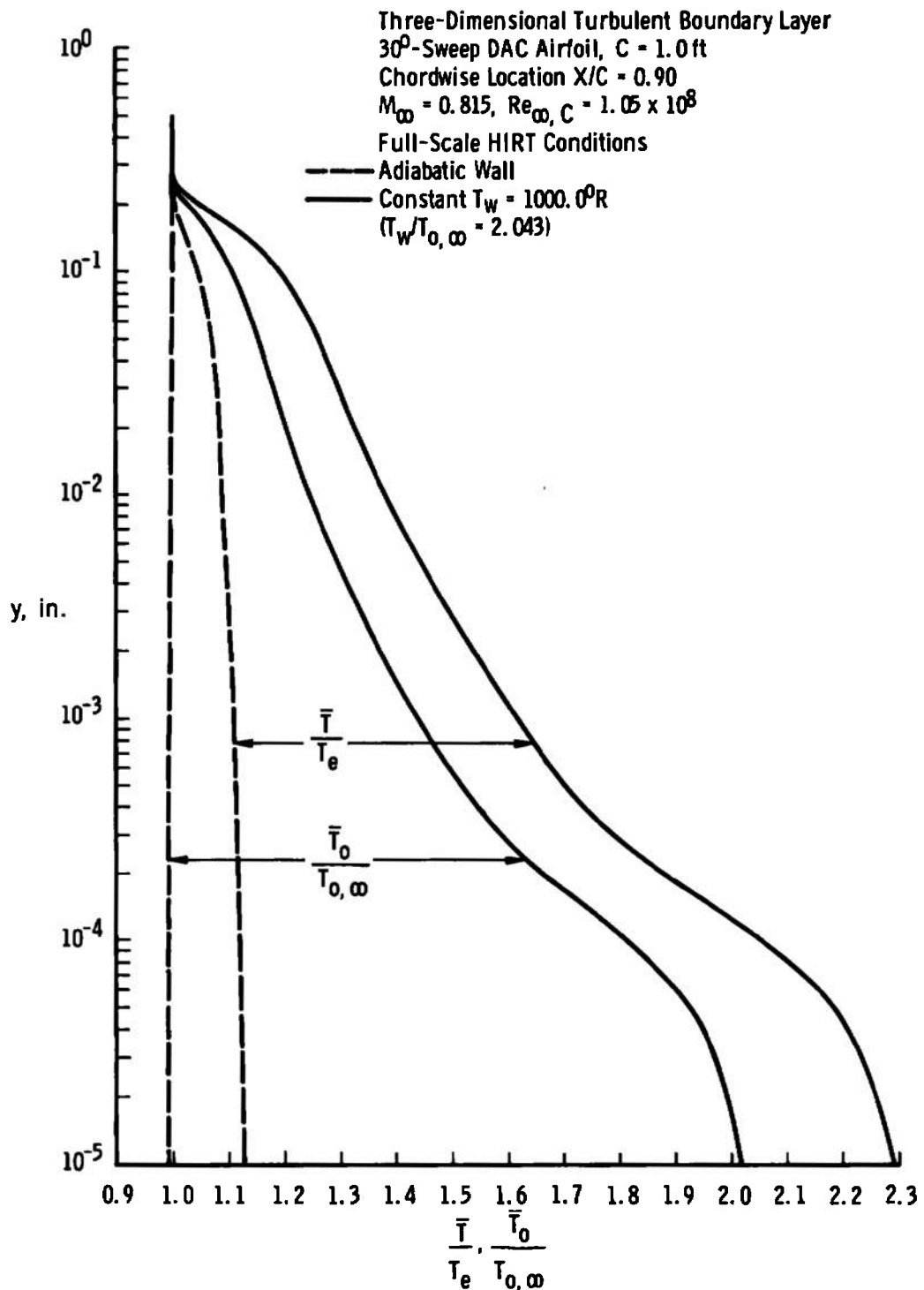
Fig. 34 Hot-Wall Effects on Turbulent Boundary-Layer Temperature Profiles

TABLE I
NACA 63$_1$-012 AIRFOIL ORDINATES AND INVISCID
SURFACE VELOCITY DISTRIBUTION*

| X/C, percent	Y/C, percent	$\left(\dfrac{U_e}{V_\infty \cos \Lambda}\right)^2$	$\dfrac{U_e}{V_\infty \cos \Lambda}$	$\dfrac{\Delta U_{e,a}}{V_\infty \cos \Lambda}$
0.0	0.0	0.0	0.0	2.336
0.50	0.935	0.750	0.866	1.695
0.75	1.194	0.925	0.962	1.513
1.25	1.519	1.005	1.003	1.266
2.50	2.102	1.129	1.063	0.933
5.00	2.925	1.217	1.103	0.682
7.50	3.542	1.261	1.123	0.559
10.00	4.039	1.294	1.138	0.484
15.00	4.799	1.330	1.153	0.387
20.00	5.342	1.349	1.161	0.326
25.00	5.712	1.362	1.167	0.283
30.00	5.930	1.370	1.170	0.249
35.00	6.000	1.366	1.169	0.221
40.00	5.920	1.348	1.161	0.196
45.00	5.704	1.317	1.148	0.174
50.00	5.370	1.276	1.130	0.155
55.00	4.935	1.229	1.109	0.137
60.00	4.420	1.181	1.087	0.121
65.00	3.840	1.131	1.063	0.106
70.00	3.210	1.076	1.037	0.091
75.00	2.556	1.023	1.011	0.079
80.00	1.902	0.969	0.984	0.067
85.00	1.274	0.920	0.959	0.055
90.00	0.707	0.871	0.933	0.042
95.00	0.250	0.826	0.909	0.029
100.00	0.0	0.791	0.889	0.0

Leading Edge Radius = 1.087 percent C

*Table taken from Abbott and von Doenhoff (Ref. 28, p. 337)

APPENDIX III
IMPLICIT FINITE-DIFFERENCE SOLUTION OF GOVERNING BOUNDARY-LAYER EQUATIONS

The governing turbulent boundary-layer equations for flow over an infinite yawed airfoil as derived in Section 2.6 of the present report form a set of coupled, nonlinear, parabolic, partial differential equations with the transformed coordinates ξ and η as the independent variables. For completeness, these governing equations (Eqs. (38), (39), and (40)) are repeated below with primes denoting partial differentiation with respect to the η-coordinate:

x - MOMENTUM

$$\ell^* f''' + \left[\frac{\partial \ell^*}{\partial \eta} + f\right] f'' + \beta[\theta - (f')^2] = 2\xi\left[f'\frac{\partial f'}{\partial \xi} - f''\frac{\partial f}{\partial \xi}\right] \qquad \text{(III-1)}$$

z - MOMENTUM

$$\ell^* c'' + \left[\frac{\partial \ell^*}{\partial \eta} + f\right] c' = 2\xi\left[f'\frac{\partial c}{\partial \xi} - c'\frac{\partial f}{\partial \xi}\right] \qquad \text{(III-2)}$$

ENERGY

$$\left(\frac{\ell^{**}}{\text{Pr}}\right) g'' + \left[\frac{\partial}{\partial \eta}\left(\frac{\ell^{**}}{\text{Pr}}\right) + f\right] g' + \Omega' = 2\xi\left[f'\frac{\partial g}{\partial \xi} - g'\frac{\partial f}{\partial \xi}\right] \qquad \text{(III-3)}$$

with the definitions

$$f' = \frac{\overline{u}}{U_e} \qquad \text{(III-4)}$$

$$c = \frac{\overline{w}}{W_e} \qquad \text{(III-5)}$$

$$g = \frac{\overline{H}}{H_e} \qquad \text{(III-6)}$$

$$\theta = \frac{\rho_e}{\overline{\rho}} = \frac{\overline{T}}{T_e} \qquad \text{(III-7)}$$

$$\ell = \frac{\bar{\rho}\mu}{\rho_e \mu_e} \tag{III-8}$$

$$\ell^* = \ell[1 + \frac{\epsilon}{\mu}] \tag{III-9}$$

$$\ell^{**} = \ell\left[1 + \frac{\epsilon}{\mu} \frac{Pr}{Pr_t}\right] \tag{III-10}$$

$$\beta = \frac{2\xi}{U_e} \frac{dU_e}{d\xi} \tag{III-11}$$

$$\Omega = \ell\left[\frac{\epsilon}{\mu}\left(1 - \frac{1}{Pr_t}\right) + \left(1 - \frac{1}{Pr}\right)\right]\left[\frac{U_e^2}{H_e} f'f'' + \frac{W_e^2}{H_e} cc'\right] \tag{III-12}$$

The boundary conditions are:

MOMENTUM

$$\left.\begin{array}{l} f(\xi,\eta = 0) = 0 \\[2mm] f'(\xi,\eta = 0) = 0 \\[2mm] \lim_{\eta \to \infty} f'(\xi,\eta) = 1 \end{array}\right\} \tag{III-13}$$

$$\left.\begin{array}{l} c(\xi,\eta = 0) = 0 \\[2mm] \lim_{\eta \to \infty} c(\xi,\eta) = 1 \end{array}\right\} \tag{III-14}$$

ENERGY

$$\left.\begin{array}{ll} g(\xi,\eta = 0) = \dfrac{H_w}{H_e} = \dfrac{h_w}{H_e} = g_w & \text{(Prescribed Wall Enthalpy)} \\[4mm] g'(\xi,\eta = 0) = 0 & \text{(Adiabatic Wall)} \\[4mm] \lim_{\eta \to \infty} g(\xi,\eta) = 1 & \end{array}\right\} \tag{III-15}$$

Following the approach by Blottner (Ref. 46) and Davis (Ref. 47), the momentum and energy equations (III-1, -2, and -3) are rewritten in "standard" form for a parabolic partial differential equation as

$$\frac{\partial^2 W}{\partial \eta^2} + a_1 \frac{\partial W}{\partial \eta} + a_2 W + a_3 + a_4 \frac{\partial W}{\partial \xi} = 0 \qquad \text{(III-16)}$$

where $W = f'$ for the x-momentum equation, $W = c$ for the z-momentum equation, and $W = g$ for the energy equation. Using Eqs. (III-1, -2, and -3), one finds the coefficients α_1 through α_4 in linearized form:

x-MOMENTUM

$$a_1 = \frac{\dfrac{\partial \ell^*}{\partial \eta} + f + 2\xi \dfrac{\partial f}{\partial \xi}}{\ell^*} \qquad \text{(III-17)}$$

$$a_2 = \frac{-\beta f'}{\ell^*} \qquad \text{(III-18)}$$

$$a_3 = \frac{\beta \theta}{\ell^*} \qquad \text{(III-19)}$$

$$a_4 = \frac{-2\xi f'}{\ell^*} \qquad \text{(III-20)}$$

z-MOMENTUM

$$a_1 = \frac{\dfrac{\partial \ell^*}{\partial \eta} + f + 2\xi \dfrac{\partial f}{\partial \xi}}{\ell^*} \qquad \text{(III-21)}$$

$$a_2 = 0 \qquad \text{(III-22)}$$

$$a_3 = 0 \qquad \text{(III-23)}$$

$$a_4 = \frac{-2\xi f'}{\ell^*} \qquad \text{(III-24)}$$

ENERGY

$$a_1 = \frac{\dfrac{\partial}{\partial \eta}\left(\dfrac{\ell^{**}}{\mathrm{Pr}}\right) + f + 2\xi \dfrac{\partial f}{\partial \xi}}{\left(\dfrac{\ell^{**}}{\mathrm{Pr}}\right)} \qquad \text{(III-25)}$$

$$a_2 = 0 \qquad \text{(III-26)}$$

$$a_3 = \frac{\Omega'}{\left(\frac{\ell^{**}}{Pr}\right)} \qquad (III\text{-}27)$$

$$a_4 = \frac{-2\xi\ell'}{\left(\frac{\ell^{**}}{Pr}\right)} \qquad (III\text{-}28)$$

The η derivatives in Eq. (III-16) are replaced with finite-difference quotients which allow variable grid spacing in the η direction in order to concentrate grid points in the region near the body surface where the dependent variables change most rapidly. The derivative in the ξ direction in Eq. (III-16) is handled in the usual manner as a two-point backward difference between points (m+1, n) and (m, n), whereas all η derivatives are evaluated at point (m+1, n) according to the grid mesh shown below.

Station
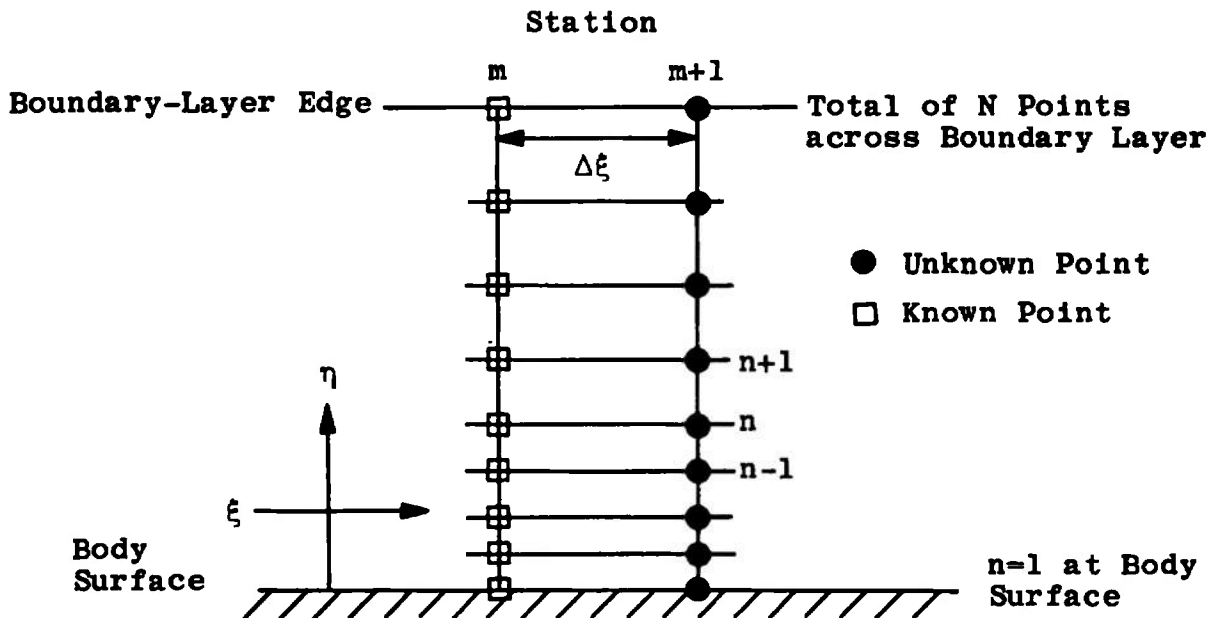
The solution is assumed to be known at point (m, n) and unknown at point (m+1, n) so that the finite-difference scheme to be constructed will be implicit in nature. The finite-difference replacements for the derivatives are as follows (see Appendix IV of Ref. 13 for derivation):

$$\left[\frac{\partial^2 W}{\partial \eta^2}\right]_{m+1,n} = \frac{2[W_{n+1} + KW_{n-1} - (1+K)W_n]_{m+1}}{D_2} \qquad (III\text{-}29)$$

85

$$\left[\frac{\partial W}{\partial \eta}\right]_{m+1,n} = \frac{\left[W_{n+1} - K^2 W_{n-1} - (1 - K^2) W_n\right]_{m+1}}{D_1} \quad \text{(III-30)}$$

$$\left[\frac{\partial W}{\partial \xi}\right]_{m+1,n} = \frac{W_{m+1,n} - W_{m,n}}{\Delta \xi} \quad \text{(III-31)}$$

where

$$D_1 = (\eta_{n+1} - \eta_n) + K^2(\eta_n - \eta_{n-1}) \quad \text{(III-32)}$$

$$D_2 = (\eta_{n+1} - \eta_n)^2 + K(\eta_n - \eta_{n-1})^2 \quad \text{(III-33)}$$

$$K = \frac{\eta_{n+1} - \eta_n}{\eta_n - \eta_{n-1}} \text{ (constant)} \quad \text{(III-34)}$$

$$\zeta = \eta_2 - \eta_1 \text{ (constant)} \quad \text{(III-35)}$$

The finite-difference form of Eq. (III-16) becomes, upon substitution of Eqs. (III-29, -30, and -31),

$$\bar{A}_n W_{m+1,n+1} + \bar{B}_n W_{m+1,n} + \bar{C}_n W_{m+1,n-1} = \bar{D}_n \quad \text{(III-36)}$$

where

$$\bar{A}_n = \frac{2}{D_2} + \frac{\alpha_1}{D_1} \quad \text{(III-37)}$$

$$\bar{B}_n = \frac{-2(1 + K)}{D_2} - \frac{\alpha_1(1 - K^2)}{D_1} + \alpha_2 + \frac{\alpha_4}{\Delta \xi} \quad \text{(III-38)}$$

$$\bar{C}_n = \frac{2K}{D_2} - \frac{K^2 \alpha_1}{D_1} \quad \text{(III-39)}$$

$$\bar{D}_n = -\alpha_3 + \frac{\alpha_4 W_{m,n}}{\Delta \xi} \quad \text{(III-40)}$$

For Eq. (III-36) to be linear, the coefficients A_n, B_n, C_n, and D_n must be treated as known quantities at point n; more will follow on this subject later. The important point is that Eq. (III-36) represents a set of simultaneous linear algebraic equations under this restriction.

Since the simultaneous linear algebraic equations resulting from Eq. (III-36) are of a special form (tridiagonal), an efficient method of

solution on a digital computer is available from Richtmyer and Morton (Ref. 48, pp. 198-201 and 274-282). For this procedure the boundary condition at the outer edge (n = N) must have a specified value $W_{m+1,N}$; special procedures (see Appendix IV) are required at the wall (n = 1). Because of the special form of Eq. (III-36), the relation

$$W_{m+1,n} = E_n W_{m+1,n+1} + e_n, \quad 2 \leq n \leq N-1 \tag{III-41}$$

exists where

$$E_2 = \frac{-(\bar{A}_2 + \bar{C}_2 F_3)}{\bar{B}_2 + \bar{C}_2 F_2} \tag{III-42}$$

$$e_2 = \frac{\bar{D}_2 - \bar{C}_2 F_1}{\bar{B}_2 + \bar{C}_2 F_2} \tag{III-43}$$

$$E_n = \frac{-\bar{A}_n}{\bar{B}_n + \bar{C}_n E_{n-1}} \left.\right\} \tag{III-44}$$

$$e_n = \frac{\bar{D}_n - \bar{C}_n e_{n-1}}{\bar{B}_n + \bar{C}_n E_{n-1}} \left.\right\} \quad 3 \leq n \leq N-1 \tag{III-45}$$

with the numerical constants F_1, F_2, and F_3 defined as in Appendix IV. The quantities E_n and e_n are computed from Eqs. (III-42) through (III-45) starting with n = 2 and progressing to n = N-1. The solution $W_{m+1,n}$ is then obtained by evaluating Eq. (III-41) from n = N-1 to n = 2 with the wall value (n = 1) evaluated from Eq. (IV-10) of Appendix IV according to

$$W_{m+1,1} = F_1 + F_2 W_{m+1,2} + F_3 W_{m+1,3} \tag{III-46}$$

where F_1, F_2, and F_3 are numerical constants defined in Appendix IV.

Knowing the distribution of the f' and θ profiles across the boundary layer from the above procedure, one can evaluate the transformed stream function f from

$$f(\xi,\eta) = \int_0^\eta f'(\xi,\eta) \, d\eta \tag{III-47}$$

where the integral is numerically integrated using the well-known trapezoidal rule, viz.,

$$f(\xi,\eta = \eta_n) = \sum_{i=2}^{n} [f'(\xi,\eta = \eta_i) + f'(\xi,\eta = \eta_{i-1})] D_i \tag{III-48}$$

with

$$D_i = \frac{\eta_i - \eta_{i-1}}{2} \qquad (III\text{-}49)$$

Inversion from the transformed (ξ, η) plane to the physical (x, y) plane is, from Eq. (63),

$$y = \frac{\sqrt{2\xi}}{\rho_e U_e} \int_o^\eta \frac{\rho_e}{\rho} d\eta \qquad (III\text{-}50)$$

where

$$\frac{\rho_e}{\rho} = \frac{\bar{T}}{T_e} = \theta \qquad (III\text{-}51)$$

because of the constancy of static pressure across the boundary layer. Again, using the trapezoidal rule method of numerical integration yields

$$y_n = \frac{\sqrt{2\xi}}{\rho_e U_e} \sum_{i=2}^{n} [\theta(\xi, \eta = \eta_i) + \theta(\xi, \eta = \eta_{i-1})] D_i \qquad (III\text{-}52)$$

with D_i given by Eq. (III-49). The relationship between ξ and x is determined from integration of Eq. (31)

$$\xi = \int_o^x \rho_e \mu_e U_e \, dx \qquad (III\text{-}53)$$

using trapezoidal rule numerical integration to advance from station m to station m+1; i.e.,

$$\xi_{m+1} = \xi_m + [(\rho_e \mu_e U_e)_m + (\rho_e \mu_e U_e)_{m+1}] \frac{\Delta x}{2} \qquad (III\text{-}54)$$

where Δx is the x-direction step size integration increment defined by

$$\Delta x = x_{m+1} - x_m \qquad (III\text{-}55)$$

Note that arbitrary x-direction station locations are allowed via the above approach; e.g., one can decrease the x-direction step size in regions of strong adverse pressure gradient in order to accurately define the location of boundary-layer separation.

The variable η-direction grid mesh used in the present work is taken from Smith and Cebeci (Ref. 49). The various constants used herein are as follows:

$$N = 161, K = 1.063, \zeta = 0.0010$$

Experience with varying these constants and observing their influence on the resultant numerical solution has indicated that the above choices are adequate under the present subsonic and transonic high Reynolds number flow conditions. These values may not be satisfactory, however, for other body geometries and flow conditions; thus, the influence of the variable grid mesh constants should be ascertained for each new investigation.

The mathematical basis of the above tridiagonal matrix procedure applied to the solution of boundary-layer problems is from Flügge-Lotz and Blottner (Ref. 50). The present application differs from their original work in one important aspect: the linearized difference equations herein are uncoupled and solved separately. In Flügge-Lotz and Blottner's approach, the difference equations remain coupled and require additional machine storage and manipulations for solution. With the present uncoupled approach, the difference equations are iterated to convergence at each station along the body; thus, one must pay the price of iteration. Through this procedure the linearizing coefficients α_1 through α_4 are evaluated at each station using the results of the previous iteration. Iteration at a given station is continued until successive values of f', c, and g differ by less than 0.10 percent from the corresponding value of the preceding cycle. Typically, about three to eight iterations per station are required for both laminar and turbulent cases, with the number of iterations per station increasing as the pressure gradient parameter, β, increases. Use of the above procedure gives a final solution at each station which is exact in the sense that it represents a converged iterated solution to the governing nonlinear partial differential equations written in finite-difference form.

Along the stagnation or attachment line of a blunt-nosed infinite extent yawed airfoil where $\xi = 0$ since x = 0, the governing boundary-layer equations (III-1), (III-2), and (III-3) reduce to the following ordinary, nonlinear, differential equations:

x-MOMENTUM

$$\ell^* f''' + \left[\frac{\partial \ell^*}{\partial \eta} + f\right] f'' + \beta[\theta - (f')^2] = 0 \qquad \text{(III-56)}$$

z-MOMENTUM

$$\ell^* c'' + \left[\frac{\partial \ell^*}{\partial \eta} + f\right] c' = 0 \qquad \text{(III-57)}$$

ENERGY

$$\left(\frac{\ell^{**}}{Pr}\right)g'' + \left[\frac{\partial}{\partial\eta}\left(\frac{\ell^{**}}{Pr}\right) + f\right]g' + \Omega' = 0 \qquad \text{(III-58)}$$

with the boundary conditions (III-13) through (III-15). In order to obtain starting profiles for the finite-difference scheme to march downstream, Eqs. (III-56), (III-57), and (III-58) are solved in the following manner by using the tridiagonal matrix procedure described previously. Along the stagnation or attachment line, $\xi = 0$ so that $\alpha_4 = 0$ in both of the momentum equations, as well as in the energy equation; in addition, the term containing ξ in α_1 of both the momentum and energy equations vanishes. Furthermore, $\beta = 1$ at $\xi = 0$ under the restriction that

$$U_e \approx \left[\frac{dU_e}{dx}\right]_{x=0} x$$

near x = 0. Initial guesses for f', c, and g are input to the analysis as

$$f'_I = 1 - \exp(-\eta) \qquad \text{(III-59)}$$

$$c_I = f'_I \qquad \text{(III-60)}$$

$$g_I = g_w + (1 - g_w)f'_I \qquad \text{(III-61)}$$

where the subscript I denotes the initial approximation. The equations are then iterated to convergence in the same manner described previously; an averaging scheme is used to speed convergence. Typically, about 10 to 20 iterations are required to generate a converged initial solution for a laminar boundary layer. Approximately 60 iterations are required for a converged turbulent boundary-layer solution.

By the use of the above procedures the numerical solution of any two-point boundary-value problem governed by either linear or nonlinear ordinary differential equations, as well as sets of coupled parabolic partial differential equations (either linear or nonlinear) is reduced to subroutine status on a digital computer in that only the coefficients α_1 through α_4 must be defined in conjunction with the required boundary conditions for each new problem. Based on experience with analyses of this type, the use of the iterative tridiagonal matrix approach where applicable is highly recommended.

APPENDIX IV
## FINITE-DIFFERENCE FORMALISM OF WALL BOUNDARY CONDITIONS

Evaluation of heat-transfer rate and shear stress at the body surface requires numerical determination of the wall derivatives $g'(\xi, \eta = 0)$, $c'(\xi, \eta = 0)$, and $f''(\xi, \eta = 0)$ since

$$\dot{q}_w \propto g'(\xi, \eta - 0)$$

$$\tau_{w,x} \propto f''(\xi, \eta = 0)$$

$$\tau_{w,z} \propto c'(\xi, \eta = 0)$$

as shown in Eqs. (59), (61), and (62). Consistent with the variable η-direction grid mesh spacing defined in Appendix III, the wall derivatives are evaluated in the present work by application of the three-point Lagrangian interpolation formula (Ref. 51, pp. 71-77) evaluated according to the following diagram:
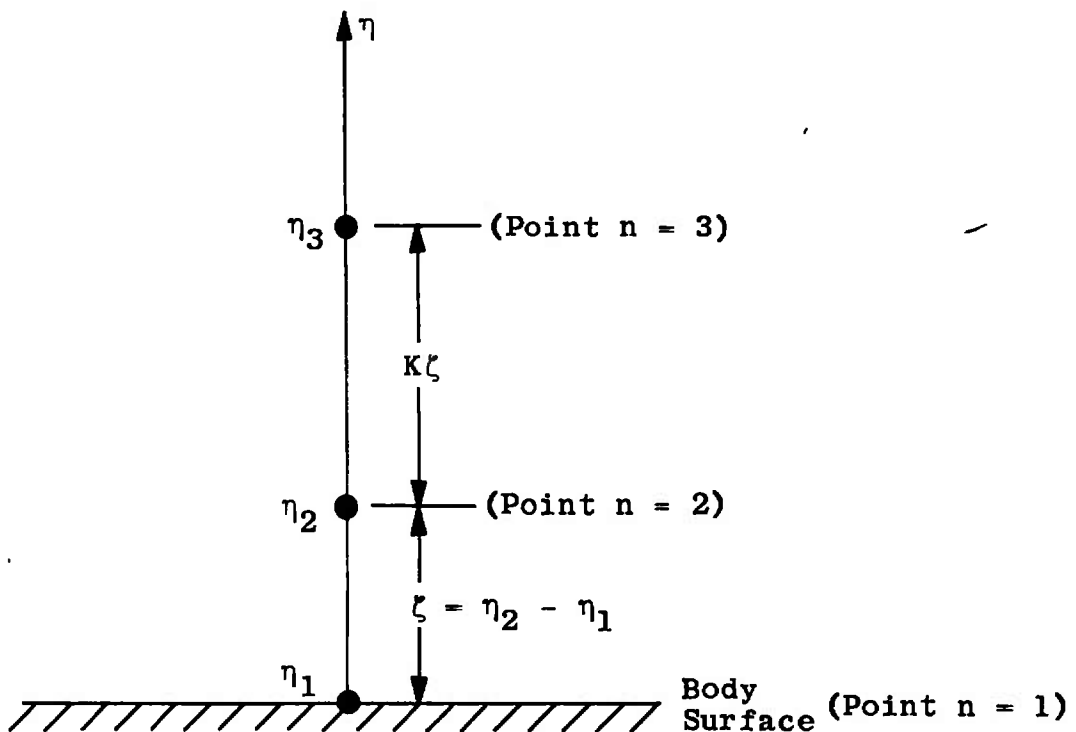
which yields, at station m+1,

$$f''(\eta=0) = \zeta[B_1(2+K)f'_{\eta_1} + B_2(1+K)f'_{\eta_2} + B_3 f'_{\eta_3}] \qquad \text{(IV-1)}$$

$$c'(\eta=0) = \zeta[B_1(2+K)c_{\eta_1} + B_2(1+K)c_{\eta_2} + B_3 c_{\eta_3}] \qquad \text{(IV-2)}$$

$$g'(\eta=0) = \zeta[B_1(2+K)g_{\eta_1} + B_2(1+K)g_{\eta_2} + B_3 g_{\eta_3}] \qquad \text{(IV-3)}$$

where

$$B_1 = \frac{-1}{\zeta^2(1+K)} \qquad \text{(IV-4)}$$

$$B_2 = \frac{+1}{K\zeta^2} \qquad \text{(IV-5)}$$

$$B_3 = \frac{-1}{\zeta^2 K(1+K)} \qquad \text{(IV-6)}$$

and

$$f'_{\eta_i} = f'(\eta = \eta_i) \qquad \text{(IV-7)}$$

$$c_{\eta_i} = c(\eta = \eta_i) \qquad \text{(IV-8)}$$

$$g_{\eta_i} = g(\eta = \eta_i) \qquad \text{(IV-9)}$$

with i = 1, 2, and 3. The parameters K and ζ are defined by Eqs. (III-34) and (III-35), respectively, in Appendix III. The use of the three-point Lagrangian interpolation formula for the wall derivatives is consistent with the formulation of the variable grid spacing derivatives presented in Appendix IV of Ref. 13 and follows the work of Smith and Cebecci (Ref. 49, Appendix C).

As stated in Appendix III, the tridiagonal matrix procedure requires special formalism at the wall. With reference to the above-presented sketch (which is taken to apply at the body station m+1 where the unknown solution is to be determined), assume that the points n = 1, 2, and 3 are related according to the general relation

$$W_1 = F_1 + F_2 W_2 + F_3 W_3 \qquad \text{(IV-10)}$$

where F_1, F_2, and F_3 are numerical constants to be determined and W is the generalized dependent variable defined in conjunction with Eq. (III-16) of Appendix III; note that

$$W_1 = W_{m+1,n=1}$$
$$W_2 = W_{m+1,n=2} \Bigg\}$$
$$W_3 = W_{m+1,n=3}$$

(IV-11)

Using Eq. (IV-10) in Eq. (III-36) of Appendix III evaluated at the point n = 2 yields

$$\overline{A}_2 W_3 + \overline{B}_2 W_2 + \overline{C}_2(F_1 + F_2 W_2 + F_3 W_3) = \overline{D}_2$$

(IV-12)

which can be grouped in the form

$$W_2 = \frac{-(\overline{A}_2 + \overline{C}_2 F_3)}{\overline{B}_2 + \overline{C}_2 F_2} W_3 + \frac{\overline{D}_2 - \overline{C}_2 F_1}{\overline{B}_2 + \overline{C}_2 F_2}$$

(IV-13)

Evaluating Eq. (III-41) of Appendix III at the point n = 2 yields

$$W_2 = E_2 W_3 + e_2$$

(IV-14)

which, upon comparison of Eqs. (IV-13) and (IV-14), results in the relationships

$$E_2 = \frac{-(\overline{A}_2 + \overline{C}_2 F_3)}{\overline{B}_2 + \overline{C}_2 F_2}$$

(IV-15)

$$e_2 = \frac{\overline{D}_2 - \overline{C}_2 F_1}{\overline{B}_2 + \overline{C}_2 F_2}$$

(IV-16)

corresponding to Eqs. (III-42) and (III-43) of Appendix III.

To evaluate the numerical constants F_1, F_2, and F_3 in Eq. (IV-10), suppose that the first derivative of the W function is prescribed to be the boundary condition at the wall point n = 1. Using the difference expression given by Eq. (IV-1) results in

$$W_1' = \left(\frac{\partial W}{\partial \eta}\right)_{n=1} = \zeta[B_1(2+K)W_1 + B_2(1+K)W_2 + B_3 W_3]$$

(IV-17)

Upon writing Eq. (IV-17) in the form

$$W_1 = \frac{-B_2(1+K)}{B_1(2+K)} W_2 + \frac{-B_3}{B_1(2+K)} W_3 + \frac{W_1'}{\zeta B_1(2+K)}$$

(IV-18)

93

and comparing Eqs. (IV-10) and (IV-18), the numerical constants F_1, F_2, and F_3 become defined as

$$F_1 = \frac{W_1'}{\zeta B_1 (2+K)} = \frac{-\zeta (1+K) W_1'}{2+K} \qquad \text{(IV-19)}$$

$$F_2 = \frac{-B_2 (1+K)}{B_1 (2+K)} = \frac{(1+K)^2}{K(2+K)} \qquad \text{(IV-20)}$$

$$F_3 = \frac{-B_3}{B_1 (2+K)} = \frac{-1}{K(2+K)} \qquad \text{(IV-21)}$$

where use has been made of Eqs. (IV-4), (IV-5), and (IV-6).

Now suppose that the value of the W function is prescribed to be the boundary condition at the wall point n = 1; e.g., $W_1 = W_w$. For this condition Eq. (IV-10) becomes

$$W_1 = F_1 + F_2 W_2 + F_3 W_3 = W_w \qquad \text{(IV-22)}$$

which requires that

$$F_1 = W_w \qquad \text{(IV-23)}$$

$$F_2 = 0 \qquad \text{(IV-24)}$$

$$F_3 = 0 \qquad \text{(IV-25)}$$

In summary of the above-derived boundary conditions relative to numerical solution of the boundary-layer equations via the tridiagonal matrix procedure, the following examples illustrate application to the wall boundary conditions of interest in the current work:

x-MOMENTUM EQUATION BOUNDARY CONDITION
GIVEN BY EQ. (III-13)

$$\text{Set: } F_1 = 0$$

$$F_2 = 0$$

$$F_3 = 0$$

$\underline{z}$-MOMENTUM EQUATION BOUNDARY CONDITION GIVEN BY EQ. (III-14)

$$\text{Set:} \quad F_1 = 0$$
$$F_2 = 0$$
$$F_3 = 0$$

ENERGY EQUATION BOUNDARY CONDITION FOR PRESCRIBED WALL TEMPERATURE g_w GIVEN BY EQ. (III-15)

$$\text{Set:} \quad F_1 = g_w$$
$$F_2 = 0$$
$$F_3 = 0$$

ENERGY EQUATION BOUNDARY CONDITION FOR ADIABATIC WALL GIVEN BY EQ. (III-15)

$$\text{Set:} \quad F_1 = 0$$

F_2 Defined by Eq. (IV-20)

F_3 Defined by Eq. (IV-21)

It should be noted that the above formalism allows completely general wall boundary conditions which can vary with respect to location on the body surface, e.g., variable wall temperature prescribed over the forward section of an airfoil with the aft section adiabatic.

DOCUMENT CONTROL DATA - R & D

(Security classification of title, body of abstract and indexing annotation must be entered when the overall report is classified)

1 ORIGINATING ACTIVITY (Corporate author)	2a. REPORT SECURITY CLASSIFICATION
Arnold Engineering Development Center Arnold Air Force Station, Tennessee 37389	UNCLASSIFIED 2b GROUP N/A

3 REPORT TITLE

NUMERICAL CALCULATION OF THE SUBSONIC AND TRANSONIC TURBULENT BOUNDARY LAYER ON AN INFINITE YAWED AIRFOIL

4 DESCRIPTIVE NOTES *(Type of report and inclusive dates)*

Final Report - April 1972 through April 1973

5. AUTHOR(S) *(First name, middle initial, last name)*

John C. Adams, Jr., ARO, Inc.

6 REPORT DATE	7a. TOTAL NO OF PAGES	7b. NO OF REFS
July 1973	108	51

8a CONTRACT OR GRANT NO	9a. ORIGINATOR'S REPORT NUMBER(S)
b. PROJECT NO	AEDC-TR-73-112
c. Program Element 65802F	9b OTHER REPORT NO(S) *(Any other numbers that may be assigned this report)*
d.	ARO-VKF-TR-73-52

10 DISTRIBUTION STATEMENT

Approved for public release; distribution unlimited.

11 SUPPLEMENTARY NOTES	12 SPONSORING MILITARY ACTIVITY
Available in DDC.	Arnold Engineering Development Center Air Force Systems Command Arnold AF Station, Tenn. 37389

13. ABSTRACT Formulation and application of a three-dimensional compressible turbulent boundary-layer analysis is presented for subsonic and transonic flow over a yawed airfoil of infinite extent. The governing turbulent boundary-layer equations are integrated using an implicit finite-difference procedure in conjunction with a scalar eddy viscosity model of three-dimensional turbulence. Comparisons with other analysis techniques as well as experimental measurements under subsonic wind tunnel conditions are presented to establish and ascertain the basic validity and applicability of the current technique. Also considered are the effects of a hot wall on the transonic, three-dimensional, turbulent boundary layer which have practical application to transonic Space Shuttle reentry, where the wing surface temperature may reach soak values on the order of twice the free-stream stagnation temperature because of the hypersonic high-heating phase of the reentry trajectory. Ground testing of Space Shuttle configurations under continuous transonic flow conditions with an adiabatic wall may not be totally applicable to actual Shuttle entry; airfoil static stall angle, maximum lift coefficient, local skin-friction, and other turbulent boundary-layer parameters are strongly affected by hot-wall relative to adiabatic-wall conditions

DD FORM 1473
1 NOV 65

14. KEY WORDS	LINK A		LINK B		LINK C	
	ROLE	WT	ROLE	WT	ROLE	WT
turbulent boundary layer						
numerical analysis						
subsonic flow						
transonic flow						
airfoils						
yaw						
Space Shuttle						
reentry						

1. Yawed airfoils

2 airfoils --

AFSC
Arnold AFS Tenn.